IFT - UNESP
INSTITUTO DE FÍSICA TEÓRICA

DISSERTAÇÃO DE MESTRADO

IFT-D.002/2023

Allee effect across spatial scales:

a statistical-physics approach to population dynamics

Daniel Cardoso Pereira Jorge

Orientador

Ricardo Martinez-Garcia

Julho de 2023

Jorge, Daniel Cardoso Pereira
J82a Allee effect across spatial scales: a statistical-physics approach to population dynamics / Daniel Cardoso Pereira Jorge. – São Paulo, 2023
97 f.

Dissertação (mestrado) – Universidade Estadual Paulista (Unesp), Instituto de Física Teórica (IFT), São Paulo
Orientador: Ricardo Martínez-García

1. Biofisica. 2. Física. 3. Modelos matemáticos. I. Título

Sistema de geração automática de fichas catalográficas da Unesp. Biblioteca do Instituto de Física Teórica (IFT), São Paulo. Dados fornecidos pelo autor(a).

Agradecimentos

Primeiramente à minha família. Em especial aos meus pais, Ari Borges Pereira Jorge e Simone Cerqueira Cardoso, por sempre estar ao meu lado e incentivar meus estudos. Aos meus tios, Rui Pereira Jorge, Suzana Cardoso e Veronica Zorek e aos meu primos Carolina Figueiredo, João Zorek e Leonardo Tosta, por todo o apoio, cuidado e presença na minha vida. Agradeço imensamente aos meus colegas soteropolitanos que estiveram próximos a mim nessa trajetória, Amanda Lima, Cleber Figueiredo, Felipe Trotte, Filipe Cruz, Johnathan Dantas, Leonardo Barbosa, Rebeca Dourado, Robert Araujo, Saada Cerqueira e Ysla França. Obrigado pelos momentos de convivência, aprendizado e apoio; sem vocês eu não teria as forças para estar onde estou.

O meu pleno agradecimento à Universidade Estadual Paulista pelo ensino de alta qualidade, me proporcionando um aprendizado que vai além das áreas da Física. Obrigado por todas as vivências e oportunidades de imersão no meio cientifico. A todo o setor técnico administrativo, terceirizados e servidores do Instituto de Física Teórica, obrigado por proporcionar o funcionamento desta instituição. A todo o corpo docente do Instituto de Física Teórica, por todas as contribuições em meu processo de formação. Devo imensos agradecimentos a todo o corpo estudantil do Instituto de Física Teórica pela organização de eventos, coloquinhos, trocas de conhecimento e fraternidade. Em especial, gostaria de ressaltar meu agradecimento a Eggon Vianna, Isabela Maietto, João Pedro Gomides, Luisa Ferreira, Matheus Carvo, Rodrigo Pitombo. Obrigado por fazer de São Paulo uma cidade acolhedora onde pude encontrar uma comunidade. Gostaria de agradecer por tornarem esta cidade um lugar que pude chamar de casa.

Aos estudantes e postdocs do meu grupo de pesquisa no Instituto de Física Teórica: Benjamin Figueiredo, Gabriel Andreguetto, Jesus Encinas, João Valeriano, Pablo de Castro, Rafael Menezes, Vivian Dornelas. Agradeço pelas inúmeras contribuições para a pesquisa apresentada nessa tese. Os seus comentários, ensinamentos e discussões acrescentaram substancialmente na qualidade do trabalho. Além do aspecto científico, gostaria de agradecer pela amizade e por todos os momentos de convivência. A presença de vocês na trajetória do meu mestrado foi crucial.

Switching languages for my international folks. I want to thank my lab mates at Princeton University for being so welcoming and terrific people. My 6 months there were filled with joy and I want to express my gratitude for each of you. Eduardo Colombo, Harrison Watson, Kelly Finke, Merlijn Staps, Sebastian Michel-Mata, and Yuriy Pichugin, your contributions to my life were beyond science and I very much appreciate your companionship. Also, I have nothing but extreme gratitude for being part of the Real Food Coop at Princeton, thank you for including me in this community. Thank you, Bella

Hubble, Dinie Zheng, Elie Svoll, Felix Kleeman, Kennedy Primus, Kevin Zhang, Naomi Frim-Abrams, and many others, my experience at Princeton would never be the same without all of you. My special thanks to Kelly Finke and Felix Kleeman, you are wonderful people and I am so grateful for every moment with you. Finally, I want to express my great gratitude to my Princeton supervisor, Corina Tarnita. Beyond your amazing mentorship, you are a wonderful person and made me feel welcome and belong to the department. You created an environment where I could contribute and learn a lot of new science. Thank you for all of the time, patience and mentorship.

Finally and most importantly, I have no words but extreme gratitude for my supervisor Ricardo Martinez-Garcia. They say that the best humans are *human*, and I can see it clearly with you. The care that you give to your work and to dealing with different people with distinct needs is inspiring. You created a welcoming and fruitful environment where everyone felt comfortable contributing, expressing their views, and being heard. You were always by my side reasoning my ideas with me and allowing them to flourish. Your mentorship went beyond our scientific project and helped me through several aspects of *being* a scientist. Your guidance allowed me to develop more critical thinking and creativity. I want to express my enormous appreciation for you as a mentor and as a person. Thank you.

Por fim, gostaria de agradecer à Fundação de Amparo à Pesquisa do Estado de São Paulo (FAPESP), que apoiou minha pesquisa a partir dos processos no. 2020/15643-8 e 2022/06202-3. Obrigado por possibilitar o avanço da ciência no Brasil.

Resumo

Interações intraespecíficas são peças fundamentais na dinâmica populacional porque estabelecem relações entre o fitness dos indivíduos e a densidade populacional. O efeito Allee é definido como uma correlação positiva entre qualquer componente do fitness de um organismo focal e a densidade populacional, e pode levar a uma dependência positiva entre a taxa de crescimento populacional per capita com a densidade populacional. A estrutura espacial da população é a chave para determinar se e até que ponto um efeito Allee se manifestará no nível demográfico, visto que ela determina como os indivíduos interagem uns com os outros. No entanto, os modelos espaciais existentes para estudar o efeito Allee impõem uma estrutura espacial fixa, o que limita nossa compreensão de como um efeito Allee e a dinâmica espacial impactam conjuntamente a dinâmica populacional. Para preencher essa lacuna, introduzimos um formalismo teórico espacialmente explícito onde a estrutura espacial e a dinâmica populacional são propriedades emergentes das taxas demográficas e de movimento em nível individual. Construímos o modelo ao nível do indivíduo, definindo taxas demográficas e de movimento levando a uma dinâmica populacional estocástica que exploramos através de simulações numéricas. Para entender melhor o resultado dessas simulações numéricas, escrevemos uma equação mestra para a dinâmica da probabilidade de encontrar a população em um determinado estado e usamos o formalismo Doi-Peliti para derivar uma equação determinística para a densidade populacional. A população apresenta uma variedade de padrões espaciais que determinam as consequências demográficas de um efeito Allee no nível individuo. Mostramos que o agrupamento de organismos aumenta a abundância populacional e permite que as populações sobrevivam em ambientes mais hostis e em densidades populacionais globais mais baixas. Além disso, a agregação pode impedir que o efeito Allee no nível do indivíduo se manifeste no nível da população ou restringi-lo a uma escala local. Esses resultados fornecem uma compreensão mecanicista de como o efeitos Allee pode operar para diferentes estruturas populacionais e emergir no nível da população. Nossos resultados destacam o poder do formalismo matemático da física estatística para investigar tópicos interdisciplinares.

Palavras chave: Efeito Allee; Modelagem matemática; Formação de Padrões; Efeito Allee de grupo; Transições críticas.

Área de pesquisa: Física; Física biológica; Modelagem matemática; Sistemas complexos.

Abstract

Intraspecific interactions are key drivers of population dynamics because they establish relations between individual fitness and population density. The component Allee effect is defined as a positive correlation between any fitness component of a focal organism and population density, and it can lead to positive density dependence in the population per capita growth rate. The spatial population structure is key to determining whether and to which extent a component Allee effect will manifest at the demographic level because it determines how individuals interact with one another. However, existing spatial models to study the Allee effect impose a fixed spatial structure, which limits our understanding of how a component Allee effect and the spatial dynamics jointly impact the population dynamics. To fill this gap, we introduce a spatially-explicit theoretical framework where spatial structure and population dynamics are emergent properties of the individual-level demographic and movement rates. We build the model at the level of the individual, defining demographic and movement rates leading to a stochastic population dynamics that we explore using numerical simulations. To better understand the outcome of these numerical simulations, we write a Master equation for the dynamics of the probability of finding the population at a given state and use the Doi-Peliti formalism to derive a deterministic equation for the population density. Depending on the intensity of the individual-level processes the population exhibits a variety of spatial patterns that determine the demographic-level by-products of an existing individual-level component Allee effect. We find that aggregation increases population abundance and allows populations to survive in harsher environments and at lower global population densities. Moreover, aggregation can prevent the component Allee effect from manifesting at the population level or restrict it to a local scale. These results provide a mechanistic understanding of how Allee effects might operate for different spatial population structures and show at the population level. Our results highlight the power of the mathematical formalism of statistical physics to investigate cross-disciplinary topics.

Key words: Allee effect; Mathematical modeling; Pattern formation; Group-Allee

effect; Critical transitions.

Research area: Physics; Biological Physics; Mathematical modeling; Complex Systems.

Contents

Chapter 1

Introduction

Intraspecific interactions are critical to understanding population ecology because they define how demographic rates depend on population density and ultimately drive population dynamics. A component Alle effect occurs whenever the presence of conspecifics increases any component of the fitness of the organisms, which can translate to a positive density dependence in the population per capita growth rate [1, 2, 3]. Populations subjected to Allee effects are of great concern in conservation because their survivability is significantly impacted by population density, making them especially vulnerable when population sizes are small. In fact, those populations might have thresholds for population survival that manifest in sudden extinctions, existence of alternative stable states, and hysteresis [3, 4, 5, 6]. A mechanistic understanding of how the individual-level processes and interactions that underlie the Allee effect is then key to understanding the trends and patterns observed in population dynamics.

The existence of a component Allee effect can have a positive impact on several different components of the fitness, such as offspring survival, mating success, or fecundity [3, 7, 8]. In some fish, rotifer, and mammals such as marmots, the presence of conspecifics changes the environmental conditions locally, improving habitat quality and individual fitness [9, 10, 11, 12]. Especially in group-living organisms, cooperative behaviors such as group vigilance, nursing, resource sharing, and social foraging also make individuals more competent in the presence of conspecifics [13, 14, 15, 16, 17, 18]. Allee effects are also frequent in sexually reproducing species. In motile organisms, females are more likely to find mates at larger population sizes [19, 20, 21, 22]. In sessile organisms, such as pollinators or broadcast spawners, fecundation is more likely at high population densities [23, 24, 25, 26, 27].

Whenever one or more components Allee effects result in a positive correlation between the net per-capita growth rate and the population size or density, we have a demographic Allee effect [1, 3]. This type of Allee effect is related to the positive impact that conspecific interactions at the individual level have on the

population. This positive density-dependence is easier to identify at low population densities because competition hinders its effect in more crowded scenarios [3]. The presence of a demographic Allee effect requires the existence of at least one component Allee effect, but the opposite is not true. In fact, no demographic Allee effect is observed for several populations with well-documented component Allee effects [3, 28, 29, 30]. For a demographic Allee effect to occur, we need that the overall fitness of the individuals to increase, rather than only a fitness component.

Organisms modify the environment within a certain range and can only interact with other individuals if they are within an interaction-specific range. Therefore, the fitness of a focal individual can only be influenced by the presence of conspecifics within this range. Moreover, Allee effects often require direct interaction between at least two organisms. Thus, the spatial population structure is key to determining whether and to which extent a component Allee effect will manifest at the demographic level [28, 29, 31]. Back to Allee's seminal experiments, several studies have investigated the impact of the spatial population structure, and more specifically of aggregation, on Allee effects [32]. For instance, some plant populations produce more and heavier seeds if distributed in clumps [24, 25]. Plant aggregates can also facilitate nearby individuals because they attract pollinators to them, which extends the facilitation range beyond the scale of a single cluster of plants [33], and ameliorate physical stresses [34]. Broadcast spawners subjected to an Allee effect, such as the red sea urchin *Strongylocentrotus franciscanus*, can survive at low abundances by aggregating [26, 27]. Finally, several social species form spatially segregated groups, which could contribute to population persistence in harsh environmental conditions [18, 35, 36]. Aggregation and group living are thus ubiquitous features of populations subjected to Allee effects, and they strongly influence the emergent population dynamics. To explain how these spatial features impact populations subjected to component Allee effects, recent studies have introduced the group-level Allee effect, defined as any positive association between the organism's fitness and group size [35]. However, a theoretical framework describing how group-level Allee effects emerge from component Allee effects and the individual-level processes responsible for aggregation and group formation is lacking.

Over the last decades, theoretical studies have been key to developing much of our current understanding of Allee effects [4, 5, 37, 38, 39, 40, 41, 42]. Several models, either deterministic or stochastic, consider well-mixed populations and

disregard spatial degrees of freedom [43, 44, 45]. The effect of space has been investigated mainly using meta-population models, which divides the population into sub-units, groups or clusters, and describe the population dynamics within and between them [30, 46]. These frameworks already incorporate group-level Allee effects because they restrict fitness benefits due to intraspecific interactions to each meta-population and have helped to explain why component Allee effects rarely many manifest at the demographic level in group-living species [3, 30]. However, meta-population models impose the existence of groups in the stationary state, rather than allowing them to emerge. On the other hand, models that incorporate space explicitly are able to explain how a non-uniform spatial organization of organisms impacts the outcome of ecological dynamics, such as species invasions, in the presence of Allee effects [47, 48] or Allee-effect features, such as the Allee threshold [31]. However, a clear link between both meta-population and spatially explicit frameworks is still lacking. In this thesis, we aim to fill this gap by introducing a theoretical framework to investigate Allee effects across different levels of spatial organization.

The thesis is structured in the following way. In Chapter 2, we introduce the basic concepts regarding the Allee effect, the mechanisms that can generate it, and its ecological consequences. In Chapter 3, we present a stochastic and spatially explicit individual-based description of a population with density-dependent reproduction mimicking a component Allee effect. This description is the most fundamental level at which we can describe a population, allowing us to explicitly model the relationship between the mechanism responsible for the component Allee effect and individual birth and death rates. In Chapter 4, we shift towards the population scale by using the Doi-Peliti formalism to derive a deterministic equation for the dynamics of the population density out of the individual-level description. This density equation allows us to do a linear stability analysis to investigate in which conditions individuals aggregate due to individual-level interactions and to study the population-level consequences of the component Allee effect depending on the spatial population structure. Finally, in Chapter 5, we zoom out of the spatially explicit description by deriving a meta-population model. We use this approach to investigate the emergence of group-level Allee effects and, consequently, determine the conditions for a demographic Allee effect in the total population to emerge. Our results recapitulate several observations on the interplay between spatial structure, group, and demographic Allee effects, providing a unifying theoretical framework to investigate the topic. More gen-

erally, this thesis provides a guide on how to use the mathematical tools from statistical mechanics to describe the dynamics of a population out of the underlying features of its individuals.

Chapter 2

Allee effect

Most organisms are born alongside conspecifics and interact with them multiple times across their life history. Therefore, the nature of those interactions and their outcomes are major components of the ecology of each species. Competition has always been considered one of the main components dictating intra-specific dynamics. All populations are subjected to some sort of competition, such as for resources, territory, mates, or any other factor necessary for survival or breeding [49, 50, 51]. In fact, since conspecifics require similar resources, intraspecific competition is usually more impactful than competition between different species [52]. The effect of competition becomes higher with the increase of populational density and always surpasses the impacts of positive interactions among conspecifics. Consequently, populations cannot grow indefinitely and a carrying capacity is set [53]. Competition is also paramount for the theory of natural selection by driving the evolution of traits that allow organisms to out-compete their conspecifics.

Positive interactions, such as cooperation, didn't have the same highlight for a long time. Classical ecology theory states that, in a population, the fitness of the organisms should decrease with population density [3, 51, 54]. This means that, even when acknowledging the existence of positive interactions, ecologists did not consider that their effects on population growth could be stronger than those of competition. According to this hypothesis, an organism would always be better off in a smaller population due to less competition [32]. The role of positive interactions would be to partially ease the effect of negative interactions at higher densities. In evolutionary theory, however, cooperation was a topic of controversy. In fact, Darwin posed it as a major problem in the classical theory of natural selection [55]. The idea that an organism would decrease its own fitness to buffer a presumable competitor and that this behavior would persist in evolutionary time seemed to conflict with the *survival of the fittest*. A great body of work has been dedicated to solving this controversy to this day [56, 57, 58, 59].

Several species increase their population density by aggregating [60]. This be-

havior would be in contradiction to the idea that competition always dominates and strengthens at higher densities. Professor Warder Clyde Allee was fascinated that the most common dispersion pattern among organisms was clumped, implying that increasing population density might be beneficial. Allee was interested in the mechanisms that promote animal aggregation and the consequences of it, which led him to years of experimental work. A large portion of his studies focused on aquatic species and how they are able to improve habitat quality by changing the chemistry of the water [32]. He demonstrated that goldfish release protective chemicals in the water, significantly buffering their survival at higher population densities [9]. For several years, Allee gathered substantial evidence that high densities have beneficial effects on some species, conflicting with the traditional ecology predictions. This realization implied that lower densities could lack the benefits of aggregation, resulting in poorer performance, which Allee called under-crowding or inverse density dependence [54]. A natural extension of this reasoning is that for some species there could be a density threshold below which population growth would be negative, leading to local extinction [3].

Allee's main interest in investigating this subject was understanding the evolutionary origins of sociality. He suggested that aggregation, and the benefits that arise from it, is a very primitive stage in the evolution of social groups [54]. He believed that in the presence of cooperation, or "proto-cooperation" since he believed that animals do not have any "intent", natural selection would push for the evolution of aggregation and increased cooperation [3]. Aggregation seems to be so important for species subjected to under-crowding that several of those have evolved mechanisms that enable aggregation in order to avoid extinction [61].

Today, the legacy of Allee's work goes beyond cooperation and comprises any mechanism that benefit organisms' crowding. The Allee principle, later renamed as the Allee effect, is defined as any type of positive relation between conspecific population density or size and the fitness of the individuals [62]. The intuition behind the Allee effect is fairly simple. If there is a benefit related to the presence of conspecifics, the more we are the more we are buffering each other. If we are not abundant enough, the benefits will not be as effective. The Allee effect has major implications for the study of population dynamics and species conservation. A population subject to this effect is particularly at risk of extinction because its survival probability is greatly impacted by population density, endangering it

at lower abundances [3]. Throughout this chapter, we will introduce examples of Allee effects in distinct natural systems, and discuss how and when these Allee effect impacts population dynamics.

2.1 Mechanisms for Allee effect

Throughout his work, Allee tried to maintain his framework general enough, so that it could describe various scenarios. However, the way in which positive density dependence emerges is extremely dependent on the specific biology of each system. In fact, Allee effects can arise from a wide range of distinct mechanisms that are present across the tree of life [3]. Although most of Allee's work focused on cooperation between conspecifics, or proto-cooperation as he preferred, positive density dependence can emerge from much more general ecological processes, such as predation or inbreeding [63, 64].

The Allee effect definition is centered around fitness. "Fitness" is a very general concept, broadly representing the individual reproductive success, and it is usually not straightforward to measure [65]. Allee effects can arise from any contributions to any component of the fitness. For instance, a mechanism that increases reproduction rate with population density can generate an Allee effect nearly in the same way as a mechanism that reduces mortality. Another key point is that a single mechanisms can influence distinct fitness components in different ways. For example, conditioning an environment allows organisms to increase the survival fitness component, such as the aquatic species in Allee's seminal experiments [32]. However, maintaining the environment under adequate conditions has energetic costs which can lead to fewer offspring, diminishing the reproduction fitness components. Thus, it is challenging to predict the overall effect of a single mechanism in the fitness of an organism. For the purposes of this section, we will only consider the positive effects of mechanisms on individual fitness, regardless of the overall outcome. However, the conundrum will be further discussed in the next section.

For the remainder of the present section, we will review the main mechanisms responsible for Allee effects to arise. We will provide a brief description of the generating mechanism, how it leads to positive density dependence, and finally discuss examples of living systems in which the discussed mechanism can be found.

Habitat conditioning. Some living beings are able to change the environmental conditions locally, improving habitat quality and individual fitness [3, 7, 8]. This can scale with conspecific local abundance, as more individuals would reflect in more and better conditioning of the habitat. Organisms can alter their environment in several ways. For instance, they can change physical features around them that can benefit their conspecifics. Whenever the temperature goes too low, several animals tend to aggregate to thermoregulate, such as little brown bats[66], Alphine marmots [10] and bobwhite quails [32]. Alternatively, organisms can alter their environment chemically. By secreting protective substances, organisms such as goldfish [9], starfish [3] and some rotifers [11] can increase population fitness. Also, some alleopathic plants can release chemicals that are toxic for invasive plants [67].

Social behavior. Organisms may depend on social interactions for various aspects of survival and reproduction [18]. Especially in group-living organisms, social behaviors such as group vigilance, nursing, resource sharing, social foraging, information sharing, and collective decision-making can enhance resource acquisition, predator defense, and reproductive success [3]. As population density decreases, the availability and effectiveness of these cooperative interactions may decline. For example, in cooperative breeding species like the African wild dog, a decrease in population density can reduce the number of helpers available to assist with rearing offspring, leading to decreased reproductive success [16]. Anti-predator social strategies are key for the persistence of several species. Some monkeys species, exhibit better vigilance and improved protection against predators in higher population sizes [68, 69]. To effectively locate food resources, which are often temporary and unevenly distributed, predators can benefit from social foraging behavior. For instance, bats share information regarding feeding locations among members of the colony and can emit social calls to actively recruit and coordinate foraging activities with unrelated group members [13, 70, 71].

Sexual reproduction Most multicellular eukaryotes, and some unicellular ones, need conspecifics to reproduce. For these species, low population densities reduce mating opportunities which can significantly diminish the fitness of organisms. In Sessile organisms such as polinators or broadcast spawners, fecundation efficiency is greatly affected by population density. For instance, aggregates of plants are able to attract more pollinators, and thus produce more and heavier

seeds [24, 25]. In motile species at low population densities, individuals may not be able to find mates [19, 20, 21, 22]. This limited availability of potential mates can lead to reduced reproductive success and a decline in the population growth rate. Furthermore, in some species, sexual reproduction may involve complex mating behaviors or mate choice preferences that require larger populations to function effectively. These behaviors may rely on the presence of a sufficient number of individuals displaying specific traits or engaging in specific courtship rituals [3, 61].

Predation. Increasing population size can lower the per capita predation risk [3, 63, 72]. When a predator-prey system is subjected to a type II functional response, the predation rate saturates for high prey populations [19]. In this limit, the consumption rate remains constant regardless of increases in prey density. The saturation can be associated with the limited capacity for predators to process their food [73]. For instance, the abundance of prey can lead to an increased number of predators reaching satiation and, consequently, stopping predating temporarily [74]. Predation generates an Allee effect when the increase in prey abundance, followed by the increase of the predator population, decreases the rate of predation per prey. Generalist predators are often the primary contributors to the occurrence of Allee effects in prey populations. This is because generalist predators exhibit less sensitivity to changes in prey density compared to specialist [63]. As a result, when a prey population decreases, a generalist predator population may not change significantly. Thus, an Allee effect occurs where the rate of prey decline surpasses the decrease in predator numbers and consumption rates. Evidence for this mechanism for Allee effect have been found in ocean skater, caribou and island foxes [3, 75]

Inbreeding. In smaller populations there are fewer mating options. A natural consequence of this is increased levels of inbreeding. When individuals mate with close relatives, they are more likely to inherit and express harmful recessive alleles that are typically masked in outbred populations [64, 76, 77]. The accumulation of these deleterious alleles can lead to a range of negative effects on various fitness-related traits, such as reduced fertility, lower survival rates, impaired growth and development, and increased susceptibility to diseases and environmental stresses. Consequently, the Allee effect can be intensified as inbreeding further compromises the population's ability to rebound and recover from de-

clining numbers [3]. Evidences of increased inbreeding in smaller populations have been find in species of plants and butterflies [78, 79, 80].

2.2 Component and Demographic Allee effects

To understand the ecological consequences of Allee effects, we must connect its underlying mechanism with the observed patterns of population dynamics. This connection is especially important because often the existence of an Allee effect does not influence the dynamics of the population at all [3]. To understand why individual-level Allee effect may not manifest at the population level, it is useful to draw the distinction between what we call "component" and "demographic" Allee effects [1]. These two levels of Allee effects reflect how the fitness of the organisms is affected by the presence of others. So far in this Chapter, we have only been considering the component Allee effect, which is a positive association between population density, or size, and one (or many) components of individual fitness, such as offspring survival, mating success, or fecundity [3, 7, 8]. On the other hand, the demographic Allee effect only happens if this association impacts the total overall fitness of the organisms. Therefore, the demographic Allee effect is a population-level emergent property and it manifests as a positive correlation between the net per-capita growth rate and the population size.

The existence of a demographic Allee effect requires the presence of one or more underlying component Allee effects. The opposite is not true because a positive density dependence on one fitness component can be completely compensated by an equal or stronger negative density dependence on another component. A fairly simple example of this situation in nature happens with some sea urchins. As broadcast spawners, they require a higher population density to increase their fecundation efficiency, displaying a component Allee effect [2]. However, at lower densities the decreased competition for resources enhances gamete production [81]. For the Caribbean long-spined urchin (*Diadema antillarum*), the component Allee effect responsible for increasing fecundation efficiency is compensated by a higher sperm production under reduced competition. Therefore, a demographic Allee effect does not occur.

It is not obvious at all if a component Allee effect will translate to the demographic level even if one knows everything about the mechanisms generating it and its effects. All of the other processes present, which are situation dependent, can affect the fitness in ways that can compensate for the positive density depen-

dence contribution from the component Allee effect. Therefore, a demographic Allee effect is the result of not only the mechanisms that trigger positive density dependence but of all underlying processes involved in the biological system, which are very often related in a nonlinear and intricate way.

2.3 Weak and strong Allee effects

Given that a demographic Allee effect does happen, it can do so in two qualitatively distinct ways. We have already established that populations with demographic positive density dependence experience under-crowding if their population densities, or sizes, are too low. That is, the per-capita growth rate is greatly diminished in the absence of conspecifics. The magnitude of the cost related to this under-crowding is key for the overall dynamics of a population.

For instance, if it is particularly costly for a population to maintain low densities, its per-capita growth rate can become negative for sparse conditions. This is a Strong Allee effect scenario, in which it exists a minimum population density or size, termed the Allee threshold, below which the per-capita growth rate becomes negative [3, 8]. A population below this threshold is subjected to an accelerated decrease in population size until it reaches extinction. On the other hand, in a situation in which the per-capita growth rate decreases with population density or size, but never goes below zero, defines a weak Allee effect. Whether an Allee effect is weak or strong is key to determining if a population can recover from losses in abundance. Making such a distinction is also crucial for understanding if a species can invade an environment. For instance, in the presence of a strong Allee effect, a population is only able to invade if it is already above the Allee threshold from the beginning [82].

Further intuition about the demographic Allee effect can be obtained through mathematical modeling [45]. Given a population of n individuals, we can separate its per-capita growth rate in three main components: An intrinsic density independent growth rate r that encompasses the performance of the organisms when alone; a positive density dependence βn rate, linear in n; and a negative density dependence rate $-\gamma n^2$, quadratic in n. The choices in the dependencies in n for the last two terms are such that the negative density dependence will always overcome the positive one at very high abundances, as we discussed in previous sections. This is necessary otherwise the population would grow unbounded. Mathematically, this choice for the per-capita growth rate leads to the

following model

$$\text{Per-capita growth rate} = r + \beta n - \gamma n^2. \tag{2.1}$$

This is a phenomenological description but this model will be derived out of individual-level processes in the next chapter. In Figure 2.1 we present the curves for the weak and strong Allee effect, together with the curve of the logistic model ($\beta = 0$ and negative density dependence linear in n) as the traditional description without Allee effect. This cubic model has two stable stationary solutions and one unstable. One of the stable stationary solutions is the extinction state because, with no individuals in the system, nothing can happen. The second stable stationary state, ρ_+, and the unstable one, ρ_-, are the roots of the quadratic equation $r + \beta\rho - \gamma\rho^2 = 0$,

$$\rho_\pm = \frac{\beta \pm \sqrt{\beta^2 + 4\gamma r}}{2\gamma}. \tag{2.2}$$

These two states represent the population carrying capacity ρ_+ and the Allee threshold ρ_-. This can be seen through the strong Allee effect curve in Figure 2.1. ρ_+ is the larger root of the equation, where the competition has overcome the positive density-dependent interaction. Therefore, if a population gets larger than rho_+, the per-capita growth rate becomes negative and takes the population size backto ρ_+. Conversely, if the population size becomes slightly smaller than rho_+, the per-capita growth rate is positive, and the system is pushed towards ρ_+, hence the term stable. On the other hand, if the population gets below ρ_-, it tends to extinction and if it gets above it, it goes towards the carrying capacity, i.e. the Allee threshold. Therefore, any perturbation to the ρ_- population size would drive the system away from it, hence the term unstable.

The condition for a strong Allee effect to occur is given by $r < 0$, and $r \geq 0$ for the weak Allee effect. It does not depend on the positive or negative density dependence parameters, β and γ. Therefore, the occurrence of a strong Allee effect does not imply harsher competition or weaker cooperation. Strong Allee effects occur an isolated individual, which is not subjected to either of those interaction types, is not able to grow on its own. In those cases, the population requires the mechanism related to the positive density dependence to survive. The necessity of the positive interaction explains the existence of a population threshold, which is the minimum amount of cooperation, or any other mechanism, necessary to

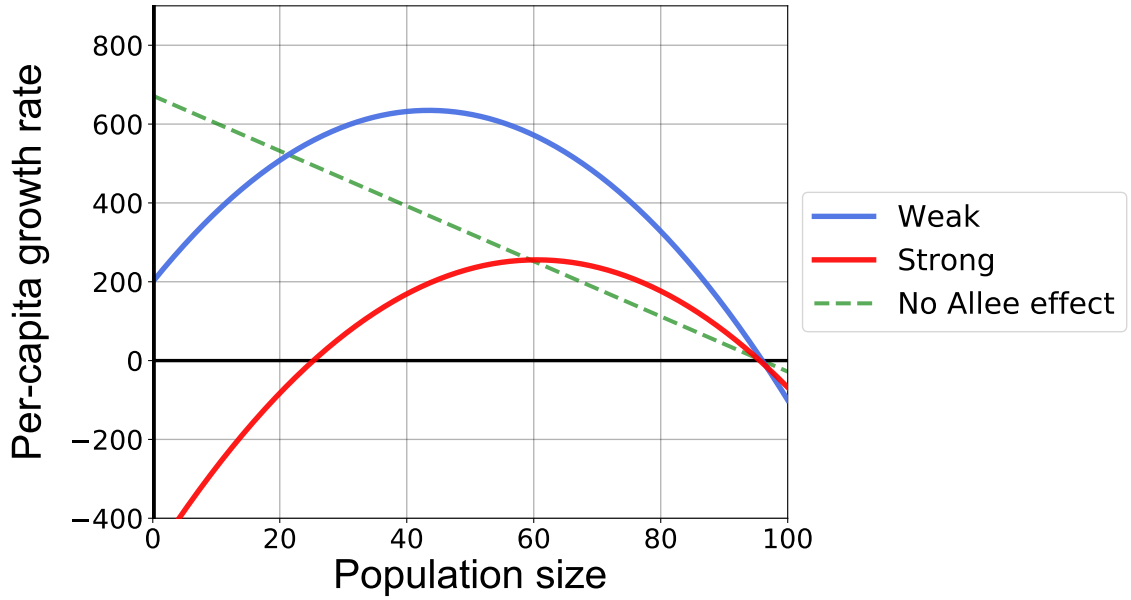

Figure 2.1: Per-capita growth rate in a population subjected to: weak Allee effect (blue), strong Allee effect (red), or no Allee effect (dashed green). The filled curves were generated by the model (2.1). The dashed curve was generated using the logistic model: Per-capita growth rate $= r(1 - n/K)$, where K is the carrying capacity.

sustain the population. A classical example in which strong Allee effects are observed are through social species [16]. Evolution pushes individuals to excel in groups by enhancing the positive interactions or reducing competition, increasing β or decreasing γ, at the expense of lower fitness when alone, decreasing r. Thus, the strong Allee effect may not be a bad scenario at all but a natural step towards sociality [83].

2.4 Spatial structure and Group-Allee effect

Up until this point, a key point regarding this entire framework has only been addressed tangentially, the role of space. Populations live in a physical world with spatial dimensions, and their distribution along the landscape is as ecologically important as their abundance. The possibility for an interaction among organisms to occur requires not only their existence but also that they are close enough (Fig. 2.2-a and b). As a consequence, the fitness of an individual depends on their position, creating a feedback loop between spatial distribution and abundance, which shapes both simultaneously [84, 85].

In the literature, there are several studies addressing the interplay between

ecological interactions and spatial structure. For instance, in arid ecosystems, vegetation patterns can appear due to short-range facilitation and long-range growth–inhibition [86, 87, 88, 89]. Central-foraging organisms, such as termites, can also drive pattern formation due to the competition in regions close their home-range [90, 91]. Due to the Allee effect driven by pollination success, certain plant populations produce more and heavier seeds when arranged in clumped populations [24, 25]. Each of these clumps can further facilitate neighbor plant groups by attracting pollinators to them, showing that the facilitation interaction range goes beyond the scale of a single aggregate [33]. Previous works have shown that clumped population structure can diminish the Allee effect threshold allowing populations to survive in low densities[26, 27, 29, 35, 36]. Thus, although Allee gave a lot of attention to aggregation, the way such emergent spatial structure forms can be as important. For instance, a single large aggregate can behave significantly differently than a population composed of several smaller groups isolated from each other, and different from populations distributed in more complex patterns [92].

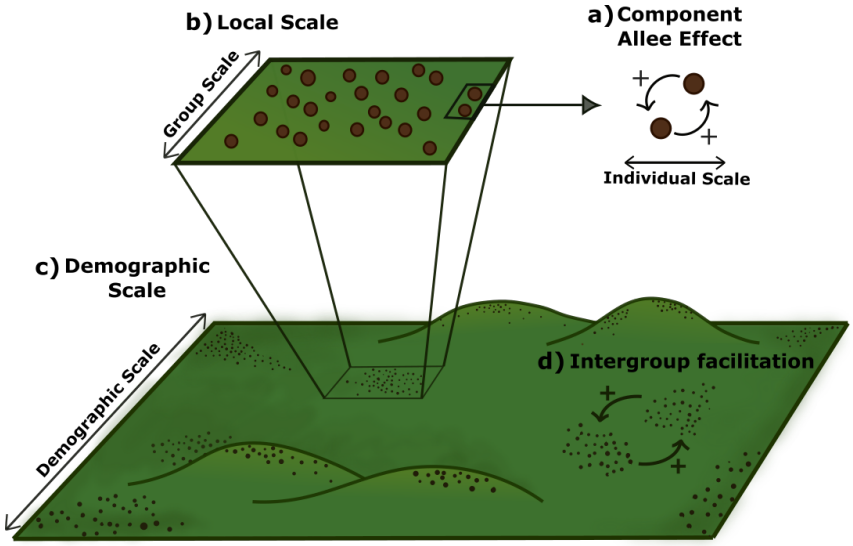

Figure 2.2: Allee effect across spatial scales. The component Allee effect (a) is a result of interactions between individuals that manifests at a (b) local scale around a focal organism. At the demographic scale (c), individuals are spatially scattered, possibly forming aggregates. In the presence of aggregates, the population has a fourth characteristic scale, defining inter-group facilitation (d)

A major consequence of spatial structure is the possibility for a demographic Allee effects to be only present on a local scale, rather than at the level of the whole population [3, 30], (Fig. 2.2-b and c). This scale-dependence has puzzled

ecologists for a long time and has important implications in the design of field studies because a demographic Allee effect that could be measured in the field would not necessarily show up in the whole population dynamics [18]. This problem was mostly addressed for group-living species, which have a spatial structure composed of isolated clumps of individuals. To solve this conundrum, the concept of Group Allee effect was created and defined as any type of positive relationship between the fitness of the individuals and the the size of the group they live in [35]. The key word here is group, rather than population size. This is a consequence of the fact that the range of the positive density-dependence interactions is finite and may not exceed group boundaries [3]. In this case, the groups seem to become the new ecological unity, rather than the individual. Groups are created, compete and die. Therefore, the dynamics of the population shifts to being dictated by the number of groups rather than the number of individuals. Since in this framework groups are not facilitating each other, this population dynamics should be qualitatively a simple logistic-type description (Fig 2.1, No Allee effect). Of course, the group Allee effect framework has some limitations, since several species have spatial structures in between isolated groups and uniformly distributed. In addition, some group populations experience inter-group facilitation, which extends the Allee effect beyond the boundaries of the groups [24, 25], (Fig. 2.2-d).

From a theoretical point of view, the group Allee effect has been mostly studied using of meta-population models. This description segregates the population into several sub-populations, i.e. meta-populations, that can interact [30, 46]. Therefore, the population is mapped into a network in which each node represents a group and links represent any inter-group interaction. This description has helped explain, from a theoretical point of view, why component Allee effects rarely manifest at the demographic level in group-living species [3, 30]. However, meta-population models impose a fixed spatial structure, which limits our understanding of how a component Allee effect and the spatial dynamics jointly determine the existence of demographic Allee effects. Furthermore, these existing models are unable to draw comparisons between structured and mixed populations while fixing the features of the individuals because they are already formulated at the population level and thus lack a clear description of how individual-level processes affect organisms' fitness.

Throughout the rest of this thesis, we aim to fill this gap by introducing a spatially-explicit theoretical framework where spatial structure and population

dynamics are emergent properties of individual-level processes. This way, the group Allee effect could be able to emerge as a property of a set of spatial structures, rather than an imposed definition.

Chapter 3

Individual scale

At the heart of understanding the ecology of a population lies the necessity to comprehend it from the level of the individuals. With this description, we can capture the spatiotemporal population dynamics of the system by incorporating any ecological interaction, such as competition, predation, cooperation, movement, and birth-death dynamics tracking single individuals [93]. Another key component of our proposed individual-based model is stochasticity, due to the inherent uncertainty and variability of ecological systems. The randomness of events, such as births, deaths, and migrations, can have a significant impact on population dynamics [94]. By incorporating stochasticity, individual-based models can capture the random events that shape population growth, fluctuations, and persistence. This chapter will focus on building and analyzing a stochastic individual-based model for Allee effect in the presence of space. By emphasizing the significance of individuals, we aim to construct a comprehensive understanding of how the Allee effect can emerge from individual-level processes and its consequences manifest at larger scales. In addition, this chapter will lay the theoretical foundations for the subsequent development of our model.

3.1 Individual-level processes

We consider a population with density-independent birth, death, and movement and also account for density-dependent processes. Specifically, individuals interact via binary reproductive facilitation and ternary competition [45]. Therefore, we assume a component Allee effect as a facilitation interaction between two individuals that increases their reproduction rates. As a simplifying assumption, the organisms in this model will be asexual. Reproductive facilitation is common even in species with asexual reproduction. For example, when individuals need the presence of conspecifics to reach the physiological condition to reproduce [3]. Some examples of species exhibiting asexual reproduction and reproduc-

tive facilitation are self-fertile snails, and parthenogenetic female lizards [95, 96]. In addition to pairwise facilitation, our model also assumes competition due to crowding effects. Mathematically, we model this crowding effect as a mortality induced by the encounter of triplet of organisms. This is a way to model competition as a process that will always overcome the facilitation, as the number of triples in a population grows faster than the number of pairs at large population sizes [45]. Therefore, competition is the dominant interaction at large population sizes, which limits population growth up to a carrying capacity. The combination of binary reproductive facilitation and ternary competition results in a hump-shaped relationship between per capita reproduction rate and local density of individuals similar to that reported by Allee in his experiments with laboratory populations of the flour beetle [32, 54], and portrayed in Figure 2.1.

The previous processes and interactions can be summarized in the following set of demographic reactions

$$\bigcirc \xrightarrow{b} \bigcirc + \bigcirc \tag{3.1a}$$

$$\bigcirc \xrightarrow{d} \varnothing \tag{3.1b}$$

$$\bigcirc + \bigcirc \xrightarrow{\beta} \bigcirc + \bigcirc + \bigcirc \tag{3.1c}$$

$$\bigcirc + \bigcirc + \bigcirc \xrightarrow{\gamma} \bigcirc + \bigcirc \tag{3.1d}$$

(3.1a) and (3.1b) represent density-independent birth and death, which happen at rates b and d respectively. (3.1c) represents a binary cooperative interaction in which two individuals interact at rate β and produce a third individual. The last reaction, (3.20), describes ternary competition happening at a rate γ. A more detailed explanation of what those rates mean will be given in the following section. This set of processes is one of the mathematically simplest ways of modeling a component Allee effect at the individual level [45]. Demographically, this model is equivalent to equation 2.1. Conversely, one can think of many alternative density-dependent processes that can result in a component Allee effect, such as presented previously (See section 2.1). Any of these other processes can be incorporated into a modeling framework like the one presented here.

In order to incorporate spatial dynamics into our model, we assume that individuals are situated within the sites of a one-dimensional regular lattice with periodic boundary conditions. This choice allows us to account for the spatial arrangement of individuals and their interactions within a defined landscape.

However, it is important to note that the principles and methodologies we employ can be easily extended to more complex and realistic two-dimensional landscapes, if desired. We label each lattice node with an integer index $i \in [0, N]$, and denote the spatial coordinate with $x \in [0, L]$. The distance between two adjacent lattice nodes is given by δx such that the spatial coordinate of the i-th node is $x_i = i\,\delta x$. We assume individuals can only move to their nearest neighbors, performing a random walk through the lattice. We can express individual random movement using the reaction notation of (3.1) as

$$\bigcirc_x \xrightarrow{h} \bigcirc_{x\pm\delta x}, \tag{3.2}$$

where h is the jump transition rate and δx is the displacement length. These choices result in a diffusive movement with diffusion coefficient $D = h\,\delta x^2$.

Making the model spatially explicit also requires inter-individual interactions to depend on the relative location of organisms. Two individuals only interact if they are close enough, and the strength of such interaction can also depend on the distance between them. Therefore, density-dependent interactions in (3.1c)-(3.1d) only occur if individuals are within an interaction-specific range. This key aspect underscores the significance of spatial scales in our study. By considering specific ranges, we can determine how the Allee effect is shaped by the local density, rather than the global one as we did in (2.1).

To account for the spatial extent of the interactions between individuals, we modify to the demographic rates in the reactions (3.1c) and (3.1d). Specifically, we define that two individuals facilitate each other if their distance is shorter than the facilitation range R_f. Consequently, a focal individual located at x reproduces at a rate $\beta/2R_f$. This process can be represented in terms of reactions as:

$$\bigcirc_x + \bigcirc_{x'} \xrightarrow{\frac{\beta}{2R_f}} \bigcirc_x + \bigcirc_{x'} + \bigcirc_x \tag{3.3}$$

provided that $|x - x'| \leq R_f$. Therefore, the positive density dependence scales with a local population size within the R_f range. The negative density dependence works similarly. We consider that a focal individual at location x can die due to competition by forming triplets with two neighbors at locations x' and x''. The rate of this process is $\gamma/4R_c^2$, given that the distance between the focal individual and each of its two neighbors is shorter than or equal to the competition range $|x - x'| \leq R_c$ and $|x - x''| \leq R_c$. In terms of reactions, we can write this

process as

$$\bigcirc_x + \bigcirc_{x'} + \bigcirc_{x''} \xrightarrow{\frac{\gamma}{4R_c^2}} \bigcirc_{x'} + \bigcirc_{x''} \tag{3.4}$$

Lastly, it is important to observe that in both the facilitation and competition terms, we assume that the non-local reaction rates remain constant within a certain interaction range, regardless of the actual distance between individuals. To model this interaction range, we utilize a top-hat function for the interaction kernel. The factors dividing the rates β and γ serve as normalization factors for the top-hat kernel. This normalization ensures that the birth and death rates depend on population density rather than population size. In other words, it takes into account the overall density of individuals in the population, allowing for a more accurate representation of the impact of interactions on population dynamics.

3.2 Reaction rates

The set of reactions introduced in the previous section fully dictates the rules of our model. From now on, we will focus on analyzing them using the mathematical formalism developed to study many-body problems in statistical mechanics. Firstly, we need to formally explain what we mean when we talk about "rates". Let's take for example the density-independent birth rate b. We will look at a single individual and turn off all of the other reactions for now. After a time-step Δt, this individual has a probability of reproducing p_b. A key assumption of this framework is that this probability is constant. After a time interval $T = M\Delta t$, the probability that the organism has an offspring of N individuals is given by the binomial distribution [97].

$$P(N, M) = p_b^N (1 - p_b)^N \frac{M!}{N!(M-N)!}. \tag{3.5}$$

That is, the probability of giving birth N times, p_b^N, times the probability of not giving birth $M - N$ times, $(1 - p_b)^N$, times the number of ways this process can be organized, $\frac{M!}{N!(M-N)!}$. This last term takes into account the number of offspring does not depend on the order of the events, only on the number of times that the organism was able to reproduce. The average number of offspring after M time-steps, λ, is given by $\lambda = Mp_b$. Thus, on average, a proportion p_b of the time-steps yields in reproduction, as expected.

This is, however, a discrete in-time description of this reproduction process. In

order to translate this description to continuous we need to take the limit $\Delta t \to 0$, while maintaining T constant. This of course yields in $M \to \infty$. Also, if the time-step is going to zero, so is the probability that the organism will reproduce in this step, $p_b \to 0$. We can then use $p_b = \frac{\lambda}{M}$ in equation (3.5) and take the limit of $M \to \infty$

$$\lim_{M\to\infty} P(N,M) = \lim_{M\to\infty} \left(\frac{\lambda}{M}\right)^N \left(1-\frac{\lambda}{M}\right)^{M-N} \frac{M!}{N!(M-N)!}, \tag{3.6}$$

$$= \frac{\lambda^N}{N!} \lim_{M\to\infty} \frac{M!}{(M-N)!} M^{-N} \left(1-\frac{\lambda}{M}\right)^{M-N}. \tag{3.7}$$

As M goes to infinity, the first term $\frac{M!}{(M-N)!}M^{-N}$ goes to 1, while

$$\lim_{M\to\infty} \left(1-\frac{\lambda}{M}\right)^{M-N} = e^{-\lambda}. \tag{3.8}$$

The whole limit is then given by

$$\lim_{M\to\infty} P(N,M) = \frac{\lambda^N}{N!} e^{-\lambda} \tag{3.9}$$

which is the Poisson distribution [97]. Finally, since λ is linear in relation to T

$$\lambda = Mp_b = \frac{p_b}{\Delta t} T \tag{3.10}$$

we can define the rate o density-independent birth as

$$b = \lim_{\Delta t, p_b \to 0} \frac{p_b}{\Delta t} = \frac{\lambda}{T}. \tag{3.11}$$

A rate is then given by the expected number of offspring generated in an interval, λ, divided by the interval length, T. Therefore, the probability distribution of an offspring N being generated after a time interval T is

$$P(N,T) = \frac{(bT)^N}{N!} e^{-bT}. \tag{3.12}$$

3.3 Global transition rates

With the reaction rates defined, the next step is to define the rates at the configuration of the population changes on time given these reaction rates. To do this, we need to look at the population-level, rather than the individual one. Our model is composed of indistinguishable individuals in a lattice. Therefore, the state of the system only depends on the number of individuals at each lattice site. We can represent the lattice configuration by a vector η that specifies the number of individuals in each lattice node: $\eta = \{...n_{i-1}, n_i, n_{i+1}...\}$ where n_i is the number of individuals at the lattice node i. In order to determine how this system evolves in time, we need to obtain the rates at which this configuration η changes in time, which we will call the global transition rates, Ω.

There are three ways in which η can change. An individual in a site i can reproduce ($n_i \rightarrow n_i + 1$), die ($n_i \rightarrow n_i - 1$) or move to a nearest neighbor site ($\{n_i, n_{i+1}\} \rightarrow \{n_i - 1, n_{i+1} + 1\}$). Each of these changes is related to a global transition rate Ω. An intermediate step towards those transition rates is the demographic ones. A demographic rate W is the direct result of a reaction rate at the individual level (See Figure 3.1). For instance, W_b is the rate at which any individual in the population will go through density-independent birth. These rates are going to change as the configurations of the lattice also change. For example, as a population increases, the rate at which a birth reaction happens is higher, simply because there are more individuals able to reproduce. For the remainder of this section, we will obtain the demographic and global transition rates of the model.

Contribution of birth processes to the global transition rates

Reproduction processes contribute to the creation of individuals in a focal lattice position x via density-independent reproduction and facilitation. These processes are represented by the following reactions

$$\bigcirc_x \xrightarrow{b} \bigcirc_x + \bigcirc_x, \tag{3.13}$$

$$\bigcirc_x + \bigcirc_{x'} \xrightarrow{\frac{\beta}{2R_f}} \bigcirc_x + \bigcirc_{x'} + \bigcirc_x, \tag{3.14}$$

where the facilitation reaction (3.14) can only happen if $|x - x'| \leq R_f$. The global transition rate resulting from these birth processes can be decomposed into two demographic rates W, one corresponding to each of the reactions that can poten-

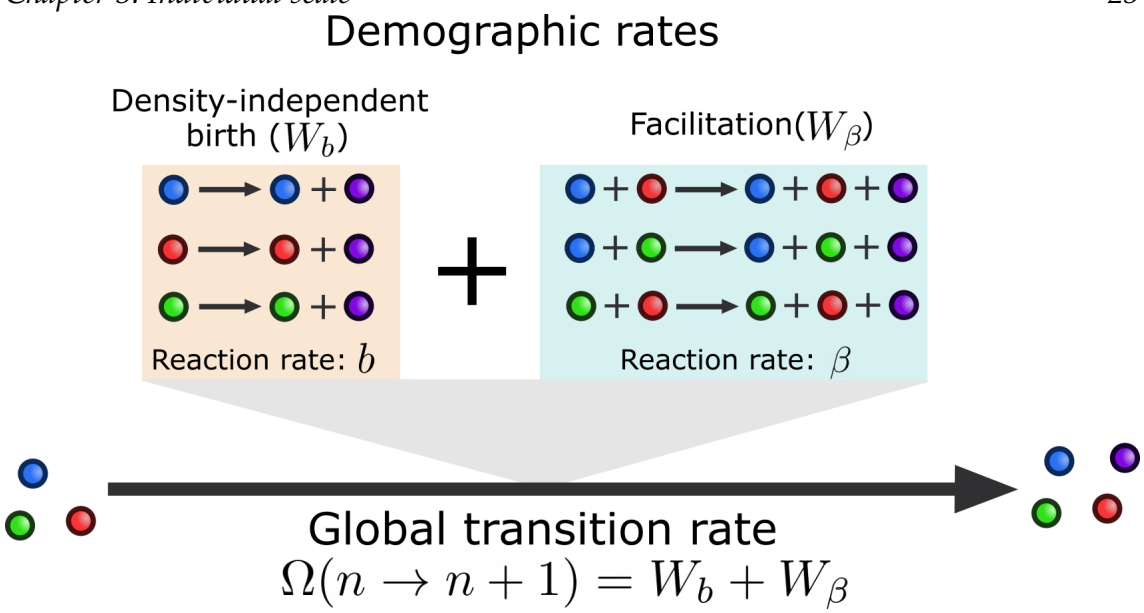

Figure 3.1: Relationship between the reaction, demographic, and global transition rates for the non-spatial model (See (3.1a)-(3.1d)). The transition from $n \to n+1$ can happen due to any reaction that results in reproduction. Thus, the global transition rate is a sum of the demographic rates of the density-independent birth (W_b) and facilitation (W_β) reactions, i.e. $\Omega(n \to n+1) = W_b + W_\beta$. A demographic rate is its corresponding reaction rate times the number of ways that this reaction can occur in the population (orange and blue rectangles).

tially contribute to the transition from a configuration η to $\eta' = \{n_x + 1\}_\eta$:

$$\Omega(\eta \to \{n_x + 1\}_\eta) = W_b(n_x) + W_\beta(\eta, x), \tag{3.15}$$

here, $\{n_x + 1\}_\eta$ denotes a lattice configuration with all sites having the same number of individuals as in the configuration η except the node with spatial coordinate x, where the occupancy has increased in one unity. $W_b(n_x)$ and $W_\beta(\eta, x)$ are the demographic rates in which the reactions for density-independent birth (3.13) and facilitation (3.14) generate one individual at the position x.

For the density-independent birth, the rate at which a focal individual reproduces is independent of the number of surrounding individuals. Therefore, the demographic rate corresponding to it should scale linearly with the number of individuals in the position x [45]. Each individual contributes with a rate b to the overall demographic rate, thus, by summing all of the contributions we have

$$W_b(n_x) = b\, n_x, \tag{3.16}$$

However, for the facilitation demographic rate, we need to take into account the spatial range of the interaction and thus the fact that reproduction at the lattice coordinate x depends on the number of individuals within the range $|x - x'| \leq R_f$. For instance, the demographic rate at which the facilitation reaction (3.14) generates an individual at x changes depending on whether x' is equal or different from x. This difference exists because pairwise facilitation only increases the number of individuals at x half of the times if $x' \neq x$, leading to a new individual at x' the other half. For $x = x'$, however, the new individual is always located at x. Thus, considering both the number of pairs we can form for both $x = x'$ and $x \neq x'$, the facilitation demographic rate is

$$W_\beta(\eta, x) = \frac{\beta}{2R_f}\left[\overbrace{\binom{n_x}{2}}^{x'=x} + \underbrace{\frac{1}{2}(N_x^f - n_x)n_x}_{x'\neq x}\right] \tag{3.17}$$

where N_x^f denotes the number of individuals within the range R_f centered at x. The expression simplifies to

$$W_\beta(\eta, x) = \frac{\beta\, n_x}{4\, R_f}\left(N_x^f - 1\right). \tag{3.18}$$

Contribution of death processes to the demographic transition rates

Individuals die in each lattice coordinate x due to reactions of density-independent death and competition. These reactions can be expressed as

$$\bigcirc_x \xrightarrow{d} \varnothing, \tag{3.19}$$

$$\bigcirc_x + \bigcirc_{x'} + \bigcirc_{x''} \xrightarrow{\frac{\gamma}{4R_c^2}} \bigcirc_{x'} + \bigcirc_{x''}. \tag{3.20}$$

The competition reaction (3.20) can only happen given that all individuals are within the focal individual's range $|x - x'| \leq R_c$ and $|x - x''| \leq R_c$. The global transition rate due to death processes is the sum of each reaction's contributions

$$\Omega(\eta \to \{n_x - 1\}_\eta) = W_d(n_x) + W_\gamma(\eta, x) \tag{3.21}$$

where $W_d(n_x)$ and $W_\gamma(\eta, x)$ are the demographic rates in which the density-independent death and competition reactions, (3.19) and (3.20) respectively, elim-

inate an individual at lattice coordinate x. Similarly to the density-independent birth process, the density-independent death demographic rate also increases linearly with n_x

$$W_d(n_x) = d\, n_x. \tag{3.22}$$

For the ternary competition demographic rate, we once again need to take into account the interaction range $|x - x'| \leq R_c$ and $|x - x''| \leq R_c$. For instance, if all individuals are in distinct positions, this reaction only affects the focal site i one-third of the times. Similarly, if two individuals are at the coordinate x, the probability that any of them die is two-thirds. Finally, if the organisms are all in the same position x, the number of individuals in x will always decrease after the reaction. The combination of all these possible combinations results in the following demographic rate

$$W_\gamma(\eta, x) = \frac{\gamma}{4R_c^2}\left[\overbrace{\binom{n_x}{3}}^{x=x'=x''} + \underbrace{\frac{2}{3}\binom{n_x}{2}(N_x^c - n_x)}_{x=x'\neq x'' \text{ and } x=x''\neq x'} + \overbrace{\frac{1}{3}n_x\binom{N_x^c - n_x}{2}}^{x\neq x'\neq x''} \right] \tag{3.23}$$

where N_x^c denotes the number of individuals within the range R_c centered at x. The expression in (3.23) simplifies to

$$W_\gamma(\eta, x) = \frac{\gamma}{6}\frac{n_x}{4R_c^2}(N_x^c - 1)(N_x^c - 2). \tag{3.24}$$

Contribution of movement to the demographic transition rates

The reaction that leads to individual movement is

$$\bigcirc_x \xrightarrow{h} \bigcirc_{x\pm\delta x}. \tag{3.25}$$

where the subscript indicates the location of the individual in spatial coordinates. Because this is a density-independent process, the global rate is linear in n_x and is given by

$$\Omega(\eta \to \{n_x - 1, n_{x'} + 1\}_\eta) = h n_x, \tag{3.26}$$

where, $x' = x + \delta x$ is a nearest neighbor of x.

3.3.1 Master equation

At this point, we have derived the global rates at which our system can change. In this section, we will focus on how we can describe the whole dynamics of the population, given an initial condition. Of course, our model is stochastic, therefore, an initial condition and the set of parameters do not fully determine the trajectory. The probabilistic aspect of such a model means that the time evolution of the system is subjected to randomness.

A way to deal with stochasticity is to focus on how the probabilities of observing the system in a given configuration evolve over time. Once again, we can write a possible configuration of the system as $\eta = \{...n_{i-1},\ n_i,\ n_{i+1}...\}$ where n_i is the number of individuals at the lattice node i. The Master equation characterizes the evolution of the probability that a system is in a specific configuration η at a given time t, $P(\eta, t)$ [97]. In our case, the Master equation describes how the probability of finding a certain population size and spatial distribution of individuals across the lattice nodes changes with time.

To construct the Master equation, we start with the global transition rates, $\Omega(\eta \to \eta')$, derived in the previous section. Here, η' represents an arbitrary configuration of the lattice and Ω defines the probabilistic transitions between η and η'. Next, let's say we have full knowledge about the probabilities of observing the system at all possible configurations η at time t, i.e. we know $P(\eta, t)$ for all η at a given t. After a small time interval Δt, the probability that the system is in the configuration η is the sum of two distinct possibilities. First, after a time-step Δt, a configuration η' can become η with probability $\Omega(\eta' \to \eta)\Delta t$. This can be derived directly from equation (3.12), where the probability that the reactions associated to $\Omega(\eta' \to \eta)$ happens once is

$$P(1, \Delta t) = \Omega(\eta' \to \eta)\Delta t \, \exp\left[-\Omega(\eta' \to \eta)\Delta t\right] \tag{3.27}$$

which in the small Δt limit becomes

$$P(1, \Delta t) \approx \Omega(\eta' \to \eta)\Delta t \, \left[1 - \Omega(\eta' \to \eta)\Delta t\right] \approx \Omega(\eta' \to \eta)\Delta t. \tag{3.28}$$

Of course, there is also the possibility that a transition from $\eta \to \eta'$ happens due to the occurrence of multiple reactions within the time interval Δt. However, the probability of those situations depends on Δt in higher orders and can be neglected. We can also have the possibility that the system was already in η and

no reaction occurred. This scenario has a probability

$$P(0,\Delta t) = \exp\left[-\sum_{\eta'}\Omega(\eta' \to \eta)\Delta t\right]. \tag{3.29}$$

The sum in η' represents that we are looking at all the possible transition rates that could take the system out of η. In the small Δt limit, the expression becomes

$$P(0,\Delta t) \approx 1 - \sum_{\eta'}\Omega(\eta' \to \eta)\Delta t. \tag{3.30}$$

Putting together (3.28) and (3.30), the probability that the system is observed at a configuration η after a time step Δt is

$$P(\eta, t+\Delta t) = \sum_{\eta'}\left[\Omega(\eta' \to \eta)\Delta t P(\eta', t)\right] + \left(1 - \sum_{\eta'}\Omega(\eta \to \eta')\Delta t\right) P(\eta, t). \tag{3.31}$$

The first term on the right side of (3.31) corresponds to the probability that the system was in a configuration η' at time t and transitioned to η. The second term is the probability that the system was in η at time t and nothing happened. We can divide both sides of (3.31) by Δt and rearrange the equation to obtain

$$\frac{P(\eta, t+\Delta t) - P(\eta, t)}{\Delta t} = \sum_{\eta'}\Omega(\eta' \to \eta)P(\eta', t) + \Omega(\eta \to \eta')P(\eta, t), \tag{3.32}$$

which taking the limit of $\Delta t \to 0$ yields

$$\frac{\partial P(\eta, t)}{\partial t} = \sum_{\eta'}\Omega(\eta' \to \eta)P(\eta', t) - \Omega(\eta \to \eta')P(\eta, t). \tag{3.33}$$

This is the master equation, which we derived without making any approximation. In fact, the master equation gives the exact and deterministic evolution of the probability of finding the system at a given configuration η. However, obtaining the solution to such an equation is very hard and very often even impossible. The next chapter will focus on approximations we can do to further explore the system.

For our specific dynamics of interest. We can obtain the Master equation by replacing (3.15), (3.21), and (3.26) for the global transition rates into (3.33). For

convenience, we scale $\beta \to 2\beta$ and $\gamma \to 2\gamma$ and map the positions to their lattice site counterparts $x \mapsto i$.

$$\begin{aligned}\frac{\partial P(\eta,t)}{\partial t} &= b\sum_i (n_i-1)P\left(\{n_i-1\}_\eta,t\right) - n_i P(\eta,t)\\ &+d\sum_i (n_i+1)P\left(\{n_i+1\}_\eta,t\right) - n_i P(\eta,t)\\ &+\frac{\beta}{2R_f}\sum_i (n_i-1)(N_i^f-2)P\left(\{n_i-1\}_\eta,t\right) - n_i(N_i^f-1)P(\eta,t)\\ &+\frac{\gamma}{4R_c^2}\sum_i (n_i+1)N_i^c(N_i^c-1)P\left(\{n_i+1\}_\eta,t\right) - n_i(N_i^c-1)(N_i^c-2)P\left(\eta,t\right)\\ &+h\sum_{\langle ij\rangle}(n_i+1)P\left(\{n_i+1,\, n_j-1\}_\eta,t\right) - n_i P(\eta,t). \end{aligned} \tag{3.34}$$

The notation $\langle ij\rangle$ specifies that the sum is performed over the nearest neighbors of i.

3.4 Numerical simulation

The master equation is a very powerful but hard to manipulate and analyze tool. An alternative approach is to numerically simulate the sequence of stochastic reactions to generate multiple realizations of the population dynamics. In the following, we will refer to each of these realizations as a model trajectory. By generating several trajectories of the system, we can estimate the probabilities of observing each configuration throughout the time evolution. Also, every single trajectory allows us to quantify the emergent properties of the system. In this section, we will present the Gillespie algorithm [98, 99], used to simulate stochastic processes with constant reaction rates. Furthermore, we'll generate trajectories and explore the model results.

3.4.1 Gillespie algorithm

The Gillespie algorithm is a widely used and efficient method to generate realizations of a stochastic process [98, 99]. Starting from a given lattice configuration, the time evolution of the system follows two main steps. First, we sample the time it takes for the next reaction to happen, i.e. the waiting time τ. This time interval is a random variable, and consequently, it is associated with a probability

distribution. In Section 3.2 we derived the probability that no reaction happens after a time interval T, as a special case of equation (3.12).

$$P(0,T) = \exp\left(-\Omega_{\eta}^{\text{OUT}} T\right), \tag{3.35}$$

where

$$\Omega_{\eta}^{\text{OUT}} = \sum_{\eta'} \Omega(\eta \to \eta') \tag{3.36}$$

is the sum of all possible global transition rates that go away from η, i.e. the total exit rate. We can interpret equation (3.35) as the probability that the time interval T is larger than the waiting time τ. Therefore, given the probability distribution for waiting time $p(\tau)$, we can write the relation

$$P(0,T) = \int_{T}^{\infty} p(\tau) dt. \tag{3.37}$$

From the fundamental theorem o calculus, we can write

$$p(t) = -\frac{dP(0,t)}{dt} = \Omega_{\eta}^{\text{OUT}} \exp\left(-\Omega_{\eta}^{\text{OUT}} \tau\right), \tag{3.38}$$

which is an exponential distribution with mean $1/\Omega_{\eta}^{\text{OUT}}$ [97].

The second step of the algorithm is to sample which reaction takes place based on how each of them contributes to the total rate. The probability that the system will experience a transition $\eta \to \eta'$ given that a random reaction occurred is

$$P(\eta \to \eta') = \frac{\Omega(\eta \to \eta')}{\Omega_{\eta}^{\text{OUT}}}. \tag{3.39}$$

That is, the probability of a transition $\eta \to \eta'$ to occur given a reaction, $P(\eta \to \eta')$, is equal to how much of the total transition rates this reaction comprises. [97]. We can then express the Gillespie algorithm as:

1. At the beginning of the simulation, choose an initial condition for the number of individuals in each lattice node.

2. Compute all the possible global transition rates $\Omega(\eta \to \eta')$ from the current configuration, η, to any other possible configuration η' and calculate $\Omega_{\eta}^{\text{OUT}}$

3. Sample the waiting time τ, from an exponential distribution with mean equal to $1/\Omega_{\eta}^{\text{OUT}}$.

4. Sample which of the possible transitions $\eta \rightarrow \eta'$ will take place out of the distribution $P(\eta \rightarrow \eta')$.

5. Update the time and the configuration of the population to the new sampled values: $t \rightarrow t + \tau$ and $\eta \rightarrow \eta'$.

6. Repeat steps 2 to 5 until the desired simulation time is reached.

3.4.2 Model simulation

With the Gillespie algorithm in hand, we perform numerical simulations of our model, summarized by the set of reactions (3.1)-(3.4). For now, we want to explore qualitatively the properties of the emergent population dynamics that results from the individual-level reactions. Our simulations start from a spatially uniform initial condition and all the replicas for a given model parameterization use the same initial condition. Regarding the model parameterization, we fix all the rates of the individual-level reactions except the movement rate, h. By changing the movement of the individuals for different simulations we will allow for distinct spatial organizations to emerge. Since we are not changing any of the demographic birth/death rates, by comparing those simulations we can see how an emerging spatial organization alone affects some of the properties of the population dynamics. In Figure 3.2 we show some representative model realizations for different values of the movement rate h.

For high diffusion, i.e. high values of h, the population reaches a steady state with a uniform spatial distribution of organisms (Fig. 3.2a, b). Therefore, the overall dynamics becomes spatially independent. In fact, the average population in the steady state can be predicted by the non-spatial model presented in equation (2.1), black dashed line in Figure 3.2g. In the next chapter, we will show how this high-diffusion scenario results in that non-spatial model. As diffusion decreases, however, individuals start to aggregate and the population develops a spatial pattern characterized by isolated clumps of organisms interspersed with unpopulated regions (Fig. 3.2c-f). Surprisingly, the total population size increases in the stationary state due to aggregation (Fig. 3.2g). By organizing the population into seemingly isolated groups, the system is able to host more individuals. Smaller diffusion results in more segregated groups, which greatly affects the population in the stationary state (Fig. 3.2c-f). This result indicates that when individuals are more constrained within their groups, the system's carrying capacity increases.

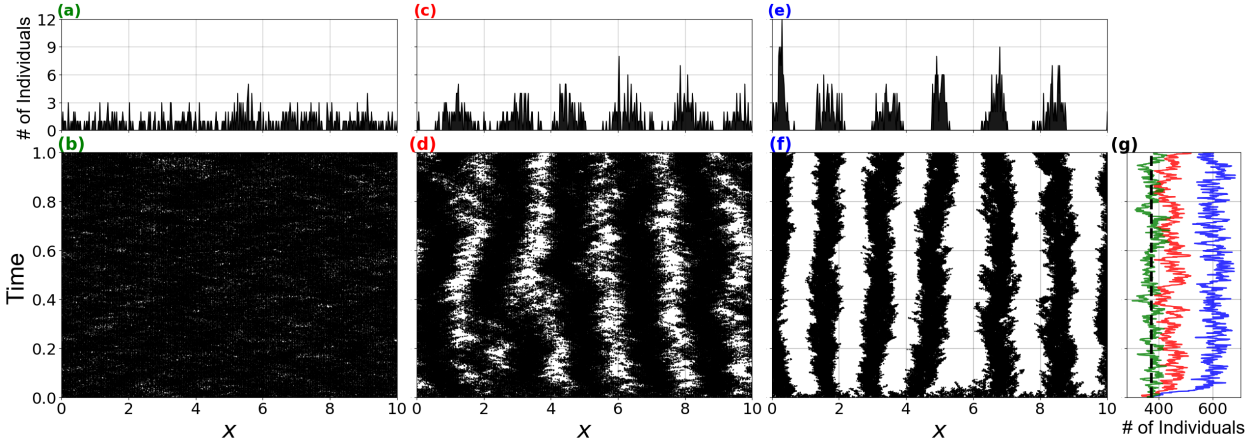

Figure 3.2: Emergence of spatial patterns for different diffusion regimes. Spatial distribution of individuals resulting from the individual-based stochastic model for (a-b, $D = 0.08$), intermediate (c-d, $D = 1.2$), and high diffusion (e-f, $D = 8$). Top panels (a, c, e) show the number of individuals at each lattice node at the end of a single simulation run. Bottom panels (b, d, f) show the temporal dynamics of the spatial distribution of individuals. The leftmost panel (g) shows the dynamics of population size at high (green), intermediate (red), and low (blue) diffusion together with the prediction from the non-spatial model (black-dashed line), (2.1). Bottom panels (b, d, f, g) share the same time scale in the vertical axis and top panels share the same x axis as their bottom counterparts. Other parameter values for all panels: $b = 30$, $d = 40$, $\beta = 4$, $\gamma = 0.1$, $L = 10$, $R_f = 0.75$ and $R_c = 1$, $\delta x = 0.02$; uniform initial condition.

Moreover, Figure 3.2 shows that the model is in fact able to somehow capture benefits from aggregation, although they are not fully explained yet. Unfortunately, generating the trajectories for the model is very computationally expensive, which greatly limits our exploration power. As mentioned before, the master equation itself is also very difficult to deal with. In the next chapter, we will use a field theoretical approach to further explore the system. This yields a population-level description based on an equation for the density of individuals. With those tools, we will be able to predict the steady-state population size and some of the properties of the emergent spatial patterns.

Chapter 4

Population scale

Up until this point, our description focused on how individuals are born, die and move. From this chapter on, we will shift this perspective to describe how a *population* changes. This might seem redundant since changes in the population are the direct result of demographic processes at the level of the individual. However, there are some practical and conceptual differences between both perspectives.

Firstly, by losing track of each individual process we can write how a population changes some of the properties of the underlying individual-level reactions. We have already started to set the stage for this connection by writing a master equation focusing on a configuration η, rather than tracking each individual closely. At the population scale, it does not matter which individual dies or reproduces, but where the event happened and what is the outcome locally. Also, different individual-level processes can contribute similarly to population dynamics and be merged into a single term when adopting a population-level description of the demographic processes. For instance, density-independent birth and death can be combined as a density-independent growth rate, whose sign dictates whether the population will grow or decline

In order to do this shift from an individual to a population description, we will abandon the stochastic aspect of our model. Instead, we will focus on the average population size. We will therefore use the individual-level stochastic processes to derive a mean-field deterministic description of the population, hence the population scale. The outcome of this process is a partial differential equation that describes the dynamics of a continuous population density field, in which we can use a variety of methods to further understand the properties of our model. On the downside, by abandoning the stochastic aspect of the model, we lose the effect of fluctuations on the overall dynamics. Therefore, we will always be coming back to the stochastic model to check whether any qualitative result is being neglected by the deterministic population model.

In the following sections, we detail the steps to obtain a deterministic equa-

tion for the dynamics of the density of individuals starting from the stochastic individual-level reactions. We apply the Doi-Peliti formalism, which is a field-theoretical approach, developed in the context of statistical field theory, that uses path integrals to map an individual-level stochastic dynamics to a continuum description in terms of a density field [100, 101, 102, 103]. Following the derivation of such an equation, we will use pattern formation theory to further understand the causes and consequences of the spatial structures obtained through numerical simulations in the previous chapter.

4.1 State space

Our system is composed of a set of indistinguishable individuals scattered in a lattice. For now, let's focus on a single isolated lattice site to present how the demographic component of our model can be mapped to the Doi-Peliti formalism. The only factor that determines the *state* of this system is the number of particles in it. Of course, the lower bound for the number of particles is zero and from now on we will refer to it as the vacuum state.

In order to formalize mathematically our concept of state, we can define a Fock space. The elements of a Fock space are state vectors that represent all of the possible states that the system can be in. For instance, if the system has n particles, its state can be represented by the state vector $|n\rangle$, in the Dirac notation. $|n\rangle$ is a basis vector, which means that it represents an observable configuration of the system, a basis state. More complicated states can be constructed if we consider the probabilities of observing the system in each of those basis states. We can write a general state of the system as a linear combination of the basis states weighted by the probability of observing them $P(n)$,

$$|\psi(t)\rangle = \sum_n P(n,t)\ |n\rangle\,. \tag{4.1}$$

Therefore, by understanding how to work with the basis states, we learn how to deal with more complicated ones.

4.1.1 Basis states

The most fundamental basis state is the vacuum state, representing the system without any organism. The vacuum state vector $|0\rangle$ is defined in a way that satisfies $\langle 0 \,|\, 0\rangle \equiv 1$, which is the inner product between two vacuum state vectors. The number of individuals in the system is constantly subjected to changes as the dynamics goes on. Thus we need to introduce a way for the states to be altered. This is performed by the bosonic operators of creation and annihilation of organisms, $a^\dagger$ and a respectively. Those operators act on the basis state vector following:

$$a^\dagger |n\rangle = |n+1\rangle \,, \tag{4.2}$$

$$a |n\rangle = n \,|n-1\rangle \,, \tag{4.3}$$

together with the condition $a |0\rangle = 0$ that forbides states with a negative number of particles. The $a^\dagger$ is the Hermitian conjugate of a, thus we have the following relations with the conjugate vectors

$$\langle n| \, a^\dagger = n \, \langle n-1| \,, \tag{4.4}$$

$$\langle n| \, a = \langle n+1| \,. \tag{4.5}$$

Acting those operators on basis states causes the number of individuals to change. Thus, we can use the creation operator $a^\dagger$ alongside with the vacuum state $|0\rangle$ to represent any basis state with n individuals:

$$|n\rangle = \left(a^\dagger\right)^n |0\rangle \,. \tag{4.6}$$

Since the population size is the only important quantity in a site, any operation able to change the state of a site can be represented as a composition of these creation and annihilation operators. In order to work with them, we can obtain their commutation relation, given by

$$\left[a, a^\dagger\right] \Rightarrow \left\langle n \left| a\, a^\dagger \right| n \right\rangle - \left\langle n \left| a^\dagger a \right| n \right\rangle \tag{4.7}$$

$$\langle n \mid n+1 \mid n \rangle - \langle n \mid n \mid n \rangle \tag{4.8}$$

$$\langle n \mid n \rangle \tag{4.9}$$

$$\left[a, a^\dagger\right] = 1. \tag{4.10}$$

A direct result from this relation is the projection of one basis vector into another, i.e. the inner product.

$$\langle n|m\rangle = \langle 0|\, a^n \left(a^\dagger\right)^m |0\rangle = \langle n-1|\, a^\dagger a\, |m-1\rangle + \langle n-1|m-1\rangle = m\, \langle n-1|m-1\rangle\,. \tag{4.11}$$

This is a recurrent relation, thus we can go to $m = 1$,

$$\langle n|1\rangle = \langle n-1|0\rangle \tag{4.12}$$

if $n = m = 1$, we go back to the identity $\langle 0|0\rangle = 1$. If $n \neq 1$ (i.e. $n \neq m$),

$$\langle n|1\rangle = \langle 0|\, a^{n-1}\, |0\rangle = 0. \tag{4.13}$$

Thus, because (4.13) is a recurrent relation, the projection is zero for all $n \neq m$. Therefore, applying the relation from $\langle 1|1\rangle$ to an $\langle n|n\rangle$ arbitrary projection, we have

$$\langle n|m\rangle = n!\, \delta_{n,m}. \tag{4.14}$$

Of course, we need to have a way to, from a state, obtain useful quantities, such as population size. To do this, we define the number operator $\hat{n} = a^\dagger a$, whose eigenvectors are the basis vectors and the eigenvalues are their corresponding population sizes

$$\hat{n} \left| n \right\rangle = n \left| n \right\rangle . \tag{4.15}$$

4.1.2 Introducing space

Once we have formalized a way to describe changes in the number of organisms within one isolated lattice node, we want to zoom out of a single site and look at the whole lattice. In this subsection, we generalize the formalism above to encompass space. Now, the state of the system is a composition of the state of all of lattice sites. Thus, a possible configuration η of the system can be described by the states of each individual lattice site. Mathematically, this composite state can be written as the tensor product of the states of each lattice node,

$$\left| \eta \right\rangle = \ldots \left| n_i \right\rangle \otimes \left| n_j \right\rangle \otimes \left| n_k \right\rangle \otimes \ldots \tag{4.16}$$

Also, the vacuum state is now defined when there is no particle in the entire system

$$\left| \mathbf{0} \right\rangle = \left| 0 \right\rangle \otimes \left| 0 \right\rangle \otimes \left| 0 \right\rangle \otimes \ldots \tag{4.17}$$

We can also generalize all the definitions we introduced for the single-node case to the general scenario in which we consider the whole lattice. First, Starting from the bosonic operators

$$a_i^\dagger \left| n_i \right\rangle = \left| n_i + 1 \right\rangle , \tag{4.18}$$

$$a_i \left| n_i \right\rangle = n_i \left| n_i - 1 \right\rangle , \tag{4.19}$$

and

$$\left\langle n_i \right| a_i^\dagger = n_i \left\langle n_i - 1 \right| , \tag{4.20}$$

$$\left\langle n_i \right| a_i = \left\langle n_i + 1 \right| , \tag{4.21}$$

whereby the indexes i refer to a specific site. We can also generalize the orthogonality condition for the vectors (4.14),

$$\langle n_i | m_j \rangle = n_i!\, \delta_{n_i,m_i} \delta_{i,j}. \tag{4.22}$$

Therefore, the creation and annihilation operators act on specific lattice nodes on the lattice. The commutation relation is then generalized to

$$\left[a_i, a_j^\dagger\right] = a_i a_j^\dagger - a_j^\dagger a_i = \delta_{ij}, \tag{4.23}$$

$$\left[a_i^\dagger, a_j^\dagger\right] = \left[a_i, a_j\right] = 0. \tag{4.24}$$

We can additionally construct the basis vector from the vacuum state using the creation and annihilation operators as

$$|\eta\rangle = |n_i, n_j, \ldots\rangle = \left(a_i^\dagger\right)^{n_i} \left(a_j^\dagger\right)^{n_j} \ldots |\mathbf{0}\rangle = \prod_k \left(a_k^\dagger\right)^{n_k} |\mathbf{0}\rangle \tag{4.25}$$

with projections

$$\langle \eta' | \, \eta \rangle = \delta_{\eta,\eta'} \prod_{n_k} n_k! \tag{4.26}$$

Also, the number operator is now defined as $\hat{n}_k = a_k^\dagger a_k$and its eigenvalues are the number of individuals at site k

$$\hat{n}_k \, |\ldots, n_k, n_{k+1}, \ldots\rangle = n_k \, |\ldots, n_k, n_{k+1}, \ldots\rangle \, . \tag{4.27}$$

Finally, a general state of the lattice can be constructed by considering the probabilities of observing the system at each configuration $\{\eta\}$. The state vector $|\psi(t)\rangle$ is represented as

$$|\psi(t)\rangle = \sum_\eta P(\eta, t) \; |\eta\rangle \, . \tag{4.28}$$

4.2 Quasi-Hamiltonian

Now that we know how to describe a general state in the lattice (4.28), we will focus on how this state can change through time. That is, we will derive the dynamical equation for the state vectors, which, at least formally, we can obtain by applying a time derivative on equation (4.28):

$$\frac{\partial}{\partial t}\left|\psi(t)\right\rangle = \sum_{\eta} \frac{\partial}{\partial t} P(\eta, t)\ \left|\eta\right\rangle . \tag{4.29}$$

We observe that the time evolution of the state is determined by the dynamics of the probabilities of finding the state in each configuration η. The equation that describes the dynamics of these probabilities is the master equation, derived in the previous chapter 3.3.1, equation (3.34). Inserting the Master equation in (4.29) we obtain an explicit expression for the dynamics of the state vector (4.29). Although equation (4.29) seems to be a more complicated version of the master equation, this expression resembles the Schrodinger equation, which dictates the time evolution of a quantum state [104]. The main aspect regarding the Schrodinger equation is the presence of a Hamiltonian, which is an operator that, when applied to any state, gives the time derivative of such state, apart from a multiplying constant. Writing equation (4.29) like a Schrodinger equation allows us to follow similar steps from quantum mechanics and develop a field theory for our discrete, individual-based model [105]. Therefore, we want to rearrange equation (4.29) into a Schrodinger-like equation, given by

$$\frac{\partial}{\partial t}\left|\psi(t)\right\rangle = -\hat{H}\left|\psi(t)\right\rangle . \tag{4.30}$$

With formal solution:

$$\left|\psi(t)\right\rangle = e^{-\hat{H}t}\left|\psi(0)\right\rangle . \tag{4.31}$$

Here, $\hat{H}$ is the quasi-Hamiltonian operator, which is a function of the creation and annihilation operators. The purpose of the present section is to obtain the explicit form of this quasi-Hamiltonian operator. Since the master equation is fairly big, we will work with it bit by bit. We associate each term of the master equa-

tion to a quasi-Hamiltonian operator: density-independent birth $\hat{H}_b$, density-independent death $\}hat H_d$, facilitation $\hat{H}_\beta$, competition $\hat{H}_\gamma$ and movement $\hat{H}_h$. The total quasi-hamiltonian is given by the sum of all these terms:

$$\hat{H} = \hat{H}_b + \hat{H}_d + \hat{H}_\beta + \hat{H}_\gamma + \hat{H}_h. \tag{4.32}$$

4.2.1 Density-independent birth, $\hat{H}_b$

Here, we want to express the density-independent birth process term of (4.29). By directly inserting the density-independent birth terms of (3.34) in (4.29) we have

$$\hat{H}_b \left|\psi(t)\right\rangle = -b \sum_\eta \sum_i \left[(n_i - 1) P\left(\{n_i - 1\}_\eta, t\right) - n_i P(\eta, t) \right] \left|\eta\right\rangle, \tag{4.33}$$

$$= -b \sum_\eta \sum_i \left[P\left(\{n_i - 1\}_\eta, t\right)\ (n_i - 1) \left|\eta\right\rangle - P(\eta, t)\, n_i \left|\eta\right\rangle \right], \tag{4.34}$$

$$= -b \sum_\eta \sum_i \left[P\left(\{n_i - 1\}_\eta, t\right)\ a_i^\dagger a_i^\dagger a_i \left|\{n_i - 1\}_\eta\right\rangle - P(\eta, t)\, a_i^\dagger a_i \left|\eta\right\rangle \right]. \tag{4.35}$$

Now, let's focus in the $\{n_i - 1\}$ term

$$\sum_\eta \sum_i P\left(\{n_i - 1\}_\eta, t\right)\ a_i^\dagger a_i^\dagger a_i \left|\{n_i - 1\}_\eta\right\rangle = \tag{4.36}$$

$$= \sum_{n_1} \sum_{n_2} \cdots \sum_{n_i} \cdots \sum_i P\left(\{n_i - 1\}_\eta, t\right)\ a_i^\dagger a_i^\dagger a_i \left|\{n_i - 1\}_\eta\right\rangle. \tag{4.37}$$

Where we rewrite the sum over all configurations as the sum of all possible occupations of the lattice, i.e. $\sum_\eta = \sum_{n_1} \sum_{n_2} \ldots$.By doing a shift $n_i \to n_i + 1$, and leaving all sums besides the one in n_i aside for a moment, we have

$$\sum_{n_i = -1} P\left(\{n_i\}_\eta, t\right)\ a_i^\dagger a_i^\dagger a_i \left|\{n_i\}_\eta\right\rangle = \sum_{n_i = 0} P\left(\{n_i\}_\eta, t\right)\ a_i^\dagger a_i^\dagger a_i \left|\{n_i\}_\eta\right\rangle, \tag{4.38}$$

since the state $|-1\rangle$ is impossible and, thus, has probability 0. This same reasoning and indexes operations will also be used to obtain all of the other quasi-Hamiltonian expressions throughout this section. Finally, the density-independent birth quasi-Hamiltonian becomes

$$\hat{H}_b |\psi(t)\rangle = b \sum_{\eta} \sum_{i} \left(\mathbb{I} - a_i^\dagger \right) a_i^\dagger a_i P(\eta, t) |\eta\rangle \tag{4.39}$$

$$= b \sum_{i} \left(\mathbb{I} - a_i^\dagger \right) a_i^\dagger a_i |\psi(t)\rangle , \tag{4.40}$$

with $\mathbb{I}$ being the identity operator.

4.2.2 Density-independent death, $\hat{H}_d$

Now, we want to express the density-independent death process term of (4.29). By directly inserting the terms from density-independent death of (3.34) in (4.29) we have

$$\hat{H}_d |\psi(t)\rangle = -d \sum_{\eta} \sum_{i} \left[(n_i + 1) P\left(\{n_i + 1\}_\eta, t \right) - n_i P(\eta, t) \right] |\eta\rangle \tag{4.41}$$

$$= -d \sum_{\eta} \sum_{i} \left[P\left(\{n_i + 1\}_\eta, t \right) \ (n_i + 1) |\eta\rangle - P(\eta, t)\, n_i |\eta\rangle \right] \tag{4.42}$$

$$= -d \sum_{\eta} \sum_{i} \left[P\left(\{n_i + 1\}_\eta, t \right) \ a_i |\{n_i + 1\}_\eta\rangle - P(\eta, t)\, a_i^\dagger a_i |\eta\rangle \right] \tag{4.43}$$

$$= d \sum_{\eta} \sum_{i} P(\eta, t) \left(a_i^\dagger - \mathbb{I} \right) a_i |\eta\rangle \tag{4.44}$$

$$= d \sum_{i} \left(a_i^\dagger - \mathbb{I} \right) a_i |\psi(t)\rangle . \tag{4.45}$$

4.2.3 Facilitation, $\hat{H}_\beta$

Here, we want to express the long-range facilitation process term of (4.29). By directly inserting the terms regarding the facilitation reaction of (3.34) in (4.29) we have

$$\hat{H}_\beta |\psi(t)\rangle = -\frac{\beta}{2R_f} \sum_\eta \sum_i \left[(n_i - 1)(N_i^f - 2) P\left(\{n_i - 1\}_\eta, t\right) - n_i (N_i^f - 1) P(\eta, t) \right] |\eta\rangle \tag{4.46}$$

$$= -\frac{\beta}{2R_f} \sum_\eta \sum_i \Bigg[P\left(\{n_i - 1\}_\eta, t\right) (n_i - 1)(N_i^f - 2) |\eta\rangle -$$

$$- P(\eta, t) n_i (N_i^f - 1) |\eta\rangle \Bigg], \tag{4.47}$$

$$= -\frac{\beta}{2R_f} \sum_\eta \sum_i \Bigg[P\left(\{n_i - 1\}_\eta, t\right) a_i^\dagger \left[\sum_{j \in R_f(i)} a_j^\dagger a_j \right] a_i |\{n_i + 1\}_\eta\rangle -$$

$$- P(\eta, t) a_i^\dagger \left[\sum_{j \in R_f(i)} a_j^\dagger a_j \right] a_i |\eta\rangle \Bigg], \tag{4.48}$$

$$= \frac{\beta}{2R_f} \sum_\eta \sum_i P(\eta, t) \left(\mathbb{I} - a_i^\dagger \right) \left[\sum_{j \in R_f(i)} a_j^\dagger a_j \right] a_i |\eta\rangle, \tag{4.49}$$

$$= \frac{\beta}{2R_f} \sum_i \left(\mathbb{I} - a_i^\dagger \right) \left[\sum_{j \in R_f(i)} a_j^\dagger a_j \right] a_i |\psi(t)\rangle, \tag{4.50}$$

with the $\sum_{j \in R_f(i)}$ representing the sum over all indexes within the range of facilitation R_f centered in the site i.

4.2.4 Competition, $\hat{H}_\gamma$

The expression for the term of (4.29) related to the long-range competition process is derived here. By directly inserting the terms regarding the competition reactions of (3.34) in (4.29) we have

$$\hat{H}_\gamma |\psi(t)\rangle = -\frac{\gamma}{4R_c^2} \sum_\eta \sum_i \Bigg[(n_i + 1) N_i^c (N_i^c - 1) P\left(\{n_i + 1\}_\eta, t\right) -$$

$$- n_i (N_i^c - 1)(N_i^c - 2) P(\eta, t) \Bigg] |\eta\rangle \tag{4.51}$$

$$= -\frac{\gamma}{4R_c^2}\sum_{\eta}\sum_{i}\Bigg[P\left(\{n_i+1\}_\eta,t\right)(n_i+1)N_i^c(N_i^c-1)\,|\eta\rangle - \tag{4.52}$$

$$- P(\eta,t)n_i(N_i^c-1)(N_i^c-2)\,|\eta\rangle\Bigg], \tag{4.53}$$

$$= -\frac{\gamma}{4R_c^2}\sum_{\eta}\sum_{i}\Bigg[P\left(\{n_i+1\}_\eta,t\right)\Bigg[\sum_{j,k\in R_c(i)} a_j^\dagger a_k^\dagger a_k a_j\Bigg]\,a_i\,|\{n_i+1\}_\eta\rangle - \tag{4.54}$$

$$- P(\eta,t)a_i^\dagger\Bigg[\sum_{j,k\in R_c(i)} a_j^\dagger a_k^\dagger a_k a_j\Bigg]\,a_i\,|\eta\rangle\Bigg], \tag{4.55}$$

$$= \frac{\gamma}{4R_c^2}\sum_{\eta}\sum_{i}P(\eta,t)\left(\mathbb{I}-a_i^\dagger\right)\Bigg[\sum_{j,k\in R_c(i)} a_j^\dagger a_k^\dagger a_k a_j\Bigg]\,a_i\,|\eta\rangle\,, \tag{4.56}$$

$$= \frac{\gamma}{4R_c^2}\sum_{i}\left(\mathbb{I}-a_i^\dagger\right)\Bigg[\sum_{j,k\in R_c(i)} a_j^\dagger a_k^\dagger a_k a_j\Bigg]\,a_i\,|\psi(t)\rangle\,, \tag{4.57}$$

with $\sum_{j,k\in R_c(i)} = \sum_{j\in R_c(i)}\sum_{k\in R_c(i)}$.

4.2.5 Movement, $\hat{H}_h$

And finally, we want to express the random walk process term of (4.29). By directly inserting (3.34) in (4.29) we have

$$\hat{H}_h\,|\psi(t)\rangle = -h\sum_{\eta}\sum_{\langle ij\rangle}\Bigg[(n_i+1)P\left(\{n_j-1,\,n_i+1\}_\eta,t\right) - n_iP(\eta,t)\Bigg]\,|\eta\rangle\,. \tag{4.58}$$

Considering that we have an infinite lattice (or periodic boundary conditions), we can write

$$\hat{H}_{i\to j} = h\sum_{\langle ij\rangle}(n_i+1)P\left(\{n_j-1,\,n_i+1\}_\eta,t\right) - n_iP(\eta,t), \tag{4.59}$$

$$\hat{H}_{j\to i} = h\sum_{\langle ij\rangle}(n_j+1)P\left(\{n_j+1,\,n_i-1\}_\eta,t\right) - n_jP(\eta,t), \tag{4.60}$$

such that $\hat{H}_{i\to j} = \hat{H}_{j\to i}$. Thus, we can write

$$\hat{H}_h \left|\psi(t)\right\rangle = \frac{1}{2}\Big[\hat{H}_{i\to j}\left|\psi(t)\right\rangle + \hat{H}_{j\to i}\left|\psi(t)\right\rangle\Big]. \tag{4.61}$$

This choice might seem to be complicating things, but it will be useful in a moment. For the first term:

$$\hat{H}_{i\to j}\left|\psi(t)\right\rangle = -\frac{h}{2}\sum_{\eta}\sum_{\langle ij\rangle}\Big[(n_i+1)P\left(\{n_j-1,\, n_i+1\}_\eta, t\right) - n_i P(\eta,t)\Big]\left|\eta\right\rangle, \tag{4.62}$$

$$= -\frac{h}{2}\sum_{\eta}\sum_{\langle ij\rangle}\Big[P\left(\{n_j-1,\, n_i+1\}_\eta, t\right)(n_i+1)\left|\eta\right\rangle - P(\eta,t)n_i\left|\eta\right\rangle\Big], \tag{4.63}$$

$$= -\frac{h}{2}\sum_{\eta}\sum_{\langle ij\rangle}\Big[P\left(\{n_j-1,\, n_i+1\}_\eta, t\right)a_i^\dagger a_j\left|\{n_j-1,\, n_i+1\}_\eta\right\rangle - \tag{4.64}$$

$$- P(\eta,t)a_i^\dagger a_i\left|\eta\right\rangle\Big], \tag{4.65}$$

$$= \frac{h}{2}\sum_{\eta}\sum_{\langle ij\rangle}P(\eta,t)\,a_i^\dagger\left(a_i - a_j\right)\left|\eta\right\rangle, \tag{4.66}$$

$$= \frac{h}{2}\sum_{\langle ij\rangle}a_i^\dagger\left(a_i - a_j\right)\left|\psi(t)\right\rangle. \tag{4.67}$$

The second term, $\hat{H}_{j\to i}\left|\psi(t)\right\rangle$, can be obtained by the exact same math and has the result:

$$\hat{H}_{j\to i}\left|\psi(t)\right\rangle = \frac{h}{2}\sum_{\langle ij\rangle}a_j^\dagger\left(a_j - a_i\right)\left|\psi(t)\right\rangle. \tag{4.68}$$

Finally, we have:

$$\hat{H}_h\left|\psi(t)\right\rangle = \frac{1}{2}\Big[H_{i\to j}\left|\psi(t)\right\rangle + H_{j\to i}\left|\psi(t)\right\rangle\Big] = \frac{h}{2}\sum_{\langle ij\rangle}\left(a_i^\dagger - a_j^\dagger\right)\left(a_i - a_j\right)\left|\psi(t)\right\rangle. \tag{4.69}$$

4.2.6 The total quasi-Hamiltonian

Finally, we can join all of the previous sub-section results to write the expression for the total quasi-Hamiltonian operator. Also, it is useful to define a local quasi-hamiltonian $\mathcal{H}_i$, given by $\hat{H}(\{a^\dagger, a\}) = \sum_i \mathcal{H}_i(\{a^\dagger, a\})$, such that we can focus on the dynamics of each lattice. The expression for this local quasi-Hamiltonian is

$$\mathcal{H}_i(\{a^\dagger, a\}) = b\left(\mathbb{I} - a_i^\dagger\right) a_i^\dagger a_i + d\left(a_i^\dagger - \mathbb{I}\right) a_i + \frac{\beta}{2R_f}\left(\mathbb{I} - a_i^\dagger\right) a_i^\dagger \sum_{j \in R_f(i)} \left\{a_j^\dagger a_j\right\} a_i \tag{4.70}$$

$$+ \frac{\gamma}{4R_c^2}\left(a_i^\dagger - \mathbb{I}\right) \sum_{j,k \in R_c(i)} \left\{a_j^\dagger a_k^\dagger a_k a_j\right\} a_i + \frac{h}{2} \sum_{\langle ij \rangle} \left(a_i^\dagger - a_j^\dagger\right)\left(a_i - a_j\right). \tag{4.71}$$

4.3 Expected values

Now that we have described how a state can be constructed and how it can evolve, we also want to obtain the expected values of the quantities we can observe from the system. Let's then consider an observable $A(\eta, t)$. The expected value of A is by definition

$$\langle A \rangle = \sum_\eta P(\eta, t) A(\eta, t). \tag{4.72}$$

By applying $A(\eta, t)$ on $|\psi(t)\rangle$ we get to a very similar expression

$$A(\eta, t)\,|\psi(t)\rangle = \sum_\eta P(\eta, t)\, A(\eta, t)\; |\eta\rangle\,. \tag{4.73}$$

Thus, to reduce (4.73) to (4.72) we need to get rid of the basis vector $|\eta\rangle$. To do this we need a vector that projects to unity with all basis vectors. We construct this vector from the relation of projection between the basis vectors (4.26),

$$\langle \text{☼} | = \sum_{\eta'} \prod_{n_i} \frac{1}{n_i!} \langle \eta' | , \tag{4.74}$$

whereby n_i represents the occupation per site in the configuration η. We call $\langle \text{☼} |$ the abyss. As can be seen directly from the definition of the abyss (4.74), the projection of any basis $|\eta\rangle$ into the abyss is always equal to 1

$$\langle \text{☼} | \eta \rangle = 1. \tag{4.75}$$

Applying this relation on (4.73):

$$\langle \text{☼} | A(\eta, t) | \psi(t) \rangle = \sum_{\eta} P(\eta, t) A(\eta, t) \langle \text{☼} | \eta \rangle = \sum_{\eta} P(\eta, t) A(\eta, t) = \langle A \rangle. \tag{4.76}$$

We might want to express $\langle \text{☼} |$ in a more elegant way. To do this, let's drop the lattice for a bit and go back to the spatialy implicit notation. We can use the vacuum state to rewrite the basis vectors in the abyss :

$$\langle \text{☼} | = \sum_{n} \frac{1}{n!} \langle n | = \sum_{n} \langle 0 | \frac{a^n}{n!} = \langle 0 | e^a. \tag{4.77}$$

Also from the definition of the abyss (4.74), we can derive a very important expression relating the abyss with the creation operator

$$\langle \text{☼} | a^\dagger = \sum_{n=0}^{\infty} \frac{1}{n!} \langle n | a^\dagger = \sum_{n=1}^{\infty} \frac{1}{(n-1)!} \langle n - 1 | = \langle \text{☼} |. \tag{4.78}$$

Thus, the abyss is invariant under the creation operator from the right. This relation comes from an important identity

$$e^a f\left(a^\dagger\right) = f\left(a^\dagger + \mathbb{I}\right) e^a. \tag{4.79}$$

Now, we can go back to the lattice to generalize the abyss operator

$$\langle ☼| = \langle 0| \prod_j e^{a_j} = \langle 0| e^{\sum_j a_j}, \tag{4.80}$$

which leads to

$$\langle A \rangle = \langle ☼| A(\eta) |\psi(t)\rangle = \langle 0| \prod_j e^{a_j} A\left(\left\{a_i^\dagger, a_i\right\}\right) e^{-H\left(\left\{a_i^\dagger, a_i\right\}\right)t} |\psi(0)\rangle. \tag{4.81}$$

We can further simplify Eq. (4.81) using the definition of the mean value of an operator A and the identity (4.79). This simplification consists of shifting the operators with e^{a_j} using the identity, resulting in

$$\langle A \rangle = \langle ☼| A(\eta) |\psi(t)\rangle = \langle 0| A\left(\left\{a_i^\dagger + \mathbb{I}, a_i\right\}\right) e^{-H\left(\left\{a_i^\dagger + \mathbb{I}, a_i\right\}\right)t} \prod_j e^{a_j} |\psi(0)\rangle. \tag{4.82}$$

To be able to compute the expected value of A using (4.82) we still need to define an initial state vector $|\psi(0)\rangle$. This vector is given by the probabilities of observing each possible system configuration eta at time 0. We define these probabilities assuming that the organisms are randomly distributed through the lattice nodes following a Poisson distribution. This choice gives probabilities of the form.

$$P(\eta, t = 0) = \prod_i \left(\frac{\langle n_0 \rangle^{n_i}}{n_i!} e^{-\langle n_0 \rangle} \right). \tag{4.83}$$

Thus, the initial state vector is given by

$$|\psi(t = 0)\rangle = \sum_\eta P(\eta, t = 0) |\eta\rangle = \sum_{\{n_i\}} \prod_i \left(\frac{\langle n_0 \rangle^{n_i}}{n_i!} e^{-\langle n_0 \rangle} \left(a_i^\dagger\right)^{n_i} \right) |0\rangle \tag{4.84}$$

$$= \prod_i e^{-\langle n_0 \rangle} e^{\langle n_0 \rangle a_i^\dagger} |0\rangle. \tag{4.85}$$

Substituting in (4.82):

$$\langle A \rangle = \langle 0 | \, A \left(\left\{ a_i^\dagger + \mathbb{I}, \, a_i \right\} \right) e^{-H\left(\left\{ a_i^\dagger + \mathbb{I}, a_i \right\} \right) t} \prod_j e^{a_j} e^{-\langle n_0 \rangle} e^{\langle n_0 \rangle a_j^\dagger} \, | 0 \rangle \, . \tag{4.86}$$

Shifting the exponential with the operator in the right:

$$\langle A \rangle = \langle 0 | \, A \left(\left\{ a_i^\dagger + \mathbb{I}, \, a_i \right\} \right) e^{-H\left(\left\{ a_i^\dagger + \mathbb{I}, a_i \right\} \right) t} \prod_j e^{-\langle n_0 \rangle} e^{\langle n_0 \rangle \left(a_j^\dagger + \mathbb{I} \right)} e^{a_j} \, | 0 \rangle \tag{4.87}$$

$$= \langle 0 | \, A \left(\left\{ a_i^\dagger + \mathbb{I}, \, a_i \right\} \right) e^{-H\left(\left\{ a_i^\dagger + \mathbb{I}, a_i \right\} \right) t} \prod_j e^{\langle n_0 \rangle a_j^\dagger} \, | 0 \rangle \, . \tag{4.88}$$

From (4.87) to (4.88) we used the relation

$$e^a \, | 0 \rangle = \left(1 + \sum_{n=1} \frac{a^n}{n!} \right) | 0 \rangle = | 0 \rangle \, . \tag{4.89}$$

To further simplify the expression, we define:

$$\tilde{f} \left(\left\{ a_i^\dagger, a_i \right\} \right) := f \left(\left\{ a_i^\dagger + \mathbb{I}, a_i \right\} \right) \tag{4.90}$$

as a Doi-shift. Thus:

$$\langle A \rangle = \langle 0 | \, \tilde{A} \left(\left\{ a_i^\dagger, \, a_i \right\} \right) e^{-\tilde{H}\left(\left\{ a_i^\dagger, a_i \right\} \right) t} \prod_j e^{\langle n_0 \rangle a_j^\dagger} \, | 0 \rangle \, . \tag{4.91}$$

This expression is useful because we are able to pull the operator A to the vacuum state on the left. Therefore, any creation operators that are in contact with $\langle 0 |$ will be set to zero, simplifying the expression. Because of this, it is useful to organize all of the $a^\dagger$ in A to the left, i.e. normal ordering. An easy example is the number operator $\hat{n}_i = a_i^\dagger a_i$. Substituting it on equation (4.91):

$$\langle n_i \rangle = \langle 0 | \left(a_i^\dagger + \mathbb{I} \right) a_i e^{-\tilde{H}\left(\left\{ a_i^\dagger, a_i \right\} \right) t} \prod_j e^{\langle n_0 \rangle a_j^\dagger} \, | 0 \rangle \tag{4.92}$$

$$= \langle 0 | \, a_i e^{-\tilde{H}\left(\left\{ a_i^\dagger, a_i \right\} \right) t} \prod_j e^{\langle n_0 \rangle a_j^\dagger} \, | 0 \rangle \, . \tag{4.93}$$

Thus, the creation operator vanishes from the expected value. In fact, any operator that is normal ordered has this property, where the identity follows:

$$\langle ☼ | A\left(\left\{a_i^\dagger, a_i\right\}\right) = \langle ☼ | A\left(\left\{a_i^\dagger \to \mathbb{I}, a_i\right\}\right). \tag{4.94}$$

This is why we have purposefully organized our quasi-Hamiltonian to be normal ordered (4.70). Actually, we check to see that:

$$H\left(\left\{a_i^\dagger \to \mathbb{I}, a_i\right\}\right) = 0. \tag{4.95}$$

That is not a specific property of our quasi-Hamiltonian. In fact, all quasi-Hamiltonian must satisfy equation (4.95). This can be seen by taking the projection of the abyss into the state vector:

$$1 = \langle ☼ | \psi(t)\rangle = \langle ☼ | e^{-\hat{H}t} | \psi(0)\rangle = \underbrace{\langle ☼ | \psi(0)\rangle}_{=1} - \langle ☼ | \hat{H}t | \psi(0)\rangle + \dots. \tag{4.96}$$

This is a direct consequence of the normalization condition, that is, the sum of all probabilities must always be equal 1. Since $\langle ☼ | \psi(0)\rangle = 1$, all the other terms in (4.96) must be zero.

4.4 Field theory

So far, the Doi-Peliti formalism has provided a representation of our stochastic process in a Fock space. However, to obtain a population-level deterministic description of our model, we need to use a field-theory approach. This yields a path integral representation of our model dynamics, which is detailed in Appendix A. To obtain this patch-integral representation, we introduce the fields $\phi_i(t)$ and $\phi_i^*(t)$ which are the coherent states of the annihilation and creation operators, respectivelly. The Hamiltonian then becomes $\mathcal{H}(a_i^\dagger \to \phi_i(t)^*, a_i \to \phi_i(t))$. Once we defined the quasi-Hamiltonian in terms of the fields, we take the continuum limit by letting the lattice spacing $\delta x \to 0$. To this end, we redefine the fields and

parameters as

$$\frac{\phi_i(t)}{\delta x} \mapsto \phi(x,t), \quad \phi_i^*(t) \mapsto \tilde{\phi}(x,t), \quad \frac{h}{2} \mapsto \frac{D}{\delta x^2}, \tag{4.97}$$

and the quasi-hamiltonian as $H\left(\phi^*(x,t), \phi(x,t)\right) = \int \mathcal{H}\left(\phi^*(x,t), \phi(x,t)\right) dx$. The main advantage of working in this field theory representation is that we can write the expected value of any observable as

$$\langle A \rangle = \langle 0 | \, \tilde{A}\left(\left\{a_i^\dagger, \, a_i\right\}\right) e^{-\tilde{H}\left(\left\{a_i^\dagger, a_i\right\}\right)t} \prod_j e^{\langle n_0 \rangle a_j^\dagger} \, |0\rangle \tag{4.98}$$

$$= \frac{1}{\mathcal{N}} \int \mathcal{D}\left[\tilde{\phi}(x,t)\right] \mathcal{D}[\phi(x,t)] A(\phi(x,t)) e^{-S[\tilde{\phi},\phi]}, \tag{4.99}$$

whereby, the action S is given by

$$S[\phi^*(x,t), \phi(x,t)] = \int dx \int_0^t d\tau \;\; \phi^* \partial_\tau \phi + \tilde{\mathcal{H}}[\tilde{\phi}(x,\tau), \phi(x,\tau)]. \tag{4.100}$$

The $\mathcal{D}\tilde{\phi}\mathcal{D}\phi$ represents $\prod_\tau \mathrm{d}\phi_{i,\tau}\mathrm{d}\phi_{i,\tau}^*$ in the limit $\delta t \to 0$. Also, we introduce the normalization factor $\mathcal{N} = \int \mathcal{D}\tilde{\phi}\mathcal{D}\phi \exp\left[-S\left(\{\tilde{\phi}\}, \{\phi\}\right)\right]$. The term $\tilde{\mathcal{H}}$ is the Doi-shifted hamiltonian $\tilde{\mathcal{H}}(\tilde{\phi} \to \tilde{\phi} + 1, \phi \to \phi)$. Also, the operator A is expressed in terms of the fields, $A\left(a_i^\dagger \to \mathbb{I}, \, a_i \to \phi\right)$.

Finally, we obtain the dynamic equation of the fields using the stationary-action principle or principle of least action, i.e. $\frac{\delta S}{\delta \phi} = \frac{\delta S}{\delta \tilde{\phi}} = 0$. By doing so, we obtain that the terms in the action that are linear in $\tilde{\phi}$ give the equation (see Appendix A),

$$\frac{\partial \phi(x,t)}{\partial t} = \left[b - d + \frac{\beta}{2R_f} \int_{x-R_f}^{x+R_f} \phi(x',t)dx' - \frac{\gamma}{4R_c^2} \left(\int_{x-R_c}^{x+R_c} \phi(x',t)dx' \right)^2 \right] \phi + D \, \nabla_x^2 \phi. \tag{4.101}$$

4.5 Mean-field approximation

We are just about to obtain the population-level equation for our model. However, in order to do so, we need to do one crucial approximation. First, we recall the expression for the expected value of the number operator (4.92):

$$\langle \hat{n}_i \rangle = \langle a_i^\dagger a_i \rangle = \langle a_i \rangle. \tag{4.102}$$

In the continuum limit:

$$\langle a_i \rangle \mapsto \langle \phi(x,t) \rangle = \frac{1}{\mathcal{N}} \int \mathcal{D}\left[\tilde{\phi}(x,t)\right] \mathcal{D}[\phi(x,t)] \phi(x,t)) e^{-S[\tilde{\phi},\phi]} \equiv \langle \rho(x,t) \rangle. \tag{4.103}$$

Thus, the mean value of the field ϕ is equivalent to the mean population density in the continuum limit $\rho(x,t)$. The word density means that this quantity measures population size per unit of space. It describes how the density of individuals is distributed in a continuous space. If one desires to obtain the number of individuals within the interval $[x_1, x_2]$ we have to integrate this density throughout this interval

$$\int_{x_1}^{x_2} \rho(x',t) dx'. \tag{4.104}$$

Therefore, to obtain the total population size, we must integrate it over the system size

$$A = \int_0^L \rho(x,t) dx. \tag{4.105}$$

The definition of population density marks the complete transition from individual to population level.

Unfortunately, equation (4.101) does not only depend on the expected value of ϕ, i.e. ρ, but also on the mean value of higher orders of it, $\langle \phi^k \rangle$. Therefore, we would need to obtain the dynamic equation of those higher other terms, which depend on even higher terms of ϕ. This coupling between orders of ϕ makes it impossible to obtain a finite set of differential equations required to solve (4.101). This can be managed by approximating those higher-order terms as $\langle \phi^k \rangle \approx \langle \phi \rangle^k$, i.e. the mean-field approximation [97, 103]. This approximation can be thought of as setting the variance of the distribution to zero, $\sigma^2 = \langle \phi^2 \rangle - \langle \phi \rangle^2 = 0$. Therefore, it neglects the demographic fluctuations of the stochastic system and approximates the dynamics to its underlying deterministic drift [100, 101, 102, 103].

In the context of our population-dynamics model with a component Allee effect, the mean-field approximation fails to describe noise-driven consequences of the Allee effect that might be ecologically relevant at low population sizes, such as extinctions caused by demographic noise [45]. It, however, allows us to apply

tools from spatially-extended dynamical systems and obtain analytical insights of the underlying stochastic dynamics. By applying the mean-field approximation in (4.101), we obtain a partial differential equation (PDE) that describes the dynamics of the population density ρ

$$\frac{\partial \rho(x,t)}{\partial t} = \left[r + \beta\, \tilde{\rho}_f(x,t) - \gamma\, \tilde{\rho}_c^2(x,t) \right] \rho(x,t) + D\, \nabla_x^2 \rho(x,t). \tag{4.106}$$

The parameter $r = b - d$ is the intrinsic growth rate, which combines the contributions of the density-independent birth and death rates from the individual-level description of the dynamics. ∇_x^2 is the Laplacian on the spatial coordinate x. Thus, the random walk at the population-level converges into a diffusion equation, as expected. The $\tilde{\rho}_\alpha(x,t)$ terms are the non-local densities, obtained by averaging the population density within a neighborhood of range R_α for $\alpha = \{f, c\}$

$$\tilde{\rho}_\alpha(x,t) = \int G\left(\left|x - x'\right|; R_\alpha\right) \rho\left(x', t\right) \mathrm{d}x'. \tag{4.107}$$

$G(|x - x'|; R_\alpha)$ is the normalized interaction kernel for the facilitation and competition, $\alpha = \{f, c\}$,

$$G(\left|x - x'\right|; R_\alpha) = \begin{cases} \frac{1}{2R_\alpha} & \text{if } |x - x'| \leq R_\alpha \\ 0 & \text{otherwise.} \end{cases} \tag{4.108}$$

Therefore, the long-range interactions of facilitation and competition contribute to the dynamics as integrals responsible for averaging the local density over a range R_f and R_c, respectively. Importantly, when the population density is uniform across space, the non-local densities converge into the population density $\tilde{\rho}_\alpha(x,t) = \rho(t)$. Moreover, because the diffusion term disappears when the population density is uniformly distributed, this equation loses its spatial dependency and becomes

$$\frac{d\rho}{dt} = \left[r + \beta\rho + \gamma\rho^2 \right] \rho, \tag{4.109}$$

which is the cubic model presented in the first chapter (2.1). This result explains why the population in the stationary state of the high-diffusion stochastic simulations in Figure 3.2a could be predicted by this non-spatial model.

4.6 Population-level model simulation

With the mean-field approximation model finally in hand, we get to the point where we can compare it with its stochastic counterpart. To do so, we need to numerically integrate equation (4.106) and generate a trajectory of the stochastic model while fixating all of the individual-level parameters. The details regarding the numerical integration algorithm used for this equation are presented in Appendix B.

This direct comparison between the simulation outcomes of both stochastic and deterministic models returns a very good quantitative agreement (Fig. 4.1). Not only the total population size of the system (Fig.4.1a) but also the emergent spatial structure (Fig.4.1b) are captured by the mean-field approximation. This allows us to use the deterministic density equation (4.106) to investigate how and for which conditions does that spatial structure emerges and what are the population-level consequences of it.

4.7 Pattern formation

The main advantage of deriving a deterministic equation approximation to the stochastic microscopic dynamics is that we can study the emergent spatial structure through pattern formation theory [106]. Thus, to investigate whether organisms organize in a periodic spatial structure or not, we perform a well-known technique for partial differential equations, the linear stability analysis. By starting from the spatially uniform solution of (4.106), ρ_+, we can add a small spatial perturbation, $\epsilon\,\psi(x,t)$ with $\epsilon \ll 1$, and calculate whether spatial patterns emerge out of it. To do so, we track the time evolution of the this perturbation amplitude. If this amplitude decreases with time, the uniform state is also stable against spatial perturbations, and patterns do not form; if the perturbation amplitude increases, the uniform state is unstable against spatial perturbations, and spatial patterns form.

For our model equation, we consider that the system starts from the form $\rho(x,t) = \rho_+ + \epsilon\,\psi(x,t)$, where ρ_+ is the uniform stable state, ψ is the perturbation, and $\epsilon << 1$ is a small parameter modulating the amplitude of the perturbation Inserting this solution in Eq. (4.106) we get

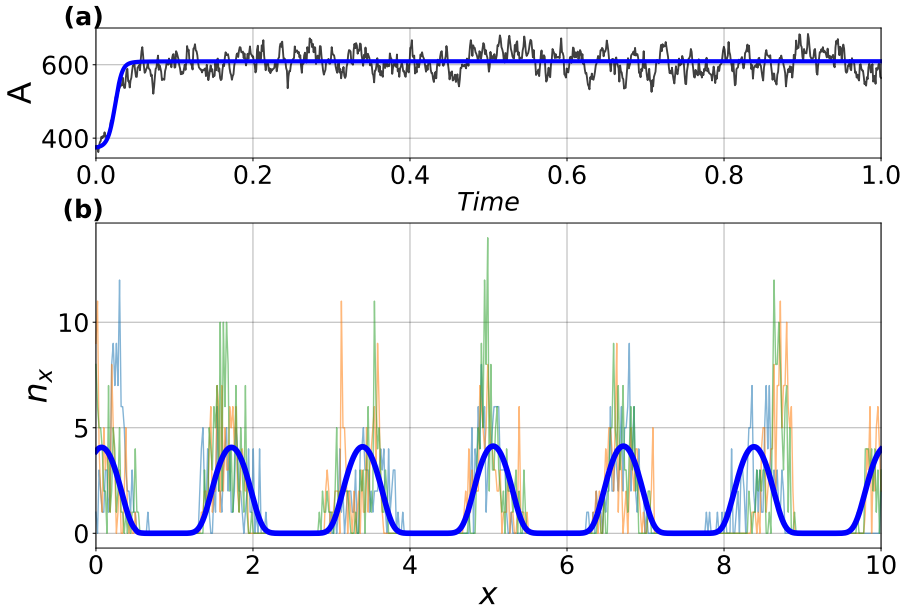

Figure 4.1: Comparison between the stochastic model and its deterministic limit. A) Population size as a function of time for a single realization of the stochastic process (black line) and the deterministic approximation (blue). B) Spatial distribution of individuals generated by the stochastic dynamics (thin blue, orange, and green lines; each line represents a snapshot of the stationary spatial distribution of individuals) and the deterministic approximation (blue thick curve). For the latter, we used an initial condition $\rho_+ + \phi(x)$, where $\phi(x)$ is a white noise uncorrelated in space with mean zero and variance $\epsilon \ll 1$, and transformed population density to size by multiplying the value of the density field in each of the PDE integration nodes by the length of the lattice mesh used in the discrete simulations δx. Parameters and lattice mesh are the same we used in Figure 3.2 (e, f). The deterministic simulations run until $t = 1500$, with $dt = 0.05$ and $dx = 0.008$. See Appendix *B* for details on the algorithm.

$$\cancel{\frac{\partial \rho_+}{\partial t}}^{\,0} + \epsilon \frac{\partial \psi}{\partial t} = r(\rho_+ + \epsilon\psi) + \beta\,(\rho_+ + \epsilon\psi) \int G_f(|x-a|)\,(\rho_+ + \epsilon\psi) da \tag{4.110}$$

$$- \gamma\,(\rho_+ + \epsilon\psi) \left[\int G_c(|x-a|)\,(\rho_+ + \epsilon\psi) da \right]^2 + D\,\nabla^2(\rho_+ + \epsilon\psi), \tag{4.111}$$

where we have introduced the simplifying notation

$$\tilde{\psi}_\alpha(x,t) = \int G_\alpha(|x-a|)\,\psi(x,t)\,da. \tag{4.112}$$

for $\alpha = \{f, c\}$. Exploiting the fact that $\rho_+ = \int G_\alpha(|x-a|)\,\rho_+\,da$, we get

$$\epsilon\frac{\partial\psi}{\partial t} = r(\rho_+ + \epsilon\psi) + \beta\,(\rho_+ + \epsilon\psi)(\rho_+ + \epsilon\tilde{\psi}_f) \tag{4.113}$$

$$- \gamma\,(\rho_+ + \epsilon\psi)\,(\rho_+ + \epsilon\tilde{\psi}_c)^2 + \epsilon D\,\nabla^2\psi. \tag{4.114}$$

The second term becomes

$$\beta\,(\rho_+ + \epsilon\psi)(\rho_+ + \epsilon\tilde{\psi}_f) = \beta\left(\rho_+^2 + \epsilon\rho_+(\psi + \tilde{\psi}_f) + \cancelto{0}{\epsilon^2\psi\tilde{\psi}_f}\right) \tag{4.115}$$

$$= \beta\left(\rho_+^2 + \epsilon\rho_+(\psi + \tilde{\psi}_f)\right). \tag{4.116}$$

The third term

$$\gamma\,(\rho_+ + \epsilon\psi)\,(\rho_+ + \epsilon\tilde{\psi}_c)^2 = \gamma\,(\rho_+ + \epsilon\psi)\,(\rho_+^2 + 2\epsilon\rho_+\tilde{\psi}_c + \cancelto{0}{\epsilon^2\tilde{\psi}_c^2}) \tag{4.117}$$

$$= \gamma\left(\rho_+^3 + \epsilon\rho_+^2(\psi + 2\tilde{\psi}_c) + \cancelto{0}{2\rho_+\epsilon^2\tilde{\psi}_c\psi}\right) \tag{4.118}$$

$$= \gamma\left(\rho_+^3 + \epsilon\rho_+^2(\psi + 2\tilde{\psi}_c)\right). \tag{4.119}$$

Now, we can reorganize the equation

$$\epsilon\frac{\partial\psi}{\partial t} = \epsilon r\psi + \epsilon\beta\,\rho_+(\psi + \tilde{\psi}_f) - \epsilon\gamma\,\rho_+^2(\psi + 2\tilde{\psi}_c) + \epsilon D\,\nabla^2\psi + \overbrace{r\rho_+ + \beta\rho_+^2 - \gamma\rho_+^3}^{\frac{\partial\rho_+}{\partial t} = 0}. \tag{4.120}$$

Dividing by ϵ and performing the Fourier transform

$$\frac{\partial\hat{\psi}}{\partial t} = r\hat{\psi} + \beta\,\rho_+(\hat{\psi} + \hat{\psi}\hat{G}_f) - \gamma\,\rho_+^2(\hat{\psi} + 2\hat{\psi}\hat{G}_c) - Dk^2\hat{\psi} \tag{4.121}$$

$$= \hat{\psi}\Big[r + \beta\,\rho_+(1 + \hat{G}_f) - \gamma\,\rho_+^2(1 + 2\hat{G}_c) - Dk^2\Big], \tag{4.122}$$

where $\hat{\psi}(k,t)$ is the Fourier transform of the perturbation and $\hat{G}_\alpha(k)$ is the Fourier transform of the kernel. Because Eq. (4.121) is a linear differential equation, it has an exponential solution $\hat{\psi}(k,t) \propto \exp(\lambda(k)t)$ whose growth rate $\lambda(k)$ is given by

$$\lambda(k) = r + \beta\,\rho_+(1+\hat{G}_f) - \gamma\,\rho_+^2(1+2\hat{G}_c) - Dk^2, \tag{4.123}$$
$$= r + \rho_+\left[\beta + \beta\hat{G}_b - \gamma\rho_+ - 2\gamma\rho_+\hat{G}_c\right] - Dk^2. \tag{4.124}$$

Using the expression for ρ_+, Eq. (2.2), in the term inside the brackets, we can reorganize the equation

$$\lambda(k) = r + \rho_+\left[\beta + \beta\hat{G}_f - \frac{\beta}{2} - \frac{\sqrt{\beta^2+4\gamma r}}{2} - 2\gamma\rho_+\hat{G}_c\right] - Dk^2 \tag{4.125}$$
$$= r + \rho_+\left[\gamma\rho_- + \beta\hat{G}_f - 2\gamma\rho_+\hat{G}_c\right] - Dk^2. \tag{4.126}$$

Using the relation

$$\rho_+\rho_- = \left[\frac{\beta+\sqrt{\beta^2+4\gamma r}}{2\gamma}\right]\left[\frac{\beta-\sqrt{\beta^2+4\gamma r}}{2\gamma}\right] = -\frac{r}{\gamma}, \tag{4.127}$$

we can simplify the equation to

$$\lambda(k) = r + \gamma\rho_+\rho_- + \rho_+\left[\beta\hat{G}_f - 2\gamma\rho_+\hat{G}_c\right] - Dk^2 \tag{4.128}$$
$$\lambda(k) = r - r + \rho_+\left[\beta\hat{G}_f - 2\gamma\rho_+\hat{G}_c\right] - Dk^2, \tag{4.129}$$

and finally obtain

$$\lambda(k) = \rho_+\left[\beta\hat{G}_f - 2\gamma\rho_+\hat{G}_c\right] - Dk^2. \tag{4.130}$$

The Fourier transform of the kernel has an explicit expression

$$\hat{G}_\alpha(k) = \frac{\sin(R_\alpha k)}{R_\alpha\,k}. \tag{4.131}$$

Thus, the growth rate $\lambda(k)$ can be expressed as

$$\lambda(k) = \rho_+\left[\beta\frac{\sin(R_f\,k)}{R_f\,k} - 2\gamma\rho_+\frac{\sin(R_c\,k)}{R_c\,k}\right] - Dk^2. \tag{4.132}$$

If $\lambda(k)$ is positive for a given wavenumber k, a perturbation with that wavenum-

ber will grow and create a regular pattern of population density. The wavenumber maximizing $\lambda(k)$ in Eq. (4.132), k_{max}, defines the dominant periodicity of the spatial pattern at short times and is related to the periodicity of the long-term spatial pattern of population density. Hence, we can estimate the number of groups m that form in a system of size L as $m \approx L k_{max}/2\pi$. Moreover, we can better understand how the different processes and interactions included in the microscopic model contribute to pattern formation by analyzing term by term all the different contributions to the perturbation growth rate.

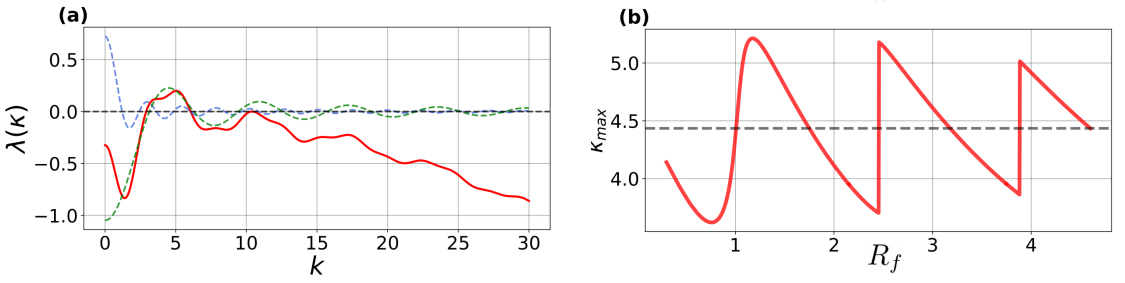

Figure 4.2: a) Perturbation growth rate as a function of the wavenumber k (red). The dashed lines represent the contributions of the facilitation (blue) and competition (green) terms to $\lambda(k)$. b) The fastest growing wavenumber, k_{max}, as a function of R_f. The grey dashed line is the number of peaks predicted in the absence of facilitation, $\beta \to 0$. We use $r = -2$, $D = 0.001$and $\beta = 1$, $\gamma = 1$. For panel (a) we choose $R_f = 2.6$.

The first understanding we can get out of the linear stability analysis is that diffusion contributes negatively to pattern formation and hence tends to homogenize population density and eliminate patterns, as observed in the stochastic simulations presented in 3.2. Second, long-range competition and facilitation enter the perturbation growth rate via the Fourier transform of their corresponding interaction kernel, which, in the case of the top-hat kernel chosen in our model, are damped oscillatory functions with interaction-specific frequency, magnitude, and sign (Fig. 4.1). The frequency of each oscillatory function is determined by the interaction range, while the magnitude is determined by the intensity of the interaction. The sign preceding each oscillatory function indicates how competition or facilitation impacts population growth, with the negative sign corresponding to competition and the positive one to facilitation. This does not mean, however, that competition hinders pattern formation while facilitation boosts it. The oscillatory functions present in the Fourier transform of the interaction kernel allow the facilitation and competition terms to oscillate between positive and negative contributions to the growth rate.

To better understand the role of long-range interactions in pattern formation,

we consider the limit cases in which each of these interactions vanishes or acts on a local scale. In the local competition limit, $R_c \to 0$, the perturbation growth rate is always negative because $\rho_+ < \beta/(2\gamma)$ when populations are uniformly distributed. Therefore, patterns do not form. However, if facilitation is local, $R_f \to 0$, or vanishes, $\beta = 0$, the perturbation growth rate can still be positive for certain wavenumbers, and patterns can potentially form. Therefore, long-range competition is a sufficient and necessary condition for pattern formation, while facilitation is not able to generate patterns by itself. Varying facilitation makes the fastest-growing wavenumber, and therefore the number of groups, oscillate around the value obtained when long-range interactions are purely competitive (Fig. 4.1b). Thus, competition sets the scale of the periodicity of the long-term spatial pattern of population density. Facilitation, on the other hand, plays a secondary role in pattern formation, rearranging the pattern periodicity around the value set by the competition range [107]. Previous studies have already identified long-range competition as a cause of spatial patterns through the establishment of the so-called exclusion regions, i.e., regions between clusters of organisms in which individuals would compete with individuals from two neighbor groups [87, 88, 103]. In fact, for low diffusion, our simulations show that the distance between aggregates is very close to the competition range R_c, as expected when patterns form due to exclusion regions [103, 108, 109]. Facilitation seems to shift a bit the size of the exclusion region so that the facilitation range of in a group would try to encompass the whole aggregate, and neighbor ones if $R_f > R_c$. In fact, the spatial patterns of population density exhibit aggregates shorter than the range of both non-local interactions, which makes the intensity of competition and facilitation inside an aggregate approximately constant.

It is important to mention that since we are dealing with a one-dimensional system, the only pattern that can emerge is a periodic sequence of aggregates. In higher dimensions, a richer set of patterns con form. [106]. However, by performing the same analysis in a two-dimensional variant of our model, we observe that the only spatial pattern that can be formed is of complete or partially isolated aggregates. That is, the spatial structure observed in one-dimension is still preserved in a two-dimension model, see Figure 4.3.

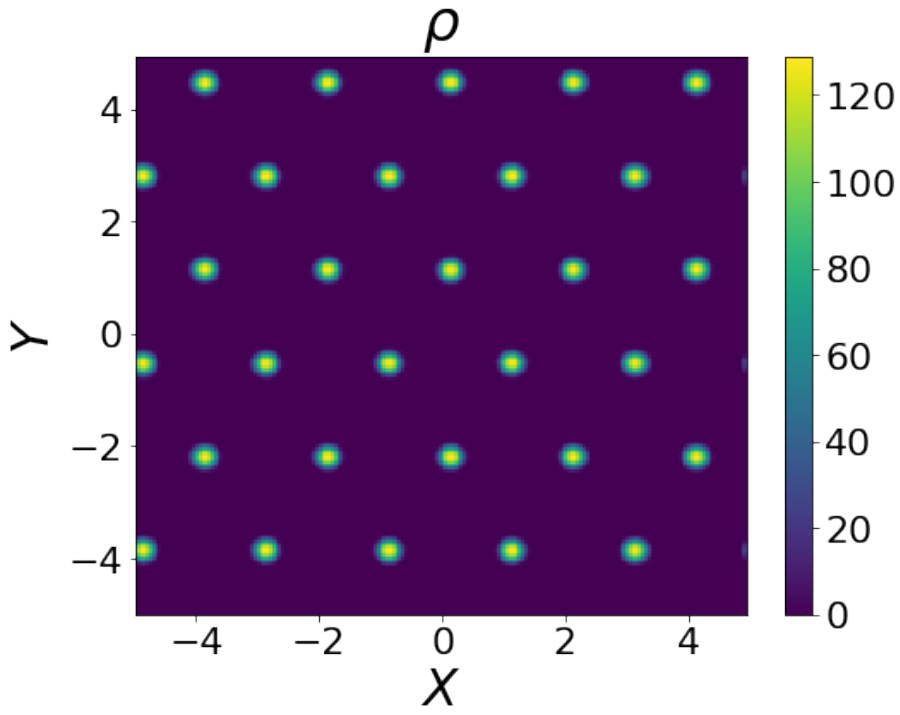

Figure 4.3: Spatial pattern of population density for the deterministic model in two dimensions. Simulations run until $\tau = 3000$, with $d\tau = 0.05$, $dx = 0.008$, and $L = 10$. The simulations used the following set of parameters: $r = -1$, $\beta = 1$, $\gamma = 1$, $R_f = 0.5$, $R_c = 1$,and $D = 10^{-3}$.

Chapter 5

Meta-populations scale

Our population-level model allowed us to understand why non-uniform patterns emerge in the population structure. However, up until this point we have not been able to explain why the carrying capacity of the system increases in the presence of those patterns. To do so, we need to once again zoom out of our current spatial scale.

When patterns are formed, the population organizes in several separated aggregates. In our current population-level model, we explicitly describe the spatial properties of the groups. Fortunately, the linear stability analysis provided a way to predict some properties of the emergent pattern based on the individual-level parameters, such as the number of aggregates in a given landscape and the distance between them. Our model can only produce periodic sequences of aggregates across the x axis, or arranged in a hexagonal lattice for the 2D model (Fig 4.3). Therefore, we do not need to track the population density across all spatial coordinates, since we know how groups are distributed. The only thing that we need to represent this system is the abundance of each group and to establish how groups interact with each other. Thus, our population can be mapped into a meta-population model.

We have touched briefly on the concept of a meta-population model before (see Chapter 2 section 2.4). In the current chapter, we will derive such a model out of our population-scale PDE system, discussing the conditions that need to be met for this approximation to be valid. This yields our group-level approximation which represents our system as a set o isolated sub-populations that can interact through facilitation if R_f is sufficiently large. This approximation will allow us to finally understand how a component Allee effect at the individual level can influence the dynamics of a spatially structured population.

5.1 Group-level approximation

Our goal in this section is to map our spatially explicit system into a meta-population model. To do so we further approximate the deterministic equation (4.106) to obtain estimates for the number of individuals within a single spatial aggregate of the stationary pattern. This approximation requires three key conditions regarding the spatial pattern:

1. All individuals within a group must interact with one another via competition and facilitation

2. Individuals of different groups must not compete with each other

3. If two groups interact with each other via facilitation, this positive interaction must reach all the individuals in both groups

The first condition requires that the competition and facilitation ranges are greater than the length of the clusters of organisms. When this condition is met, the birth/death dynamics of the cluster only depends on the number of individuals in it (if the facilitation range is smaller than the distance between groups), regardless of how they are distributed. This is not true when the facilitation range is larger than the competition range. We will discuss later. The second condition implies that the competition range must be shorter than the distance between pattern aggregates. These two conditions also require that diffusion is low so the spatial structure of the system is determined mainly by the finite-range ecological interactions. By the end of this chapter, we will explore to which extent those conditions hold as we increase diffusion. The last condition requires that, if there is inter-group facilitation, the facilitation range must be large enough to encompass all the individuals of a neighbor group. Therefore this third condition complements the first one by imposing that the strength of inter-group interactions must only depend on the number of individuals in the groups, and not on how they are distributed in the clusters. This condition is correct provided that the first two are met, except for specific values of R_f for which the facilitation range reaches neighboring clusters partially.

Given that the three conditions above are fulfilled, the non-local density $\tilde{\rho}_c$ is constant inside each aggregate. This is so because the integral that defines this averaged density in Eq. (4.107) reduces to the number of individuals within the

group, $\mathcal{N}_i$.

$$\tilde{\rho}_c(x_i,t) = \int G\left(\left|x_i - x'\right|; R_c\right) \rho\left(x',t\right) \mathrm{d}x' = \frac{\mathcal{N}_I(t)}{2R_c} \tag{5.1}$$

where x_i is the spatial coordinate of each lattice node, i, inside the aggregate "I". Following the same arguments, $\tilde{\rho}_f$ is also constant inside each group. However, since different groups can facilitate each other, the value of $\tilde{\rho}_f$ depends on the number of groups within the facilitation range R_f. Notice that this is not true for competition because the distance between groups must be larger than the competition range (condition 2). Thus we can write

$$\tilde{\rho}_f(x_i,t) = \frac{\mathcal{N}_I(t)}{2R_f} + \sum_{\langle I,J\rangle} \frac{\mathcal{N}_J(t)}{2R_f} \tag{5.2}$$

whereby J runs over the neighbors of the focal group I that are within the facilitation range. Next, we use Eqs. (5.1) and (5.2) in Eq. (4.101) to get:

$$\frac{\partial \rho(x_i,t)}{\partial t} = \left[r + \beta\frac{\mathcal{N}_I(t)}{2R_f} + \beta \sum_{\langle I,J\rangle} \frac{\mathcal{N}_J(t)}{2R_f} - \gamma\,\frac{\mathcal{N}_I^2(t)}{4R_c^2}\right]\rho(x_i,t), \tag{5.3}$$

where we have neglected the diffusion term because small diffusion is a necessary condition to have the three conditions above fulfilled. Finally, we integrate over the group length on both sides of Eq. (5.3) to obtain

$$\frac{\partial \mathcal{N}_I(t)}{\partial t} = \left[r + \frac{\beta}{2R_f}\left(\mathcal{N}_I(t) + \sum_{\langle I,J\rangle} \mathcal{N}_J(t)\right) - \gamma\,\frac{\mathcal{N}_I^2(t)}{4R_c^2}\right]\mathcal{N}_I(t). \tag{5.4}$$

Equation (5.4) marks our transition to the meta-population scale. Here, the spatial properties of the pattern are set, and the only meaningful variables that describes the state of the population are the local abundances of the aggregates. When there are no inter-group interactions, the equation of each group is independent of the others and it assumes the form of the cubic model (see (2.1)).In this limit, we recover the group Allee effect in which a fitness component of an organism increases with group size rather than with total population size/density[3, 16, 35]. That is, a component of the fitness, related to the facilitation, increases with group size rather than total population size/density.

Since there are no spatial dependencies in the parameters, and considering periodic boundary conditions, we can assume that all aggregates have the same

number of neighbors and the same aggregate size in the stationary state. In these conditions, we can introduce a parameter that gives the number of groups within the facilitation range, η. Using this parameter, we can write an ordinary differential equation to describe the dynamics of any aggregate size:

$$\frac{\partial \mathcal{N}(t)}{\partial t} = \left[r + \beta(\eta + 1) \frac{\mathcal{N}(t)}{2R_f} - \gamma \frac{\mathcal{N}^2(t)}{4R_c^2} \right] \mathcal{N}(t). \tag{5.5}$$

Eq. (5.5) is a cubic model, similar to (2.1). The presence of inter-group interactions modulates the intensity of facilitation through the η parameter. Solving Eq. (5.5) we can obtain the possible stationary group sizes $\mathcal{N}_0 = 0$ (extinction) and:

$$\mathcal{N}_{\pm} = \frac{(\eta + 1)\frac{\beta}{2R_f} \pm \sqrt{\left((\eta + 1)\frac{\beta}{2R_f}\right)^2 + \frac{r\gamma}{R_c^2}}}{\gamma / 2R_c^2}. \tag{5.6}$$

For the remainder of this chapter, we will investigate the population-level consequences of non-uniform spatial patterns of population density using the meta-population model. We will compare the results obtained using this approximation with those provided by the population and individual level models.

5.2 Population persistence

First, we will study how spatial patterns of population density influence the persistence of the population as the quality of the environment decreases. This decrease in the quality of the environment can come from a reduction can be a decrease in the food supply for the organisms, severe temperature or chemical changes in the environment, or any other factor that diminishes the abilities of organisms to survive and/or reproduce. We consider that all of those are external factors, independent of how the interactions among the conspecifics happen. Thus, they reflect a decrease in the intrinsic growth rate of the organisms, r.

We want to understand how the abundance of the total population, A, changes with r. In the absence of periodic patterns of population density, the population is uniformly distributed at a population density given by the stable solution of the cubic model, ρ_+ in Eq. (2.2). In this scenario, the total abundance $A_{uniform}$ will be given by the stable population density ρ_+ times the spatial length of the system L

$$A_{uniform} = \int_0^L \rho_+ dx = L\frac{\beta + \sqrt{\beta^2 + 4\gamma r}}{2\gamma}. \tag{5.7}$$

The same can be done to find the Allee threshold in the total abundance, i.e. the system size times the unstable equilibrium, $L\rho_-$. From Eq. (5.7), we can explicitly determine how $A_{uniform}$ changes with the intrinsic growth rate r. This expression predicts that the stable equilibrium will cease to exist if r gets too low. Therefore, we define $\tilde{r}_{uniform}$ as the critical value below which ρ_+ and ρ_- become imaginary, i.e. the term in the square root of equation (5.7) becomes negative.

$$\tilde{r}_{uniform} = -\frac{\beta^2}{4\gamma}. \tag{5.8}$$

Ecologically, this means that those states are not possible solutions for the system, and thus, the extinction state becomes the only stable equilibrium. Therefore, when $r < \tilde{r}_{uniform}$, populations will go extinct if they are uniformly distributed in space.

As we already saw from the simulations of the stochastic individual-based dynamics, aggregation increases the total abundance, 3.2. The meta-population model allows us to quantify this increase in the total abundance, $A_{patterns}$, due to the emergence of non-uniform spatial distributions of population density. Integrating the population density in the patterned state across the system size is analogous to adding the population size within each group. Given that all the conditions underlying the meta-population model are met, i.e. low diffusion and adequate values of R_f, the total abundance is given by

$$A_{patterns} = \int_0^L \rho(t,x) dx = m\,\mathcal{N}_+, \tag{5.9}$$

where $\mathcal{N}_+$ is given by Eq. (5.6) and $m \approx L\,k_{max}/2\pi$ is the number of groups within the system size L. As we discussed in Section 4.7, we can estimate this number of groups we can estimate from the pattern wavelength predicted by the wavenumber that maximizes the perturbation growth rate in Eq. (4.132), k_{max}. Equation (5.9) gives an explicit relation between $A_{patterns}$ and the intrinsic growth rate r. Similarly to the case of uniformly distributed populations, (5.9) predicts that the stable equilibrium will cease to exist for low values of r. We can calculate the critical value of the intrinsic growth rate, $\tilde{r}_{patterns}$, below which the system cannot sustain a non-zero population size,

$$\tilde{r}_{patterns} = -\gamma^{-1}\left[\frac{\beta}{2}\frac{R_c}{R_f}(\eta+1)\right]^2. \tag{5.10}$$

As expected, $\tilde{r}_{patterns}$ decreases with increasing facilitation and decreasing competition strength. In addition, $\tilde{r}_{patterns}$ decreases when the number of groups that interact with one another increases.

Defining an Allee threshold is harder when the spatial distribution of population density is not uniform. This is because it becomes space-dependent, and the Allee threshold is determined by the local density of individuals within the competition and facilitation ranges. These local densities, in turn, depend on the number and spatial arrangement of groups. If we impose that all groups must be of equal size, we can define an unstable patterned state where all groups have size $\mathcal{N}_-$. Moreover, we can interpret this state as an upper bound for the Allee threshold. Because any population spatially organized in m isolated groups with total abundance above $m\mathcal{N}_-$ will grow. If groups are independent of each other, i.e. $\mathcal{N}_+$ is real for $\eta = 0$, then a lower bound for the Allee threshold for the whole population would be $\mathcal{N}_-$. This is because a population below this value can never form a group able to sustain itself. Of course, if groups must rely on each other to survive, i.e. $\mathcal{N}_+$ only exists if $\eta > 0$, defining this lower bound would require looking at the smallest facilitation network that ensures the survival of the population

Next, we can validate the expressions obtained for the total abundance and the critical value of the intrinsic growth rate, $A_{patterns}$ and $\tilde{r}_{patterns}$, using the meta-population approximation with simulations of the individual and population-level models. In Figure 5.1 we compare the steady state abundances divided by system's length, L, for all models as we decrease r from 0 to $\tilde{r}_{patterns}$.

For the individual-level model, we run 50 independent simulations until $t = 500$ for each value of r. Then, we compute the mean total abundance of the last 400 time steps and then compute the average over an ensemble of realizations using all simulations with the same r. For the deterministic population-level model, we compute both stable and unstable patterned stationary states. First, we integrate Eq. (4.106) with $r = 0$ until the population density reaches its stationary spatial pattern and compute the population abundance by integrating the density field over the system length. Next, we decrease r in a small amount Δr and integrate Eq. (4.106) for a long time interval Δt using the stationary pattern for $r = 0$ as the initial condition. We repeat this process recursively until the r is

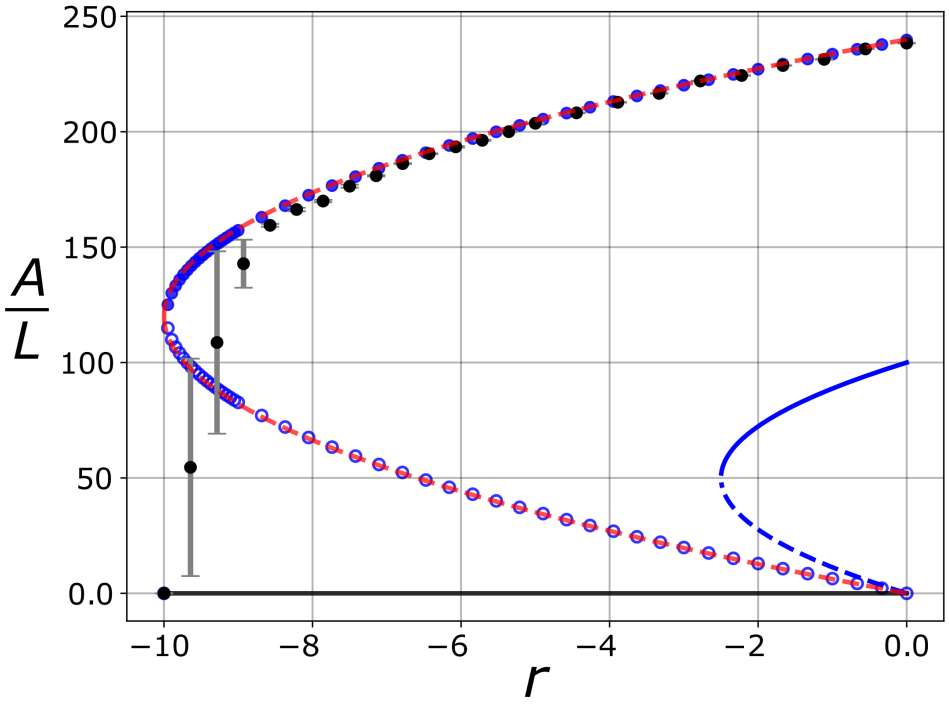

Figure 5.1: Effect of spatial self-organization on the demographic Allee affect. Population abundance (A) divided by the system's length (L) as a function of the net population growth, r, obtained from: the deterministic density equation when patterns develop, Eq. (4.106) (blue points and blue lines); the non-spatial cubic model (blue lines); the meta-population model, Eq. (5.6) (dashed red line); and the stochastic dynamics (black circles with error bars indicating the variance of 50 independent realizations). The filled points and the blue solid line represent a stable equilibrium, whereas the empty symbols and blue dashed lines represent unstable equilibrium states. The deterministic simulations run until $t = 1500$, with $dt = 0.05$ and $dx = 0.008$. The stochastic model runs until $t = 500$ with $\beta = 10^{-1}$, $\gamma = 10^{-3}$, $R_f = 0.5$, $R_c = 1$ and $\delta x = 0.02$. All simulations are done with $L = 32$ and $D = 10^{-3}$.

such that the population density vanishes. This procedure gives us the stationary values of the population abundance that are stable, ρ_+. To compute the unstable ones, we assume that $\rho_-(x,t) = \alpha\,\rho_+(x,t)$, where α is a dimensionless scaling parameter such that $0 < \alpha \leq 1$. This assumption implies that ρ_- has the same spatial structure as ρ_+ and that both solutions only differ by a factor α that makes $\rho_-(x,t) < \alpha\,\rho_+(x,t)$. Under this assumption, to compute ρ_- we need to numerically find the $0 < \alpha \leq 1$ that satisfies $\partial_t \rho_- = 0$. Because $\alpha = 1$ always satisfies this condition, we only take into account the lowest value of α, which is $\alpha = 1$ only when $r = \tilde{r}_{patterns}$.

The predictions of the meta-population model for $\tilde{r}_{patterns}$ and the total abundance $A_{patterns}$ are in excellent agreement with those of the density equation and

the outcome of the stochastic simulations (Fig. 5.1). The disagreement between the deterministic approximation and stochastic simulations appears for values of r close to $\tilde{r}_{patterns}$. In this regime, fluctuations in population size can take the population size below the Allee threshold and cause extinctions more easily [44]. Thus, fluctuations become an important driver of population dynamics in this parameter regime, and the mean-field results diverge from the stochastic ones. Also, in order to compare the total abundance of the spatially uniform and patterned solutions, we plot $A_{uniform}$ (blue line) and its unstable state (dashed blue line), see Eq.(5.7), in Figure 5.1. We observe that the number of individuals that the system can host significantly increases for the patterned solution as compared to the uniform case. Also, the Allee threshold is higher when individuals are uniformly distributed in space, see the unstable uniform state (dashed blue line) and the unstable patterned state (empty circles and red dashed line), i.e. the upper bound for the Allee threshold in the patterned state. The critical value for the intrinsic growth rate is much lower when the population density is non-uniform in space organization, $\tilde{r}_{patterns} < \tilde{r}_{uniform}$ (Fig. 5.1). As a result of these changes in $\tilde{r}$ and the Allee threshold, populations exhibiting a self-organized spatial pattern of population density and a component Allee effect can persist in harsher environments and at higher numbers than uniformly distributed populations. Finally, because spatially structured populations have lower Allee thresholds, they are less susceptible to extinctions caused by environmental perturbations and can recover after extinction following smaller fluctuations than uniformly distributed populations.

5.3 Demographic Allee effect in clumped populations

Organism grouping sets new ways in which the individual-level component Allee effect manifests at the population level and determines the Allee threshold. In the previous section, we analyzed the case where all groups have the same number of individuals. In the present section, we relax this by using Eq. (5.4) that gives the dynamics of each group independently. We analyze these possible outcomes for different numbers of groups and facilitation ranges in order to understand to which extent the component Allee effect present in the individual-level processes translates to a demographic one for the whole population.

Mimicking the one-dimensional landscape we used in all previous analyses, we consider that groups are arranged in a line. However, we do not consider

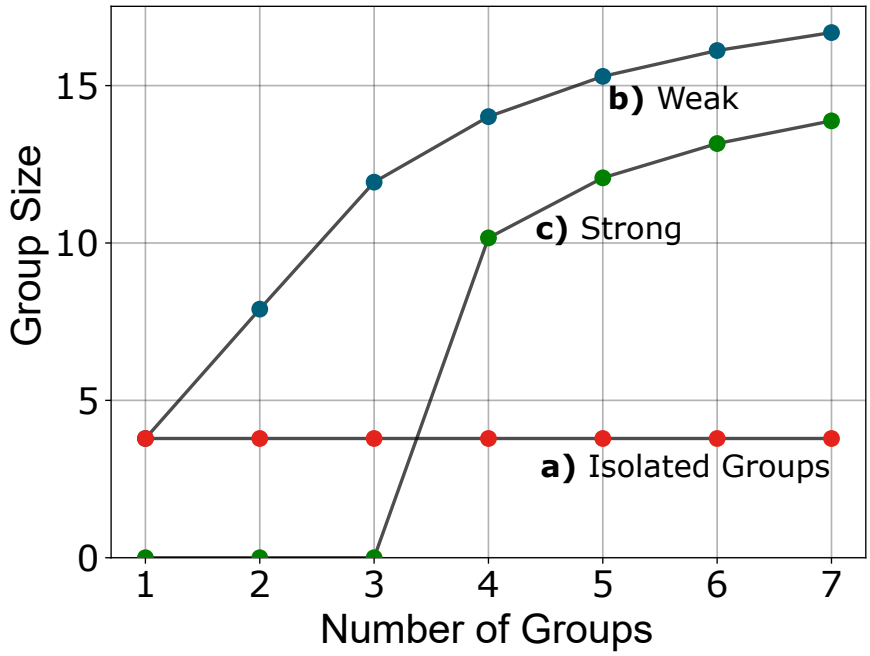

Figure 5.2: Demographic Allee effect in a population composed of groups. Here, we set the number of groups in the system and compute the size of a single group in the stationary state, $\mathcal{N}_+$. The red symbols correspond to a situation in which groups are isolated, $r = -2$ and $R_f = 0.5$; blue and green symbols correspond to cases with inter-group facilitation with $R_f = 2$ and $r = -2$ (blue) and $r = -100$ (green). For all cases, $R_c = 1$, $\beta = 10^{-1}$, and $\gamma = 10^{-3}$

periodic boundary conditions to prevent the number of groups from being effectively infinite. For short facilitation ranges, individuals in different groups do not interact with one another, which leads to the group-Allee effect limit that we already discussed earlier [3, 16, 35]. In this limit, the fitness of individuals within each aggregate only depends on group size (Fig. 5.2a), and groups are independent units. Therefore, the formation or extinction of a group does not have any effect on the others. Thus, as discussed in the previous section, the minimum population size that ensures population survival is equal to the Allee threshold of one single group, $\mathcal{N}_-$ from Eq. (5.6) with $\eta = 0$.

If the facilitation range is such that groups interact with one another, the fitness of the individuals can increase significantly due to the presence of neighbor groups. As a consequence, group size increases in the presence of more groups (Fig. 5.2b and 5.2c). For very harsh environmental conditions (low r) the population only survives if groups facilitate one another (Fig. 5.2c). More specifically, for certain net growth rates r, a population would only be able to survive provided that groups facilitate each other, which makes long-range interactions a necessary

condition for population survival. Notice, however, that when the facilitation range increases and groups rely on one another for survival, the high connectivity between groups makes the population less resistant to local perturbations that might cause global extinctions. That is, the decrease in the population of a group will affect others through the facilitation network, and can eventually lead to the total extinction of the population.

These results highlight how in this limit groups become the new ecological unit of the system. When groups do not facilitate each other (Fig. 5.2a), no demographic Allee effect can be observed in a large population. This is because the emergence of more groups is not going to boost the per-capita growth rate of the already existing ones. Thus, higher population sizes, i.e. more groups, do not result in an increase in fitness. This scenario resembles an ecological dynamics only driven by competition, where the fitness of individuals decreases with the number of groups. If we set a fixed spatial length of the system, an increase in the number of groups results in less space for others to emerge, ultimately leading to a decreased rate of group "reproduction".

When the facilitation range is such that it encompasses one focal group and its neighbors, adding more groups leads to an overall higher individual fitness for each organism (Fig. 5.2b and 5.2c). Therefore, the demographic Allee effect emerges in the presence of inter-group interactions, rather than inter-individual ones. It even sets a new type of weak and strong Allee effects, which depends on the number of groups present in the system. When a single group is able to survive alone but has increased size when other groups are nearby, we have a weak Allee-like effect at the population level. Analogously, when a population requires a minimum number of groups to survive, we have a strong Allee-like effect at the population level. Interestingly, a group-level strong Allee effect can occur while a weak Allee-like effect (or no demographic Allee effect at all) can happen at the population level. This scale-dependent intensity of the Allee effect resembles the way in which a multicellular animal, for instance, can experience no Allee effect in its population while its cells are subjected to a Strong Allee effect, i.e. if the cell count of the animal goes below a certain threshold, the organism cannot survive.

5.4 Increasing diffusion

Throughout this chapter, we have assumed that diffusion is low enough so that the first two conditions underlying the group-level approximation in Eq. (5.5)

are met. In this section, we increase the diffusion coefficient in order to evaluate within which range of diffusion those conditions remain valid (Fig. 5.3a). In the low-diffusion regime, the predictions of the meta-population approximation agree nicely with the simulated population abundances. However, as diffusion increases, diffusion takes control of the spatial dynamics, and the conditions underlying the group-level approximation stop being valid. As observed with the simulations of the stochastic individual-based dynamics (Fig. 3.2), the total population abundance decreases as diffusion increases. That is, as groups become less isolated from each other, the system is not able to host as many organisms. In fact, the population density decreases until diffusion reaches a critical value (black dashed line in Figure 5.3a), predicted by the linear stability analysis $\lambda(k_{max}) < 0$, at which patterns do not form. In this case, the population abundance is equal to that predicted by models assuming uniformly distributed individuals (See Eq. (2.1)). We also observe this decrease in population density in the spatial patterns of population density, which tend to become uniform as diffusion increases (Fig. 5.3b). Therefore, there is a continuum transition between being uniformly distributed in space and the formation of properly isolated groups.

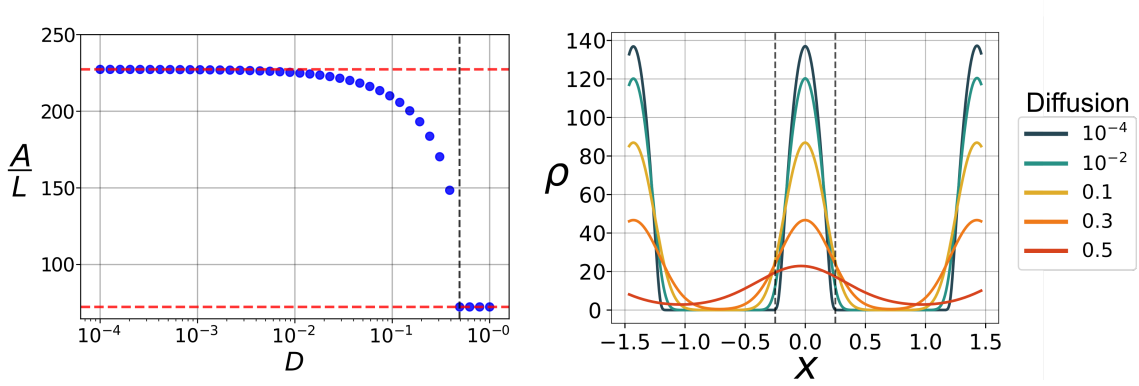

Figure 5.3: (a) Effect of increasing diffusion on the population abundance. Self-organized spatial patterns disappear when diffusion increases and the population abundance decreases from the metapopulation prediction $\mathcal{N}_+$ to the uniform solution ρ_+. (b) Effect of diffusion on spatial patterns, stationary patterns of population density for different diffusion intensities (color code indicated in the legend). The black dashed lines limit the extent of the facilitation range, R_f. Parameter values (for both panels): $t = 2 \times 10^4$, with $dt = 0.05$, $dx = 0.008$, $L = 32$ and parameters: $r = -2$, $R_f = 0.5$ and $R_c = 1$.

Chapter 6

Conclusion

In this work, we have theoretically investigated the demographic consequences of a component Allee effect across various levels of spatial organization. We started from the most straightforward set of processes leading to a demographic Allee effect, which in the non-spatial limit collapses to a cubic model [45, 110]. This individual-level description allows us to establish a mechanistic description of how the vital rates of a focal individual depend on the density of conspecifics around it. Our model, therefore, accounts for spatial processes both through the spatial population structure and the range of the different interactions among organisms. From these individual-level processes, we present a series of mathematical techniques to build a population-level description of the dynamics. Finally, when patterns do form, we derive a spatially implicit approximation of the spatially explicit original model. Building those models allows us to investigate how a component Allee effect operating at the level of the individuals can manifest across various characteristic spatial scales of the population.

We introduce a framework that incorporates a component Allee effect due to reproductive facilitation. As a consequence of this component Allee effect, the reproduction rates of a focal individual increase with the population density within this interaction-specific facilitation range R_f. We also consider growth limitation caused by intraspecific competition, which depends on population density within its range R_c. Our framework can be straightforwardly generalized to other types of individual-level interactions leading to component Allee effects, such as social behaviors, mate limitation, or environmental conditioning [3, 111]. Our work has mainly focused on quantifying features of the demographic Allee effect, such as the Allee threshold, the long-term total population size, and the lowest value of the density-independent growth rate for which the population survives, for distinct spatial distributions. Moreover, because population-level dynamics and patterns emerge from individual-level processes in our model, we can understand the origin of these observed features at the most fundamental level and frame them within a common theoretical framework.

Restricting the interactions of facilitation and competition to a finite neighborhood around each focal individual makes the Allee effect and its features to emerge on a local scale. That is, dependent on local, instead of total, population densities. The Allee threshold, for instance, is now set by the density of individuals within a given region of the landscape and thus a space-dependent quantity. This property of the Allee threshold might enable the survival of a local population in situations where the global density is very low and might help to explain field studies reporting population survival at low global population densities [26, 30, 112].

Our model also provides the appropriate theoretical framework to formalize the group Allee effect and integrate it within a unifying modeling approach [16, 18]. When the population organizes in groups, one can consider those as the fundamental units of the population. If competition acts on a longer range than facilitation, these groups are isolated units that cannot interact with one another. This results in the component Allee effect impacting only the demographics of a single group, i.e. demographic group Allee effect, and therefore the birth/death dynamics within a group is only determined by the number of individuals in it. A consequence of groups becoming independent units is the absence of the demographic Allee effect at the global population scale. Conversely, when the facilitation range is higher than the competition's, groups start to interact. In this scenario, the fitness of a group increases in the presence of neighbors. This positive correlation scales to the population level and creates an emergent demographic Allee effect in the global population dynamics. If the growth rate is low enough, the inter-group facilitation can also result in the existence of a minimum number of groups to ensure population survival.

Traditionally, group-level Allee effects like the ones described above are studied by meta-population models, that assume a fixed spatial organization of the groups of organisms. Because these models impose the spatial structure of the population rather than allowing it to emerge, they do not allow us to compare the population dynamics across spatial structures while fixing the individual-level demographic processes. Our approach, similarly to [31], differs from those models by explicitly considering the range of interaction for both reproductive facilitation and crowding effects. As a consequence, groups emerge naturally out of these individual-level processes. By shifting the scale of the system that we are interested in throughout our analysis, we are able to use different tools from statistical physics to predict the emergent properties of the model. This bottom-

up mechanistic approach allows us to identify how each individual-level process impacts each of the population-level characteristics of demographic Allee effects.

Beyond group-level processes, spatial heterogeneities in population density benefit population survival. In our model, organism aggregation minimizes competition, resulting in larger global population sizes that are less prone to extinction due to demographic fluctuations [44]. This happens because the formation of groups is a response to long-range competition. In addition, aggregation lowers the Allee threshold significantly, favoring the persistence of a local population at lower densities. This local decrease in the Allee threshold is different from the effective decrease in the global Allee threshold already discussed here. The first occurs due to a decrease in the actual value of the Allee threshold, while the latter is related to its locality. Finally, this minimization of competition allows aggregated populations to survive in harsher environments than uniformly distributed ones. That is, uniformly distributed populations exhibit a higher value of $\tilde{r}$ than populations that develop self-organized spatial patterns, which is in accordance with the literature [31]. Our approach, however, is able to explicitly show why this happens and to obtain an expression for $\tilde{r}$ out of the individual-level rates and scales that define the individual-level processes.

Our model provides the simplest framework to study Allee effects across levels of spatial organization. To give the minimal description able to capture all the complexity exhibited by populations subjected to Allee effects, we made some simplifying model assumptions. As previously discussed, we chose the reproduction facilitation component Allee effect. This assumption can be easily changed by modifying the set of individual-level demographic reactions to encompass other fitness components. Also, we assume that the rate of a long-range interaction is the same provided that the interacting individuals are within a range. Mathematically, this defines the shape of the interaction kernel as a top-hat function. The choice of another kernel would not change our results provided that they lead to spatial pattern formation [87, 108, 113]. Different mechanisms responsible for spatial pattern formation could also be considered and our results would hold, provided that spatial patterns emerge in the form of clumps of population density. We choose long-range interactions, which ultimately lead to pattern formation, because it is the most straightforward mechanism to create non-uniform spatial organization [88]. An interesting direction for future research, however, would be to consider alternative pattern-forming interactions, such as density-dependent movement or resource-consumer interactions, lead-

ing to a larger variety of spatial patterns in population density, such as labyrinths, gaps and rings [107, 114, 115, 116, 117]. Another possible direction to deepen our understanding of the inter-group facilitation network is to study how local perturbations affect population dynamics when groups interact, more specifically, how local extinctions caused by these perturbations spread through the network of interacting groups of organisms. Finally, our modeling framework is also easily extendable to include interactions between several species [118, 119], thus providing a theoretical tool to investigate community-level consequences of different component Allee effects.

To summarize our results, this work established three main ways that aggregation can influence population dynamics in the presence of Allee effects. First, aggregation enhances population density locally and thus allows the population to persist in harsh environments where uniformly distributed individuals would go extinct. Second, aggregation results in localized sub-populations that follow independent dynamics from one another and might eliminate the population-level Allee effect. Finally, aggregation decreases competition by limiting its effect to individuals within the same group. Consequently, aggregation reduces the Allee threshold and increases the total population size. More generally, our work emphasizes the potential that models developed from a rigorous description of the individual-level interactions and processes have to improve our understanding of observed patterns and trends in population dynamics.

Bibliography

[1] Philip A Stephens, William J Sutherland, and Robert P Freckleton. What is the Allee effect? *Oikos*, pages 185–190, 1999.

[2] Don R Levitan. The Allee effect in the sea. *Marine Conservation Biology: the science of maintaining the sea's biodiversity*, pages 47–57, 2005.

[3] Franck Courchamp, Ludek Berec, and Joanna Gascoigne. *Allee effects in ecology and conservation*. OUP Oxford, 2008.

[4] Russell Lande. Extinction thresholds in demographic models of territorial populations. *The American Naturalist*, 130(4):624–635, 1987.

[5] Gui-Quan Sun. Mathematical modeling of population dynamics with Allee effect. *Nonlinear Dynamics*, 85(1):1–12, 2016.

[6] Daniel Oro. Extinction, nonlinear dynamics, and sociality. In *Perturbation, behavioural feedbacks, and population dynamics in social animals: when to leave and where to go* [111], pages 114–127.

[7] H Allen Orr. Fitness and its role in evolutionary genetics. *Nature Reviews Genetics*, 10(8):531–539, 2009.

[8] JM Drake and AM Kramer. Allee effects. *Nature Education Knowledge*, 3(10):2, 2011.

[9] WC Allee and Edith S Bowen. Studies in animal aggregations: mass protection against colloidal silver among goldfishes. *Journal of Experimental Zoology*, 61(2):185–207, 1932.

[10] Philip A Stephens, Fredy Frey-roos, Walter Arnold, and Wlliam J Sutherland. Model complexity and population predictions. the alpine marmot as a case study. *Journal of Animal Ecology*, 71(2):343–361, 2002.

[11] WC Allee and GM Rosenthal. Group survival value for philodina rosola, a rotifer. *Ecology*, 30(3):395–397, 1949.

[12] Jaboury Ghazoul. Buzziness as usual? Questioning the global pollination crisis. *Trends in ecology & evolution*, 20(7):367–373, 2005.

[13] Dina KN Dechmann, Bart Kranstauber, David Gibbs, and Martin Wikelski. Group hunting—a reason for sociality in molossid bats? *PLoS one*, 5(2):e9012, 2010.

[14] Katarzyna Nowak and Phyllis C Lee. Demographic structure of zanzibar red colobus populations in unprotected coral rag and mangrove forests. *International Journal of Primatology*, 32(1):24–45, 2011.

[15] Tamaini V Snaith and Colin A Chapman. Red colobus monkeys display alternative behavioral responses to the costs of scramble competition. *Behavioral Ecology*, 19(6):1289–1296, 2008.

[16] Elena Angulo, Greg SA Rasmussen, David W Macdonald, and Franck Courchamp. Do social groups prevent Allee effect related extinctions?: The case of wild dogs. *Frontiers in zoology*, 10(1):1–14, 2013.

[17] Gloria M Luque, Tatiana Giraud, and Franck Courchamp. Allee effects in ants. *Journal of Animal Ecology*, 82(5):956–965, 2013.

[18] Elena Angulo, Gloria M Luque, Stephen D Gregory, John W Wenzel, Carmen Bessa-Gomes, Ludek Berec, and Franck Courchamp. Allee effects in social species. *Journal of Animal Ecology*, 87(1):47–58, 2018.

[19] Brian Dennis. Allee effects: population growth, critical density, and the chance of extinction. *Natural Resource Modeling*, 3(4):481–538, 1989.

[20] Martin Liermann and Ray Hilborn. Depensation: evidence, models and implications. *Fish and Fisheries*, 2(1):33–58, 2001.

[21] Ksenia Tcheslavskaia, Carlyle C Brewster, and Alexei A Sharov. Mating success of gypsy moth (lepidoptera: Lymantriidae) females in southern wisconsin. *The Great Lakes Entomologist*, 35(1):1, 2002.

[22] KA Garrett and RL Bowden. An Allee effect reduces the invasive potential of tilletia indica. *Phytopathology*, 92(11):1152–1159, 2002.

[23] Tia-Lynn Ashman, Tiffany M Knight, Janette A Steets, Priyanga Amarasekare, Martin Burd, Diane R Campbell, Michele R Dudash, Mark O

Johnston, Susan J Mazer, Randall J Mitchell, et al. Pollen limitation of plant reproduction: ecological and evolutionary causes and consequences. *Ecology*, 85(9):2408–2421, 2004.

[24] Stuart Wagenius. Scale dependence of reproductive failure in fragmented echinacea populations. *Ecology*, 87(4):931–941, 2006.

[25] Arantzazu L Luzuriaga, Adrian Escudero, María José Albert, and Luis Giménez-Benavides. Population structure effect on reproduction of a rare plant: beyond population size effect. *Botany*, 84(9):1371–1379, 2006.

[26] Carolyn J Lundquist and Louis W Botsford. Estimating larval production of a broadcast spawner: the influence of density, aggregation, and the fertilization Allee effect. *Canadian Journal of Fisheries and Aquatic Sciences*, 68(1):30–42, 2011.

[27] Claire Guy, David Smyth, and Dai Roberts. The importance of population density and inter-individual distance in conserving the european oyster ostrea edulis. *Journal of the Marine Biological Association of the United Kingdom*, 99(3):587–593, 2019.

[28] Andrew M Kramer, Brian Dennis, Andrew M Liebhold, and John M Drake. The evidence for Allee effects. *Population Ecology*, 51(3):341–354, 2009.

[29] Andrew R Kanarek, Colleen T Webb, Michael Barfield, and Robert D Holt. Allee effects, aggregation, and invasion success. *Theoretical ecology*, 6(2):153–164, 2013.

[30] AD Rijnsdorp and B van Vingerhoed. Feeding of plaice pleuronectes platessa l. and sole solea solea (l.) in relation to the effects of bottom trawling. *Journal of Sea Research*, 45(3-4):219–229, 2001.

[31] Anudeep Surendran, Michael J. Plank, and Matthew J. Simpson. Population dynamics with spatial structure and an Allee effect. *Proceedings of the Royal Society A: Mathematical, Physical and Engineering Sciences*, 476:1–19, 2020.

[32] Warder Clyde Allee. *Social life of animals.* Number Edn 1. William Heineman Ltd, London and Toronto, 1938.

[33] Solenn Le Cadre, Thomas Tully, Susan J Mazer, Jean-Baptiste Ferdy, Jacques Moret, and Nathalie Machon. Allee effects within small populations of *Aconitum napellus ssp. lusitanicum*, a protected subspecies in Northern France. *New Phytologist*, 179(4):1171–1182, 2008.

[34] Brian R Silliman, Elizabeth Schrack, Qiang He, Rebecca Cope, Amanda Santoni, Tjisse van der Heide, Ralph Jacobi, Mike Jacobi, and Johan van de Koppel. Facilitation shifts paradigms and can amplify coastal restoration efforts. *Proceedings of the National Academy of Sciences*, 112(46):14295–14300, 2015.

[35] Brian A Lerch, Ben C Nolting, and Karen C Abbott. Why are demographic Allee effects so rarely seen in social animals? *Journal of Animal Ecology*, 87(6):1547–1559, 2018.

[36] Rosie Woodroffe, Helen MK O'Neill, and Daniella Rabaiotti. Within-and between-group dynamics in an obligate cooperative breeder. *Journal of Animal Ecology*, 89(2):530–540, 2020.

[37] Vito Volterra. Population growth, equilibria, and extinction under specified breeding conditions: a development and extension of the theory of the logistic curve. *Human Biology*, 10(1):1–11, 1938.

[38] VA Kostitzin. Sur la loi logistique et ses généralisations. *Acta Biotheoretica*, 5(3):155–159, 1940.

[39] PML Tammes, H Klomp, and Maj Van Montfort. Sexual reproduction and underpopulation. *Archives Néerlandaises de Zoologie*, 16(1):105–110, 1964.

[40] Ping-Hwa Hsu and AG Fredrickson. Population-changing processes and the dynamics of sexual populations. *Mathematical Biosciences*, 26(1-2):55–78, 1975.

[41] Marjorie A Asmussen. Density-dependent selection ii. the Allee effect. *The American Naturalist*, 114(6):796–809, 1979.

[42] JM Cushing. The Allee effect in age-structured population dynamics. In Thomas G Hallam, LJ Gross, and SA Levin, editors, *Mathematical Ecology-Proceedings Of The Autumn Course Research Seminars International Ctr For Theoretical Physics*, pages 479–505. World Scientific Publ., 1988.

[43] Brian Dennis. Extinction and waiting times in birth-death processes: applications to endangered species and insect pest control. *Statistical distributions in scientific work*, 6:289–301, 1981.

[44] Brian Dennis. Allee effects in stochastic populations. *Oikos*, 96(3):389–401, 2002.

[45] Vicenç Méndez, Michael Assaf, Axel Masó-Puigdellosas, Daniel Campos, and Werner Horsthemke. Demographic stochasticity and extinction in populations with Allee effect. *Physical Review E*, 99(2):022101, 2019.

[46] Vıctor Padrón and Marıa Cristina Trevisan. Effect of aggregating behavior on population recovery on a set of habitat islands. *Mathematical biosciences*, 165(1):63–78, 2000.

[47] Gabriel Andreguetto Maciel and Frithjof Lutscher. Allee effects and population spread in patchy landscapes. *Journal of Biological Dynamics*, 9(1):109–123, 2015.

[48] Timothy H Keitt, Mark A Lewis, and Robert D Holt. Allee effects, invasion pinning, and species' borders. *The American Naturalist*, 157(2):203–216, 2001.

[49] Michael Begon, John L Harper, Colin R Townsend, et al. *Ecology. Individuals, populations and communities.* Blackwell scientific publications, 1986.

[50] Harold Sellers Colton. Some effects of environment on the growth of lymnaea columella say. *Proceedings of the Academy of Natural Sciences of Philadelphia*, pages 410–448, 1908.

[51] Raymond Pearl. *The biology of population growth*. New York: AA Knopf, 1926.

[52] Joseph H Connell. On the prevalence and relative importance of interspecific competition: evidence from field experiments. *The American Naturalist*, 122(5):661–696, 1983.

[53] Eric J Chapman and Carrie J Byron. The flexible application of carrying capacity in ecology. *Global ecology and conservation*, 13:e00365, 2018.

[54] Warder Clyde Allee, Orlando Park, Alfred E Emerson, Thomas Park, Karl P Schmidt, et al. *Principles of Animal Ecology.* Number Edn 1. WB Saundere Co. Ltd., 1949.

[55] Tim Clutton-Brock. Cooperation between non-kin in animal societies. *Nature*, 462(7269):51–57, 2009.

[56] Robert Axelrod and William D Hamilton. The evolution of cooperation. *science*, 211(4489):1390–1396, 1981.

[57] Stuart A West, Ashleigh S Griffin, and Andy Gardner. Social semantics: altruism, cooperation, mutualism, strong reciprocity and group selection. *Journal of evolutionary biology*, 20(2):415–432, 2007.

[58] Martin A Nowak, Corina E Tarnita, and Edward O Wilson. The evolution of eusociality. *Nature*, 466(7310):1057–1062, 2010.

[59] Martin A Nowak. *Evolutionary dynamics: exploring the equations of life*. Harvard university press, 2006.

[60] Warder Clyde Allee. Animal aggregations. *The Quarterly Review of Biology*, 2(3):367–398, 1927.

[61] Joanna Gascoigne, Ludek Berec, Stephen Gregory, and Franck Courchamp. Dangerously few liaisons: a review of mate-finding allee effects. *Population Ecology*, 51:355–372, 2009.

[62] EUGENE P Odum. Fundamentals of ecology. xii, 387 pp. *W. B. Saunders Co., Philadelphia, Pennsylvania, and London, England*, 1953.

[63] Joanna C Gascoigne and Romuald N Lipcius. Allee effects driven by predation. *Journal of Applied Ecology*, 41(5):801–810, 2004.

[64] Gloria M Luque, Chloé Vayssade, Benoît Facon, Thomas Guillemaud, Franck Courchamp, and Xavier Fauvergue. The genetic allee effect: a unified framework for the genetics and demography of small populations. *Ecosphere*, 7(7):e01413, 2016.

[65] Sedeer el Showk. The meaning of fitness, 2014.

[66] Quinn MR Webber and Craig KR Willis. An experimental test of effects of ambient temperature and roost quality on aggregation by little brown bats (myotis lucifugus). *Journal of Thermal Biology*, 74:174–180, 2018.

[67] Gabrielle Thiébaut, Michèle Tarayre, and Héctor Rodríguez-Pérez. Allelopathic effects of native versus invasive plants on one major invader. *Frontiers in plant science*, 10:854, 2019.

[68] Julie A Teichroeb and Pascale Sicotte. Cost-free vigilance during feeding in folivorous primates? examining the effect of predation risk, scramble competition, and infanticide threat on vigilance in ursine colobus monkeys (colobus vellerosus). *Behavioral Ecology and Sociobiology*, 66:453–466, 2012.

[69] Craig B Stanford. Avoiding predators: Expectations and evidence in primate antipredator behavior. *International Journal of Primatology*, 23(4), 2002.

[70] Gerald S Wilkinson. Information transfer at evening bat colonies. *Animal Behaviour*, 44:501–518, 1992.

[71] Gerald S Wilkinson and Janette Wenrick Boughman. Social calls coordinate foraging in greater spear-nosed bats. *Animal Behaviour*, 55(2):337–350, 1998.

[72] Andrew M Kramer and John M Drake. Experimental demonstration of population extinction due to a predator-driven allee effect. *Journal of Animal Ecology*, 79(3):633–639, 2010.

[73] Crawford S Holling. The components of predation as revealed by a study of small-mammal predation of the european pine sawfly1. *The canadian entomologist*, 91(5):293–320, 1959.

[74] Jonathan M Jeschke, Michael Kopp, and Ralph Tollrian. Predator functional responses: discriminating between handling and digesting prey. *Ecological monographs*, 72(1):95–112, 2002.

[75] WA Foster and JE Treherne. Evidence for the dilution effect in the selfish herd from fish predation on a marine insect. *Nature*, 293(5832), 1981.

[76] David H Reed and Richard Frankham. Correlation between fitness and genetic diversity. *Conservation biology*, 17(1):230–237, 2003.

[77] Richard Frankham. Inbreeding and extinction: island populations. *Conservation biology*, 12(3):665–675, 1998.

[78] Ilik Saccheri, Mikko Kuussaari, Maaria Kankare, Pia Vikman, Wilhelm Fortelius, and Ilkka Hanski. Inbreeding and extinction in a butterfly metapopulation. *Nature*, 392(6675):491–494, 1998.

[79] Yvonne Willi, Josh Van Buskirk, and Markus Fischer. A threefold genetic allee effect: population size affects cross-compatibility, inbreeding depression and drift load in the self-incompatible ranunculus reptans. *Genetics*, 169(4):2255–2265, 2005.

[80] Markus Fischer, Michael Hock, and Melanie Paschke. Low genetic variation reduces cross-compatibility and offspring fitness in populations of a narrow endemic plant with a self-incompatibility system. *Conservation genetics*, 4:325–336, 2003.

[81] DR Levitan. Skeletal changes in the test and jaws of the sea urchin diadema antillarum in response to food limitation. *Marine Biology*, 111:431–435, 1991.

[82] Caz M Taylor and Alan Hastings. Allee effects in biological invasions. *Ecology Letters*, 8(8):895–908, 2005.

[83] Deborah E Shelton and Richard E Michod. Group and individual selection during evolutionary transitions in individuality: meanings and partitions. *Philosophical Transactions of the Royal Society B*, 375(1797):20190364, 2020.

[84] MA Fuentes, MN Kuperman, and VM Kenkre. Nonlocal interaction effects on pattern formation in population dynamics. *Physical review letters*, 91(15):158104, 2003.

[85] Eduardo H Colombo, Ricardo Martínez-García, Cristóbal López, and Emilio Hernández-García. Spatial eco-evolutionary feedbacks mediate coexistence in prey-predator systems. *Scientific Reports*, 9(1):18161, 2019.

[86] Ricardo Martinez-Garcia, Ciro Cabal, Justin M Calabrese, Emilio Hernández-García, Corina E Tarnita, Cristóbal López, and Juan A Bonachela. Integrating theory and experiments to link local mechanisms and ecosystem-level consequences of vegetation patterns in drylands. *Chaos, Solitons & Fractals*, 166:112881, 2023.

[87] Ricardo Martínez-García, Justin M Calabrese, Emilio Hernández-García, and Cristóbal López. Vegetation pattern formation in semiarid systems

without facilitative mechanisms. *Geophysical Research Letters*, 40(23):6143–6147, 2013.

[88] Ricardo Martínez-García, Justin M Calabrese, Emilio Hernández-García, and Cristóbal López. Minimal mechanisms for vegetation patterns in semiarid regions. *Philosophical Transactions of the Royal Society A: Mathematical, Physical and Engineering Sciences*, 372(2027):20140068, 2014.

[89] Nicolas Barbier, Pierre Couteron, René Lefever, Vincent Deblauwe, and Olivier Lejeune. Spatial decoupling of facilitation and competition at the origin of gapped vegetation patterns. *Ecology*, 89(6):1521–1531, 2008.

[90] Gabriel Andreguetto Maciel and Ricardo Martinez-Garcia. Enhanced species coexistence in lotka-volterra competition models due to nonlocal interactions. *Journal of Theoretical Biology*, 530:110872, 2021.

[91] Corina E Tarnita, Juan A Bonachela, Efrat Sheffer, Jennifer A Guyton, Tyler C Coverdale, Ryan A Long, and Robert M Pringle. A theoretical foundation for multi-scale regular vegetation patterns. *Nature*, 541(7637):398–401, 2017.

[92] Quan-Xing Liu, Peter MJ Herman, Wolf M Mooij, Jef Huisman, Marten Scheffer, Han Olff, and Johan Van De Koppel. Pattern formation at multiple spatial scales drives the resilience of mussel bed ecosystems. *Nature communications*, 5(1):5234, 2014.

[93] Volker Grimm and Steven F Railsback. *Individual-based modeling and ecology*. Princeton university press, 2005.

[94] Brian Dennis. Allee effects in stochastic populations. *Oikos*, 96(3):389–401, 2002.

[95] D. Crews, M. Grassman, and J. Lindzey. Behavioral facilitation of reproduction in sexual and unisexual whiptail lizards. *Proceedings of the National Academy of Sciences of the United States of America*, 83(24):9547–9550, 1986.

[96] J. D. Thomas and M. Benjamin. The Effects of Population Density on Growth and Reproduction of Biomphalaria glabrata (Say) (Gasteropoda: Pulmonata). *The Journal of Animal Ecology*, 43(1):31, 1974.

[97] Raúl Toral and Pere Colet. *Stochastic numerical methods: an introduction for students and scientists*. John Wiley & Sons, 2014.

[98] Daniel T Gillespie. A general method for numerically simulating the stochastic time evolution of coupled chemical reactions. *Journal of computational physics*, 22(4):403–434, 1976.

[99] Daniel T Gillespie. Exact stochastic simulation of coupled chemical reactions. *The journal of physical chemistry*, 81(25):2340–2361, 1977.

[100] Masao Doi. Stochastic theory of diffusion-controlled reaction. *Journal of Physics A: Mathematical and General*, 9(9):1479, 1976.

[101] Luca Peliti. Path integral approach to birth-death processes on a lattice. *Journal de Physique*, 46(9):1469–1483, 1985.

[102] U. C. Täuber. *Field-Theory Approaches to Nonequilibrium Dynamics*, pages 295–348. Springer Berlin Heidelberg, Berlin, Heidelberg, 2007.

[103] Emilio Hernández-García and Cristóbal López. Clustering, advection, and patterns in a model of population dynamics with neighborhood-dependent rates. *Physical Review E*, 70(1):016216, 2004.

[104] David J Griffiths and Darrell F Schroeter. *Introduction to quantum mechanics*. Cambridge university press, 2018.

[105] JL Cardy. The mathematical beauty of physics, 1996.

[106] Mark C Cross and Pierre C Hohenberg. Pattern formation outside of equilibrium. *Reviews of modern physics*, 65(3):851, 1993.

[107] Max Rietkerk and Johan Van de Koppel. Regular pattern formation in real ecosystems. *Trends in ecology & evolution*, 23(3):169–175, 2008.

[108] Simone Pigolotti, Cristóbal López, and Emilio Hernández-García. Species clustering in competitive lotka-volterra models. *Physical review letters*, 98(25):258101, 2007.

[109] Ricardo Martinez-Garcia, Ciro Cabal, Justin M Calabrese, Emilio Hernández-García, Corina E Tarnita, Cristóbal López, and Juan A Bonachela. Integrating theory and experiments to link local mechanisms

and ecosystem-level consequences of vegetation patterns in drylands. *Chaos, Solitons & Fractals*, 166:112881, 2023.

[110] Mark Kot. Harvest models: bifurcations and breakpoints. In *Elements of Mathematical Ecology*, pages 13–25. Cambridge University Press, 2001.

[111] Daniel Oro. *Perturbation, behavioural feedbacks, and population dynamics in social animals: when to leave and where to go*. Oxford University Press, USA, 2020.

[112] Rosie Woodroffe. Demography of a recovering african wild dog (lycaon pictus) population. *Journal of Mammalogy*, 92(2):305–315, 2011.

[113] Eduardo H Colombo, Cristóbal López, and Emilio Hernández-García. Pulsed interaction signals as a route to biological pattern formation. *Physical Review Letters*, 130(5):058401, 2023.

[114] Quan-Xing Liu, Arjen Doelman, Vivi Rottschäfer, Monique de Jager, Peter MJ Herman, Max Rietkerk, and Johan van de Koppel. Phase separation explains a new class of self-organized spatial patterns in ecological systems. *Proceedings of the National Academy of Sciences*, 110(29):11905–11910, 2013.

[115] Feng Rao and Yun Kang. The complex dynamics of a diffusive prey–predator model with an Allee effect in prey. *Ecological complexity*, 28:123–144, 2016.

[116] Ricardo Martinez-Garcia, Clara Murgui, Emilio Hernández-García, and Cristóbal López. Pattern Formation in Populations with Density-Dependent Movement and Two Interaction Scales. *PLoS ONE*, 10:e0132261, 2015.

[117] Ricardo Martinez-Garcia, Corina E. Tarnita, and Juan A. Bonachela. Self-organized patterns in ecological systems: from microbial colonies to landscapes. *Emerging Topics in Life Sciences*, 6(3):245–258, 2022.

[118] Gabriel Andreguetto Maciel and Ricardo Martinez-Garcia. Enhanced species coexistence in Lotka-Volterra competition models due to nonlocal interactions. *Journal of Theoretical Biology*, 530:110872, 2021.

[119] Mario I Simoy and Marcelo N Kuperman. Non-local interaction effects in models of interacting populations. *Chaos, Solitons & Fractals*, 167:112993, 2023.

[120] Johannes Knebel. Application of statistical field theory to reaction-diffusion problems. *University of Cambridge*, 2010.

[121] Simone Cenci, Gunnar Pruessner, and Ettore Vicari. A field theoretical approach to stationarity in reaction-diffusion processes. 2015.

[122] Uwe C Täuber, Martin Howard, and Benjamin P Vollmayr-Lee. Applications of field-theoretic renormalization group methods to reaction–diffusion problems. *Journal of Physics A: Mathematical and General*, 38(17):R79, 2005.

[123] Raúl Montagne, Emilio Hernández-García, A Amengual, and Maxi San Miguel. Wound-up phase turbulence in the complex ginzburg-landau equation. *Physical Review E*, 56(1):151, 1997.

Appendix A

Path-integral representation

In this appendix, we focus on mapping this formalism into a field theory by constructing path integrals.

A.0.1 Coherent states

In order to start with the field theory for the Doi-Peliti formalism, we must define the coherent states $|\phi\rangle$. Those states are the eigenvectors of the annihilation operator a, so that:

$$a_i |\phi_i\rangle = \phi_i |\phi_i\rangle . \tag{A.1}$$

With $\phi_i \in \mathbb{C}$ We can write any vector on the Fock space from the basis vectors. Thus focusing on the site i of the lattice:

$$|\phi_i\rangle = \sum_{n_i} c_{n_i} |n_i\rangle . \tag{A.2}$$

Acting with the annihilation operator on the expression above

$$a_i |\phi_i\rangle = \sum_{n_i=0} c_{n_i} a_i |n_i\rangle \tag{A.3}$$

$$\phi_i |\phi_i\rangle = \sum_{n_i=1} c_{n_i} n_i |n_i - 1\rangle . \tag{A.4}$$

Expanding the left side of the equation with the basis vectors

$$\phi_i \sum_{n_i=0} c_{n_i} |n_i\rangle = \sum_{n_i=1} c_{n_i} n_i |n_i - 1\rangle \tag{A.5}$$

$$\phi_i \sum_{n_i=1} c_{n_i-1} |n_i - 1\rangle = \sum_{n_i=1} c_{n_i} n_i |n_i - 1\rangle \tag{A.6}$$

That is

$$\phi_i c_{n_i} = n_i c_{n_i - 1}. \tag{A.7}$$

Which, by applying it over and over, we obtain

$$c_n = c_0 \frac{\phi_i^{n_i}}{n_i!}. \tag{A.8}$$

The only free parameter is the first coefficient c_0. Thus, if we set that $\langle \phi_i | \, \phi_i \rangle \equiv 1$

$$\langle \phi_i | \, \phi_i \rangle = |c_0|^2 \sum_{n_i} \sum_{n_i'} \frac{(\phi_i^*)^{n_i}}{n_i!} \frac{(\phi_i)^{n_i'}}{n_i'!} \langle n_i | \, n_i' \rangle = |c_0|^2 \sum_{n_i} \frac{\left(|\phi_i|^2\right)^{n_i}}{n_i!} = |c_0|^2 e^{|\phi_i|^2} = 1. \tag{A.9}$$

Remembering that $\langle n_i | n_i' \rangle = n_i! \delta_{n_i, n_i'}$. Thus, $c_0 = e^{-\frac{|\phi_i|^2}{2}}$. Joining everything, we can write a coherent state as

$$|\phi_i\rangle = e^{-\frac{|\phi_i|^2}{2}} \sum_{n_i=0} \frac{\phi_i^{n_i}}{n_i!} |n_i\rangle = e^{-\frac{|\phi_i|^2}{2} + a_i^\dagger \phi_i} |0\rangle . \tag{A.10}$$

If one has two different coherent states and projects one to the other

$$\langle \varphi | \, \phi \rangle = e^{-\frac{|\phi|^2}{2} - \frac{|\varphi|^2}{2}} \sum_{n=0} \sum_{n'=0} \frac{(\varphi^*)^{n'}}{n'!} \frac{(\phi)^n}{n!} \langle n' | \, n \rangle = e^{-\frac{|\phi|^2}{2} - \frac{|\varphi|^2}{2}} \sum_{n=0} \frac{(\varphi^* \phi)^n}{n!} \tag{A.11}$$

$$= \exp\left(-\frac{|\phi|^2}{2} - \frac{|\varphi|^2}{2} + \varphi^* \phi \right). \tag{A.12}$$

Now that we have those states, let's show an important identity. First, lets once more drop the lattice indexes for the sake of clarity

$$\mathbb{I} = \sum_n \frac{1}{n!} |n\rangle \langle n| = \sum_n \sum_m \frac{1}{n!} |n\rangle \langle m| \, \delta_{m,n}. \tag{A.13}$$

Using the identity $\delta_{mn} = \frac{1}{\pi m!} \int d^2\phi e^{-|\phi|^2} (\phi^*)^m \phi^n$:

$$\mathbb{I} = \sum_n \sum_m \frac{1}{n!} |n\rangle \langle m| \frac{1}{\pi m!} \int d^2\phi \, e^{-|\phi|^2} (\phi^*)^m \phi^n \tag{A.14}$$

$$= \frac{1}{\pi} \int \sum_n \sum_m d^2\phi \, e^{-|\phi|^2} \frac{\phi^n}{n!} |n\rangle \langle m| \frac{(\phi^*)^m}{m!} \tag{A.15}$$

where the integration measure is $d^2\phi = d\phi d\phi^*$. From the definition of the coherent states

$$\mathbb{I} = \frac{1}{\pi} \int d^2\phi \; |\phi\rangle \langle\phi| \, . \tag{A.16}$$

This can be generalized to the lattice notation

$$\mathbb{I} = \int \prod_i \frac{d^2\phi_i}{\pi} \; |\{\phi\}\rangle \langle\{\phi\}| \, . \tag{A.17}$$

Whereby we introduce the multiple particle coherent state $|\{\phi\}\rangle = |\phi_1\rangle \otimes |\phi_2\rangle \otimes |\phi_3\rangle \otimes \ldots$.

A.0.2 Path integrals

Now, we get to the point where we can introduce the path integrals for the Doi-Peliti formalism. This field theory of the stochastic processes will appear naturally as we, finally, apply the continuum limit in the lattice. However, to set the stage for this limit, we need to play around with some mathematical relations. The first one was just derived from the previous section (A.17). The other is obtained by splitting the time interval $(0, t)$ in N very small pieces with length $\delta t = t/N$. Thus, we can rewrite the exponential of the hamiltonian as

$$e^{-\hat{H}t} = \lim_{\substack{\delta t \to 0 \\ N \to \infty}} (1 - \delta t \tilde{H})^{t/\delta t} \tag{A.18}$$

$$= \lim_{\substack{\delta t \to 0 \\ N \to \infty}} \underbrace{(1 - \delta t \tilde{H}) \cdot (1 - \delta t \tilde{H}) \cdots (1 - \delta t \tilde{H})}_{N \text{ pieces}} . \tag{A.19}$$

Now, we can insert the identity (A.17) in between those pieces

$$e^{-\hat{H}t} = \lim_{\substack{\delta t\to 0\\ N\to\infty}} \mathbb{I}\cdot(1-\delta t\tilde{H})\cdot\mathbb{I}\cdot(1-\delta t\tilde{H})\cdot\mathbb{I}\ldots\mathbb{I}\cdot(1-\delta t\tilde{H})\cdot\mathbb{I} \tag{A.20}$$

$$= \lim_{\substack{\delta t\to 0\\ N\to\infty}} \int \prod_i \prod_k^N \left(\frac{d\phi_i(t_k)d\phi_i^*(t_k)}{\pi}\right) |\{\phi(t)\}\rangle \langle\{\phi(t)\}| (1-\delta t\tilde{H})\times \tag{A.21}$$

$$\times |\{\phi(t-\delta t)\}\rangle \langle\{\phi(t-\delta t)\}| (1-\delta t\tilde{H})\ldots(1-\delta t\tilde{H}) |\{\phi(0)\}\rangle \langle\{\phi(0)\}| \tag{A.22}$$

We want to insert this expression on the expected value of an observable (4.91). However, as we can see, the expression becomes very large very fast. Thus, we need to work with it piece by piece. The full expression is given by

$$\langle A\rangle = \langle 0|\,\tilde{A}\left(\left\{a_i^\dagger, a_i\right\}\right)\ldots \text{ Expression (A.22) } \ldots \prod_j e^{\langle n_0\rangle a_j^\dagger}|0\rangle\,. \tag{A.23}$$

The term on the left is

$$\langle 0|\,\tilde{A}\left(\left\{a_i^\dagger, a_i\right\}\right)|\{\phi(t)\}\rangle = \langle 0|\,A\left(\left\{a_i^\dagger\to\mathbb{I}, a_i\right\}\right)|\{\phi(t)\}\rangle\,. \tag{A.24}$$

We can do this because A is normal ordered. Then, we must remember that the coherent state is an eigenvector of the annihilation operator a_i. This leads to

$$\langle 0|\,A\left(\left\{a_i^\dagger\to\mathbb{I}, a_i\right\}\right)|\{\phi(t)\}\rangle = \langle 0|\,\{\phi(t)\}\rangle\, A\left(\phi(t)\right) \tag{A.25}$$

The notation $A\left(\phi(t)\right) \equiv A\left(\{1,\phi(t)\}\right)$. Now, we only need to obtain $\langle 0|\,\{\phi(t)\}\rangle$, from the definition of the multiple particle coherent state

$$\langle 0|\,\{\phi(t)\}\rangle = \prod_i \langle 0|\,\phi_i(t)\rangle = \prod_i e^{-\frac{|\phi_i(t)|^2}{2}} \sum_{n_i=0} \frac{\phi_i(t)^{n_i}}{n_i!}\langle 0|n_i\rangle = \exp\left(-\sum_i \frac{|\phi_i(t)|^2}{2}\right). \tag{A.26}$$

The terms in the middle of (A.23) are going to be in the form

$$\langle\{\phi(t_k+\delta t)\}|\left(1-\delta t\tilde{H}\left(\left\{a_i^\dagger,a_i\right\}\right)\right)|\{\phi(t_k)\}\rangle\,. \tag{A.27}$$

Since the quasi-Hamiltonian is normal ordered, we can just use the fact that the coherent state and its conjugate are eigenvectors of a_i and $a_i^\dagger$, respectively. This leads us with:

$$\langle\{\phi(t_k+\delta t)\}|\{\phi(t_k)\}\rangle\left(1-\delta t\tilde{H}\left(\phi_i^*(t_k+\delta t),\phi_i(t_k)\right)\right). \tag{A.28}$$

The projection between two coherent states was already derived in (A.12). Thus the term $\langle\{\phi(t_k+\delta t)\}|\{\phi(t_k)\}\rangle$ becomes

$$\langle\{\phi(t_k+\delta t)\}|\{\phi(t_k)\}\rangle=\prod_i\langle\phi_i(t_k+\delta t)|\phi_i(t_k)\rangle \tag{A.29}$$

$$=\exp\left(\sum_i-\frac{|\phi_i(t_k+\delta t)|^2}{2}-\frac{|\phi_i(t_k)|^2}{2}+\phi_i^*(t_k+\delta t)\phi_i(t_k)\right). \tag{A.30}$$

Finally, the last term of (A.23)

$$\langle\{\phi(0)\}|\prod_j e^{\langle n_0\rangle a_j^\dagger}|0\rangle \tag{A.31}$$

Once again we use the fact that the conjugate of the coherent state is an eigenvector of $a^\dagger$. Thus

$$\langle\{\phi(0)\}|0\rangle\exp\left(\sum_i\langle n_0\rangle\,\phi_i^*(0)\right)=\exp\left(-\sum_i\frac{|\phi_i(0)|^2}{2}+\langle n_0\rangle\,\phi_i^*(0)\right). \tag{A.32}$$

At this point, we have organized the equation such that we got rid of all the bosonic operators. We still have to arrange it in a compact and comprehensible expression. First, we notice that by joining all of the $\left(1-\delta t\tilde{H}\left(\phi_i^*(t_k+\delta t),\phi_i(t_k)\right)\right)$ and assuming that δt is very small

$$\prod_{k}^{N-1}\left(1-\delta t\tilde{H}\left(\phi_i^*(t_k+\delta t),\phi_i(t_k)\right)\right)=\exp\left(\sum_{k}^{N-1}-\delta t\tilde{H}\left(\phi_i^*(t_k),\phi_i(t_k)\right)\right). \quad \text{(A.33)}$$

The δt difference between the arguments of the Hamiltonian is dropped when assuming $\delta t \to 0$ [120, 121, 122]. Now, if we join all of the other terms, we will have

$$\prod_i \exp\left(-\sum_j^{N-1}\left[\frac{|\phi_i(t_j+\delta t)|^2}{2}+\frac{|\phi_i(t_j)|^2}{2}-\phi_i^*(t_j+\delta t)\phi_i(t_j)\right]\right. \quad \text{(A.34)}$$

$$\left.-\frac{|\phi_i(t)|^2}{2}-\frac{|\phi_i(0)|^2}{2}+\langle n_0\rangle\phi_i^*(0)\right). \quad \text{(A.35)}$$

Focusing on the absolute value terms

$$-\sum_{j=0}^{N-1}\left[\frac{|\phi_i(t_j+\delta t)|^2}{2}\right]-\sum_{j=0}^{N-1}\left[\frac{|\phi_i(t_j)|^2}{2}\right]-\frac{|\phi_i(t)|^2}{2}-\frac{|\phi_i(0)|^2}{2}. \quad \text{(A.36)}$$

Since $t_{j+1}=t_j+\delta t$, we can make a shift on the index of the second sum

$$\sum_{j=0}^{N-1}\left[\frac{|\phi_i(t_j)|^2}{2}\right]=\sum_{j=0}^{N-1}\left[\frac{|\phi_i(t_j+\delta t)|^2}{2}\right]+\frac{|\phi_i(0)|^2}{2}-\frac{|\phi_i(t)|^2}{2}. \quad \text{(A.37)}$$

Substituting in (A.36)

$$-\sum_{j}^{N-1}\left[|\phi_i(t_j+\delta t)|^2\right]-|\phi_i(0)|^2. \quad \text{(A.38)}$$

Going back to (A.34)

$$\prod_i \exp\left(-\sum_j^{N-1}\left[|\phi_i(t_j+\delta t)|^2-\phi_i^*(t_j+\delta t)\phi_i(t_j)\right]-|\phi_i(0)|^2+\langle n_0\rangle\phi_i^*(0)\right) \tag{A.39}$$

$$=\prod_i \exp\left(-\sum_j^{N-1}\left[\frac{\phi_i(t_j+\delta t)-\phi_i(t_j)}{\delta t}\phi_i^*(t_j+\delta t)\right]\delta t+\left(\langle n_0\rangle-\phi_i(0)\right)\phi_i^*(0)\right) \tag{A.40}$$

Summing this term with the one of the quasi-Hamiltonian we get, in the limit $\delta t \to 0$

$$=\exp\left(-\left\{\int_0^t\left[\tilde{H}\left(\phi_i^*(\tau),\phi_i(\tau)\right)+\sum_i\phi_i^*(\tau)\partial_\tau\phi_i(\tau)\right]d\tau-\sum_i\left(\langle n_0\rangle-\phi_i(0)\right)\phi_i^*(0)\right\}\right) \tag{A.41}$$

.

Finally, we substitute this result into (A.23)

$$\langle A\rangle=\frac{1}{\mathcal{N}}\int\left(\prod_i\mathcal{D}\left[\phi_i^*(t)\right]\mathcal{D}[\phi_i(t)]\right)A(\phi(t))e^{-S[\phi^*(t),\phi(t)]}. \tag{A.42}$$

with

$$S\left[\phi^*(t),\phi(t)\right]=\left(\int_0^t d\tau\left(\tilde{H}\left(\phi_i^*(\tau),\phi_i(\tau)\right)+\sum_i\phi_i^*(\tau)\partial_\tau\phi_i(\tau)\right)-\sum_i\left(\langle n_0\rangle-\phi_i(0)\right)\phi_i^*(0)\right). \tag{A.43}$$

$\mathcal{D}\phi_i\mathcal{D}\phi_i^*$ represents $\prod_\tau \mathrm{d}\phi_{i,\tau}\mathrm{d}\phi_{i,\tau}^*$ in the limit $\delta t \to 0$. Also, we introduce the normalization factor $\mathcal{N}=\int\prod_i\mathcal{D}\phi_i\mathcal{D}\phi_i^*\exp\left[-S\left(\{\phi^*\},\{\phi\}\right)\right]$. The functional S is the action of the system. We finally get to introduce the continuum spatial limit. In order to do it, we let the lattice spacing $\delta x \to 0$ leading to a field theory. We need to redefine our parameters:

$$\frac{\phi_i(t)}{\delta x^d}\mapsto\phi(x,t),\quad \phi_i^*(t)\mapsto\tilde{\phi}(x,t),\quad \frac{h}{2}\mapsto\frac{D}{\delta x^2},\quad \langle n_0\rangle\mapsto\rho_0=\frac{\langle n_0\rangle}{\delta x^d}. \tag{A.44}$$

Also, this limit will take the sums on the lattice and map them into integrals

$\sum_i \to \delta x^{-d} \int d^d x$. The diffusion part of the quasi-Hamiltonian then becomes, after Doi-shifting and before applying the continuum limit

$$H_h(\phi_i^*(t)+1, \phi_i(t)) = \frac{h}{2} \sum_{\langle ij \rangle} \left(\phi_i^* - \phi_j^*\right) \left(\phi_i - \phi_j\right), \tag{A.45}$$

and after the continuum limit

$$H_h(\tilde{\phi}(x,t)+1, \phi(x,t)) = \int dx D \nabla \tilde{\phi} \cdot \nabla \phi = \int dx D \tilde{\phi} \nabla^2 \phi. \tag{A.46}$$

We played with the ∇'s by integrating by parts and assuming that the fields are zero at $x \to \infty$. Finally, the action in the continuum limit becomes

$$S[\phi^*(x,t), \phi(x,t)] = \int dx \int_0^t d\tau \;\; \tilde{\phi} \partial_\tau \phi + \tilde{\mathcal{H}}[\tilde{\phi}(x,\tau), \phi(x,\tau)]. \tag{A.47}$$

Here we drop the $\phi(0)$ term, since the system will eventually forget about the initial condition. Thus, the expected value of an observable can be obtained by summing over the fields ϕ and $\tilde{\phi}$ and weighting it by the exponential of the action.

A.0.3 Field equations

Now that we have an action that weights the contribution of the fields in the expected value, we can use it to get a mean field approximation for the number of particles. To do this we use the stationary-action principle (also called the least-action principle). Following this principle, the equation of motion for the fields ϕ and $\tilde{\phi}$ will be the ones that satisfy

$$\frac{\delta S}{\delta \phi} = \frac{\delta S}{\delta \tilde{\phi}} = 0. \tag{A.48}$$

Those are functional derivatives, defined as

$$\int \frac{\delta F}{\delta \rho} \beta(x) dx = \lim_{\varepsilon \to 0} \frac{F[\rho + \varepsilon\beta] - F[\rho]}{\varepsilon} = \left[\frac{d}{d\varepsilon} F[\rho + \varepsilon\beta]\right]_{\varepsilon=0}. \tag{A.49}$$

whereby F is a general functional of ρ. Thus, for the action

$$\int\int_0^t \frac{\delta S}{\delta\phi}\beta(\chi,\tau)d\tau d^d\chi = \left\{\frac{d}{d\varepsilon}\int\int_0^t d\tau d^d\chi\ \tilde{\phi}\partial_\tau(\phi+\varepsilon\beta) + \sum_k a_k(\phi\to\phi+\varepsilon\beta)\tilde{\phi}^k\right\}_{\varepsilon\to 0}, \tag{A.50}$$

whereby, we are arranging the quasi-Hamiltonian by the powers of the $\tilde{\phi}$ field, $\mathcal{H} = \sum_k a_k(\phi)\tilde{\phi}^k(x,t)$. Thus, $a_k(\phi)$ is the functional that multiplies the field $\tilde{\phi}$ to the power of k. Bringig the derivative and the limit $\varepsilon \to 0$ inside of the equation

$$\int\int_0^t \frac{\delta S}{\delta\phi}\beta(\chi,\tau)d\tau d^d\chi = \int\int_0^t d\tau d^d\chi\ \tilde{\phi}\partial_\tau\left[\frac{d}{d\varepsilon}(\phi+\varepsilon\beta)\right]_{\epsilon\to 0} + \tag{A.51}$$

$$+\sum_k \tilde{\phi}^k\left[\frac{d}{d\varepsilon}a_k(\phi\to\phi+\varepsilon\beta)\right]_{\epsilon\to 0} \tag{A.52}$$

The most general way of setting this expression to zero, $\dfrac{\delta S}{\delta\phi} = 0$, for any ϕ is to take $\tilde{\phi} = 0$. Now, the functional derivative in $\tilde{\phi}$

$$\int\int_0^t \frac{\delta S}{\delta\phi}\beta(\chi,\tau)d\tau d^d\chi = \left\{\frac{d}{d\varepsilon}\int\int_0^t d\tau d^d\chi\ (\tilde{\phi}+\varepsilon\beta)\partial_\tau\phi + \sum_k a_k(\phi)(\tilde{\phi}+\varepsilon\beta)^k\right\}_{\varepsilon\to 0}. \tag{A.53}$$

Organizing the equation and acting with the limit $\varepsilon \to 0$:

$$\int\int_0^t \frac{\delta S}{\delta\phi}\beta(\chi,\tau)d\tau d^d\chi = \frac{d}{d\varepsilon}\int\int_0^t d\tau d^d\chi\ \left[\partial_\tau\phi + a_1(\phi)\right]\beta + \sum_{k=2} a_k(\phi)\frac{d}{d\varepsilon}\left[(\tilde{\phi}+\varepsilon\beta)^k\right]_{\varepsilon\to 0}. \tag{A.54}$$

Because we want both functional derivatives to be zero simultaneously, we apply the condition obtained previously ($\tilde{\phi} = 0$). Since the terms in the sum in k are always going to depend on $\tilde{\phi}$ or ε^w, with $w \geq 2$, all terms will be zero. This leads to the condition

$$\partial_t\phi + a_1(\phi) = 0 \tag{A.55}$$

Therefore, only the linear in $\tilde{\phi}$ terms of the quasi-Hamiltonian are going to matter for the field equation.

Appendix B

Numerical integration of the population density equation

In this appendix, we present how to perform the numerical integration of the population-level approximation PDE. We use a second-order in time pseudospectral method detailed in [123]. The method consists in determining the time evolution of a PDE in Fourier space through a "two-step" process. With it, we obtain the density field at a time $t + 2\delta$ with an error $\mathcal{O}(\delta t^3)$. First, we Fourier transform the nonlinear PDE (4.106) and separate its linear and nonlinear terms

$$\frac{\partial \hat{\rho}(k,t)}{\partial t} = -\alpha(k)\hat{\rho}(k,t) + \Phi(k,t) \tag{B.1}$$

where $\hat{\rho}(k,t)$ is the Fourier transform of the population density field and $\alpha(k) = Dk^2 - r$ is the coefficient associated with the linear part. $\Phi(k,t)$ is the Fourier transform of the nonlinear part of the original equation

$$\Phi(k,t) = \mathcal{F}\left[\tilde{\rho}_f(x,t)\rho(x,t) - \gamma\,\tilde{\rho}_c^2(x,t)\rho(x,t)\right] \tag{B.2}$$

Setting the initial condition $\rho(x,0)$ and computing its Fourier transform $\hat{\rho}(k,0)$, the algorithm we use to integrate the equation between t and $t + 2\delta t$ is based on the following steps:

1. Compute $\Phi(x,t)$ in real space and transform it to Fourier space to obtain $\Phi(k,t)$.

2. Calculate the Fourier transform of the density field at time $t + \delta t$ (see [123] for a derivation of this expression) as,

$$\hat{\rho}(k,t+\delta t) = e^{-\alpha(k)\delta t}\hat{\rho}(k,t) + \frac{1 - e^{-\alpha(k)\delta t}}{\alpha(k)}\Phi(k,t) \tag{B.3}$$

3. Compute $\rho(x, t + \delta t)$ by Fourier transforming $\hat{\rho}(k, t + \delta t)$ and use it to calculate the nonlinear part of the original PDE in real space.

4. Compute $\Phi(k, t + \delta t)$ by Fourier transforming the result obtained in the previous step.

5. Calculate the updated field in the Fouier domain,

$$\hat{\rho}(k, t + 2\delta t) = e^{-2\alpha(k)\delta t}\hat{\rho}(k, t) + \frac{1 - e^{-2\alpha(k)\delta t}}{\alpha(k)}\Phi(k, t + \delta t) \tag{B.4}$$

Thus, in each algorithm iteration, the field $\hat{\rho}(k, t)$ goes to $\hat{\rho}(k, t + 2\delta t)$ and the process is repeated until the desired simulation time is reached. For all of the population-level model simulations, we use $dt = 0.05$, $dx = 0.008$.